Title
Nuclear Air-Brayton Combined Cycle Power Conversion Design, Physical Performance Estimation and Economic Assessment

Author
Andreades, Charalampos

Publication Date
2015

Peer reviewed|Thesis/dissertation

Nuclear Air-Brayton Combined Cycle Power Conversion Design, Physical Performance Estimation and Economic Assessment

by

Charalampos Andreades

A dissertation submitted in partial satisfaction of the

requirements for the degree of

Doctor of Philosophy

in

Engineering - Nuclear Engineering

and the Designated Emphasis

in

Energy Science and Technology

in the

Graduate Division

of the

University of California, Berkeley

Committee in charge:

Professor Per F. Peterson, Chair
Professor Jasmina Vujic
Professor Massimiliano Fratoni
Professor Lucas Davis

Summer 2015

Nuclear Air-Brayton Combined Cycle Power Conversion Design, Physical Performance Estimation and Economic Assessment

by

Charalampos Andreades

Abstract

Nuclear Air-Brayton Combined Cycle Power Conversion Design, Physical Performance Estimation and Economic Assessment

by

Charalampos Andreades

Doctor of Philosophy in Nuclear Engineering

Designated Emphasis in Energy Science and Technology

University of California, Berkeley

Professor Per F. Peterson, Chair

The combination of an increased demand for electricity for economic development in parallel with the widespread push for adoption of renewable energy sources and the trend toward liberalized markets has placed a tremendous amount of stress on generators, system operators, and consumers. Non-guaranteed cost recovery, intermittent capacity, and highly volatile market prices are all part of new electricity grids.

In order to try and remediate some of these effects, this dissertation proposes and studies the design and performance, both physical and economic, of a novel power conversion system, the Nuclear Air-Brayton Combined Cycle (NACC). The NACC is a power conversion system that takes a conventional industrial frame type gas turbine, modifies it to accept external nuclear heat at 670°C, while also maintaining its ability to co-fire with natural gas to increase temperature and power output at a very quick ramp rate. The NACC addresses the above issues by allowing the generator to gain extra revenue through the provision of ancillary services in addition to energy payments, the grid operator to have a highly flexible source of capacity to back up intermittent renewable energy sources, and the consumer to possibly see less volatile electricity prices and a reduced probability of black/brown outs.

This dissertation is split into six sections that delve into specific design and economic issues related to the NACC. The first section describes the basic design and modifications necessary to create a functional externally heated gas turbine, sets a baseline design based upon the GE 7FB, and estimates its physical performance under nominal conditions.

The second section explores the off-nominal performance of the NACC and characterizes its startup and shutdown sequences, along with some of its safety measures. The third section deals with the power ramp rate estimation of the NACC, a key performance parameter in a renewable-heavy grid that needs flexible capacity. The fourth section lays out the cost structure of the Mk1 Pebble-Bed Fluoride-salt-cooled High-temperature Reactor (FHR) with the NACC, since the NACC cannot be treated separately from its heat source.

The fifth section evaluates the cost structure of a twelve-unit Mk1 FHR and NACC, including capital construction costs, operating costs, fuel and decommissioning costs in bottom up methodology. The sixth section proposes alternative NACC configurations and scales (mobile, remote NACC) or alternative power cycles to the NACC that can be coupled to the FHR (supercritical carbon dioxide Brayton cycle).

Acknowledgements

I would like to offer a laconic but meaningful message of gratitude to certain people that have got me on, guided me down, and firmly placed me on the path I currently find myself on, realizing that this is simply an end to a chapter of long and beautiful journey.

First and foremost, I would to express my gratitude to my parents and family, who have not once stopped supporting me and have encouraged me to pursue my passions and keep a firm and realistic outlook on life.

In turn, to Deborah Roudebush, my high school physics teacher, who pushed me to excel and taught me a structured and ordered way of thinking about problems, with incessant patience and a genuine desire for improvement of her students, I cannot thank you enough.

To John J. Dorning, Whitney Stone Professor of Nuclear Science and Engineering, an undergraduate professor and friend at the University of Virginia, who offered a hint of the rigor and beauty of graduate level study and nuclear engineering, I am indebted; also the sole non-Greek person who has managed to correctly pronounce my full Greek name on the first try.

To my dear mentors, Professors Per F. Peterson and Jasmina Vujic, who opened the door and welcomed me to the warm family of the nuclear engineering department at the University of California Berkeley, who never once hesitated to provide guidance, opportunities, and a truly magnificent learning environment, I am eternally obliged.

To the wonderful faculty and staff of the Nuclear Engineering Department at the University of California at Berkeley, and by extension my colleagues in the Thermal Hydraulics laboratory, who provided a stimulating academic environment, an endless pool of learning and discussion, on philosophical as much as on technical matters, I am grateful.

To Lisa Zemelman and Noriko Katagiri, for truly making administrative matters a background thought, and always allowing full concentration on the task at hand, a heartfelt thank you.

To Lindsay Dempsey, at Generation Solutions, Peter J. Warren, at General Electric, the kind employees of Thermoflow Inc., Dr. Alex Papalexopoulos, at Ecco Intl., and all those that are unnamed, who have contributed in their own meaningful manner to my research, you remain in my mind and I extend my gratitude to you.

This research was performed using funding received from the U.S. Department of Energy Office of Nuclear Energy's Nuclear Energy University Programs.

Table of Contents

Acknowledgements i
List of Figures v
List of Tables vii
1 Introduction 1
1.1 Overview of the NACC 2
1.2 Overview of FHR Technology 3
1.3 Dissertation Structure 4
2 NACC Design and Performance under Nominal Ambient Conditions 5
2.1 Introduction 5
2.1.1 Review of Nuclear Power Conversion and Open-Air Brayton Cycle Literature 6
2.1.2 Benefits of RACC Power Conversion. 7
2.2 Commercially Available Gas Turbines 9
2.3 Two Baseline Configurations 10
2.3.1 Two Baseline RACC Cycles. 11
2.3.2 Rankine Cycle. 13
2.3.3 Base Load. 14
2.3.4 Cofiring. 15
2.3.5 Coiled Tube Air Heaters (CTAHs): 16
2.4 Additional RACC Design Issues 18
2.4.1 Turbine Blade and Nozzle Considerations. 18
2.4.2 Turbine Modification. 19
2.4.3 RACC Turbine Orientation. 20
2.5 RACC Modeling and Optimization 21
2.5.1 Brayton Cycle Optimization. 22
2.5.2 Rankine Cycle Optimization. 28
2.5.3 Alstom GT24. 28
2.6 Discussion 29
3 Nuclear Air-Brayton Combined Cycle Power Conversion Off-Nominal and Transient Performance 31

3.1 Introduction 31
3.2 Baseline Design Selection 32
3.3 Off Nominal Ambient Conditions 33
3.3.1 Off-Nominal Ambient Temperature. 33
3.3.2 Off-Nominal Elevation. 39
3.4 Start-Up 41
3.5 Shutdown 45
3.6 Load Rejection 46
3.7 Unit Trips 46
3.8 Power Ramping and Cofiring 47
3.9 Service Life and Maintenance 48
3.10 Blade Failures 49
3.11 Natural Gas Safety 49
3.12 Discussion 50
4 NACC Power Ramp Rate Calculation 51
4.1 Methodology 51
4.2 Data and analysis 52
4.3 Discussion 59
5 Mk1 FHR Cost Estimation 60
5.1 Introduction 60
5.2 Construction Costs 61
5.2.1 Preconstruction Costs 61
5.2.2 Direct Costs 62
5.2.3 Indirect Costs and Project Contingency 66
5.3 Operation and Maintenance Costs 67
5.4 Fuel Costs 70
5.5 Decommissioning Costs 72
5.6 Discussion 73
6 Supplementary Cycle Configurations and NACC Alternatives 75
6.1 Introduction 75
6.2 Simple and Combined Cycle NACC for Mobile Applications 75

6.2.1 Gas Turbine Selection and Modification 76
6.2.2 Modeling and Results 78
6.2.3 Discussion 81
6.3 Supercritical Carbon Dioxide (S-CO_2) Power Conversion 81
6.3.1 Code to Code Comparison 82
6.3.2 PB-FHR S-CO_2 Cycle Modeling and Considerations 87
6.3.3 Discussion 93
7 Conclusion 95
References 99

List of Figures

Figure 1-1. The 'duck curve" showing steep ramping needs and overgeneration risk [1]. 2
Figure 2-1. Flow schematic for a RACC power conversion system with a single stage of reheat. . 6
Figure 2-2. Compressor air outlet temperature as a function of inlet temperature and compression ratio, for a modern, large, high efficiency (89.4%) axial compressor. 10
Figure 2-3. Computer-aided-design rendering of a baseline GE 7FB gas turbine modified to introduce external air heating and reheating, with cofiring. 12
Figure 2-4. Mk1 FHR and NACC physical arrangement. 14
Figure 2-5. CTAH elevation and plan views, taken from Gilli et al. patent [19]. 17
Figure 2-6. 113-MWe Alstom GT11N2 gas turbine with an external silo combustor [22]. 20
Figure 2-7. Base-load 100-MWe THERMOFLEX® power conversion system flow diagram. 22
Figure 2-8. Peaking 241-MWe THERMOFLEX® power conversion system flow diagram. 22
Figure 2-9. Net efficiency vs. ER for GE 7FB baseline. 25
Figure 2-10. Power vs. ER for GE 7FB baseline. 25
Figure 2-11. CTAH Size vs. ER for GE 7FB baseline. 26
Figure 2-12. NACC T-s diagram for GE 7FB baseline. 26
Figure 2-13. LP pressure losses vs. net power. 27
Figure 2-14. LP pressure losses vs. net efficiency. 28
Figure 3-1. Reference THERMOFLEX® power conversion system flow diagram for base-load, 15°C nominal ambient conditions. 36
Figure 3-2. THERMOFLEX® power conversion system flow diagram for 0°C cold ambient conditions with stack recirculation. 36
Figure 3-3. THERMOFLEX® power conversion system flow diagram for 40°C warm ambient conditions with compressor inlet fogging. 37
Figure 3-4. Net FHR thermal power at different ambients, with and without GT inlet control... 38
Figure 3-5. LP/HP CTAH heat transfer ratio at different ambients, with and without GT inlet control. 38
Figure 3-6. Net baseload electrical power at different ambients, with and without GT inlet control. 38
Figure 3-7. Net baseload efficiency at different ambients, with and without GT inlet control. .. 38
Figure 3-8. Net co-firing electrical power at different ambients, with and without GT inlet control. 38
Figure 3-9. Net co-firing efficiency at different ambients, with and without GT inlet control. ... 38
Figure 3-10. Net Power (base load, BL, and co-fired, CF) at varying ambient conditions for 0 m and 1625 m elevations. 40
Figure 3-11. Efficiency (base load, BL, and co-fired, CF) at varying ambient conditions for 0 m and 1625 m elevations. 40
Figure 3-12. Relative CTAH sizes at varying ambient conditions for 0 m and 1625 m elevations. 40

Figure 3-13. Core thermal power at varying ambient conditions for 0 m and 1625 m elevations. 40
Figure 3-14. THERMOFLEX® power conversion system flow diagram for start-up. 42
Figure 3-15. Net shaft power versus shaft speed. 44
Figure 3-16. Normalized start-up parameters versus shaft speed. 45
Figure 4-1. Typical startup curve for a GT [41]. 52
Figure 4-2. THERMOFLEX® schematic of GE 7FB simple cycle. 54
Figure 4-3. Turbine efficiency as a function of TET. 55
Figure 4-4. ER as a function of TET. 55
Figure 4-5. γ as a function of TET. 56
Figure 4-6. TET as a function of TET. 57
Figure 4-7. GE 7FB ramp rates during startup. 58
Figure 5-1. Preconstruction costs as a function of units on site 62
Figure 5-2. GE 7FB CC THERMOFLEX schematic flow diagram. 64
Figure 5-3. Annual O&M Costs as a Function of FHR Units. 69
Figure 6-1. SC GE 10-1 layout w/ reactor - Isometric view. 77
Figure 6-2. SC GE 10-1 layout w/ reactor - Elevation view. 78
Figure 6-3. NACC T-s diagram - baseload and co-fired. 81
Figure 6-4. Optimized S-CO_2 Brayton cycle conditions for the SFR-100 [65]. 83
Figure 6-5. SFR-100 S-CO_2 ideal cycle results from THERMOFLEX®. 84
Figure 6-6. SFR-100 S-CO_2 detailed THERMOFLEX® results. 85
Figure 6-7. SNL S-CO_2 recompression Brayton cycle flow diagram [66]. 86
Figure 6-8. SNL S-CO_2 THERMOFLEX® cycle diagram. 86
Figure 6-9. PB-FHR S-CO_2 power conversion schematic. 88
Figure 6-10. FHR S-CO_2 T-s diagram. 90

List of Tables

Table 2-1. Commercially available 60Hz F, G, and H class turbines. Power output is the rating for a simple combustion cycle. 10
Table 2-2. Key CTAH design parameters. 18
Table 2-3. GE 7FB and Alstom GT24 parameters for conventional natural gas firing. 23
Table 2-4. Ducting air pressure loss estimation for GE 7FB baseline design. 23
Table 2-5. Expansion ratio selection results. 24
Table 2-6. Steam cycle pressure selection. 28
Table 2-7. Key RACC design parameters. 29
Table 3-1. Key RACC design parameters based on the GE 7FB. 33
Table 3-2. GE 7FB operating characteristics at varying ambient conditions. 35
Table 3-3. RACC performance at sea level and Denver, CO. 40
Table 4-1. NACC performance characteristics. 51
Table 4-2. GE 7FB state points as a function of power. 53
Table 4-3. GE 7FB operating startup and low power operating point estimations. 57
Table 4-4. GE 7FB ramp rates during startup. 58
Table 5-1. Preconstruction costs for a single unit Mk1. 61
Table 5-2. Mk1 material inventory and costs. 63
Table 5-3. GE 7FB CC material inventory and prices. 64
Table 5-4. Single unit Mk1 material inventory and scaled direct costs. 65
Table 5-5. Estimated quantities of composite materials contained in a typical 1000 MW_e PWR power plant, including field construction materials consumed [51]. 66
Table 5-6. Total indirect cost for a single unit Mk1. 66
Table 5-7. Total capital cost for a single unit Mk1 FHR. 67
Table 5-8. Annual O&M costs for Mk1. 68
Table 5-9. Estimates of Advanced NGCC operating costs (2014$) [52, 55]. 69
Table 5-10. Mk1 fuel design parameters. 70
Table 5-11. Annual uranium requirements for Mk1 core. 71
Table 5-12. Annual fuel costs for a single unit Mk1 FHR. 71
Table 5-13. Estimated specific decommissioning costs. 72
Table 5-14. Estimated decommissioning costs for a single and twelve unit Mk1. 72
Table 5-15. Overview of Mk1 costs 73
Table 6-1. Commercially available 10MWe aeroderivative GTs. 75
Table 6-2. GE 10-1 characteristics. 76
Table 6-3. SC w/ reheat optimization – Baseload. 78
Table 6-4. SC w/ reheat optimization – Co-fired. 79
Table 6-5. Rankine cycle optimization – Baseload 80
Table 6-6. Rankine cycle optimization – Co-fired. 80
Table 6-7. Co-firing efficiencies. 80

Table 6-8. Main performance parameters for ANL and SNL S-CO2 Brayton cycles. 82
Table 6-9. PB-FHR S-CO_2 cycle conservative and best estimate fixed operating parameters..... 89
Table 6-10. FHR S-CO_2 optimized parameters. 90
Table 6-11. Operating parameter comparison of NACC and S-CO2 cycles. 92
Table 6-12. Coiled tube gas heater summarized performance characteristics. 93
Table 7-1. Key NACC design parameters. 96
Table 7-2. Overview of Mk1 costs..... 97

1 Introduction

The subject of this dissertation is the study, design, and estimation of economic merit of a novel power conversion system, namely the Nuclear Air-Brayton Combined Cycle (NACC). In basic layman terms it can be described as a hybrid nuclear/natural gas (NG) turbine that derives its baseload power from nuclear heat and can provide additional power on demand by injecting NG. This configuration enables the production of a baseload of electricity while also providing quick ramping and flexible electricity on demand. The significance of such operation can be understood by first understanding the general role of energy in society and subsequently the current developments in energy needs and policy.

The strong correlation between energy availability and economic development and in turn standard of living, is one that is well understood. Energy allows for the mechanization and automation of processes, and consequently freeing up time and resources that can be devoted elsewhere and elsewise. In such a fashion, agricultural societies transition into industrial ones, and sequentially to post-industrial and service based ones. Electricity and electrification are a form of energy that drives forward economic and societal development. The main energy source for the past two and a half centuries has been and to a large extent still is coal; which leads to the next pressing issue of the late 20th and early 21st century, climate change, and in particular man-made climate change in a rapidly changing electricity sector.

Electricity liberalization and deregulation have shifted the way energy and electricity is priced, away from average cost pricing to competitive marginal cost pricing. Although in the infant years of the industry, electric utilities priced electricity at competitive rates, competing with natural gas (NG) lighting and self-generation, a need to guarantee economic viability and attractiveness to investors led to a push for regulation. This effort resulted in the large protected monopoly utilities with guaranteed cost plus pricing in the 1930's. Success in deregulating other industries, such as trucking and commercial airlines among others, led to an increased interest and resurgence of competitive pricing in many electricity markets over the past 25 years. Furthering the changing nature of electricity markets is the push for clean energy sources stemming from the United Nations Framework Convention on Climate Change of 1992 and the subsequent adoption of renewable, yet intermittent, "green" resources. This combination of changes has created a highly volatile pricing mechanism, which demands excess fast ramping flexible capacity reserves to avoid disruption of continuous electricity supply. A reference scenario is the so-called "duck-curve" in the California electricity grid, under which high penetration of intermittent renewables, namely solar, causes a quick and large dip in supply during the early evening hours. The shortage cannot be balanced at a quick enough rate within the demanded time-frame of a couple of hours by conventional resources due to their operating and physical limitations. Compounding to the situation, some of the "stand-by" plants only run a few hours a year and in turn set high market prices when called upon in order to recover their capital costs. In sum, the introduction of intermittent renewable energy sources, that try to

mitigate carbon emissions, in combination with the changing nature of electricity markets, create a volatile pricing mechanism that help to hinder a secure electricity network.

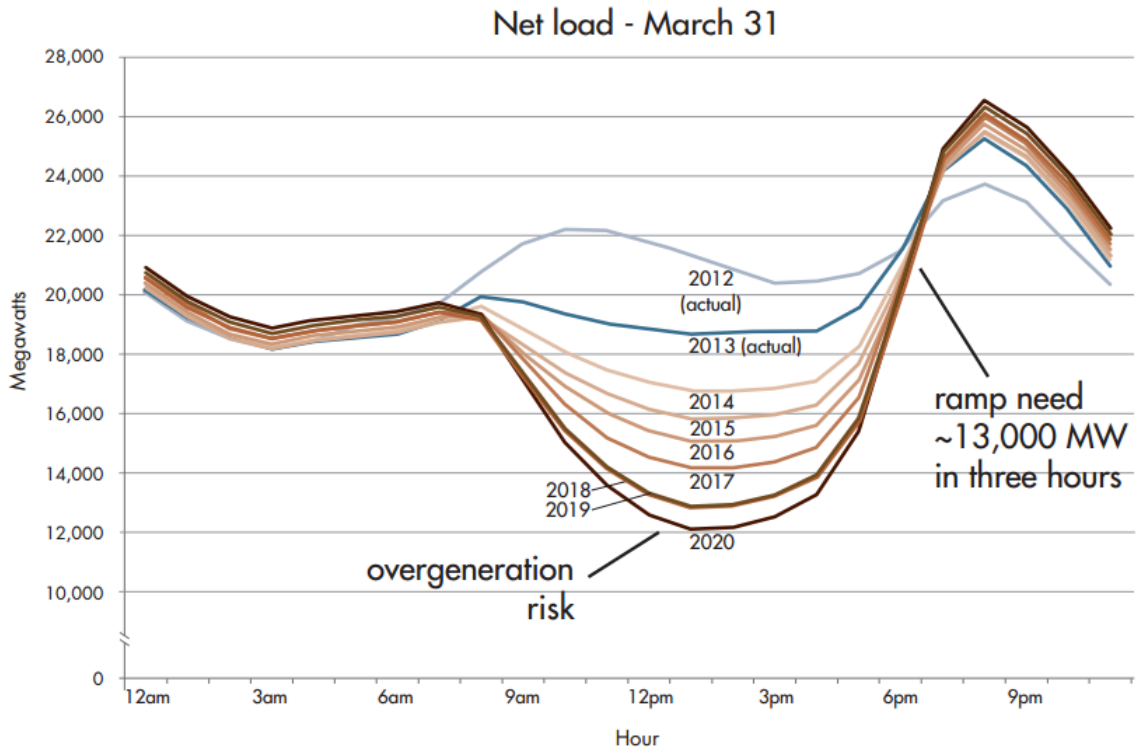

Figure 1-1. The 'duck curve" showing steep ramping needs and overgeneration risk [1].

With this background in mind, it becomes apparent that there is a clear need for a combination of reliable, flexible, and clean supply of electricity. Just such a system is the NACC, which provides a baseload of clean nuclear baseload electricity in tandem with a flexible NG peaking electricity supply to enable a clean and low-carbon grid.

1.1 Overview of the NACC

The NACC is an innovative power conversion system based on the air Brayton cycle. Traditionally, nuclear power stations have used steam Rankine cycles to convert heat to electricity, as steam turbines are a century-and-a-half-old technology that is well understood and reliable. However, steam turbines have slow response times due to several technical constraints (slow pressure buildup in the boilers, material integrity limits due to temperature swings, etc.) These characteristics render them unsuitable to a renewable heavy grid that requires quick ramping and flexible capacity. Natural gas turbines (GTs), based on the Brayton cycle, are the power conversion system of choice when it comes to providing flexible capacity. Evolutionary advances over the past fifty years in the aeronautical industry have translated into better performing and more reliable GTs in the electricity production sector.

The advances in performance and compressor design of modern GTs have been quite large. This makes it important to study whether they can be coupled to an external heat source

in the 600 to 700°C temperature range possible with molten salt coolants. For this reason it was decided to determine whether a commercially available GT could be modified to accept nuclear heat from a salt-cooled reactor, while also maintaining its ability to combust NG (and in the future hydrogen or biofuels) on demand to produce peaking electricity. A conventional commercially available GT, the GE 7FB in a combined cycle configuration, was selected and the turbine design was modified to accept external heating and a stage of reheat. A significant performance advantage over the conventional steam cycle used for light water reactors was found, due to the higher peak temperatures. Additionally, a performance advantage over conventional GTs in converting NG to electricity is also found, because NG adds heat at a higher average temperature, so the NG heat acts as a topping cycle. The overall configuration allows for a supply of steady base load nuclear electricity and quick ramping peaking electricity for grid support services, such as frequency regulation, spinning reserves, black start services, and flexiramp capacity.

1.2 Overview of FHR Technology

Although the NACC can be coupled to any external heat source that can provide heat in the 600 to 700°C temperature range (e.g. concentrating solar), the primary heat source considered in this dissertation is the fluoride-salt-cooled high-temperature reactor (FHR). The FHR is a generation IV small modular reactor technology now under development in the U.S. and China. It is a pool-type reactor that combines several technologies, namely passive decay heat removal and safety systems, graphite-matrix-coated particle fuel, fluoride salt coolant, and an open-air Brayton cycle power conversion system. The FHR uses flibe as a coolant, a lithium fluoride and beryllium fluoride salt mixture (Li_2BeF_4), which has high melting (459 °C) and boiling (1430 °C) temperatures, very low volume change on freezing (~2%), and operates at nearly atmospheric pressure in the reactor primary coolant loop. With structural materials such as 316 or 304 stainless steel, or Alloy N, FHRs can deliver heat with a core inlet temperature of 600 °C and outlet temperature of 700 °C. These characteristics allow for its coupling to NACC power conversion. The NACC provides several potential technical and operational advantages as well as economic benefits. A detailed description of the Mk1 Pebble-Bed FHR (Mk1 PB-FHR or simply Mk1) preconceptual commercial point design can be found in Andreades et al. [2].

FHRs, as well as fluid-fueled MSRs and high-temperature CSP, appear to be somewhat unique in their capability to couple to an open-cycle NACC power conversion system (PCS). Light water reactors and conventional trough-type solar collectors deliver heat at temperatures that are too low for NACC. Liquid metal reactors, which use fuel with metallic cladding, are limited to peak core outlet temperatures around 550 °C which is likewise too low to be compatible with NACC. Helium-cooled high-temperature reactors have sufficiently high core outlet temperatures, but the core inlet temperatures needed to maintain the high-pressure reactor vessel at an acceptably low temperature is too low for NACC power conversion. This leaves salts as the remaining heat transfer fluids with properties appropriate for NACC application.

1.3 Dissertation Structure

This dissertation is split into six sections that delve into specific design and economic issues related to the NACC. The first section describes the basic design and modifications necessary to create a functional externally heated GT, sets a baseline design based upon the GE 7FB, and estimates its physical performance under nominal conditions.

The second section explores the off-nominal performance of the NACC and characterizes its startup and shutdown sequences, along with some of its safety measures. The third section deals with the power ramp rate estimation of the NACC, a key performance parameter in a renewable heavy grid that needs flexible capacity. The fourth section lays out the cost structure of the Mk1 PB-FHR with the NACC, since the NACC cannot be treated separately from its heat source.

The fifth section evaluates the cost structure of a twelve-unit Mk1 PB-FHR and NACC, including capital construction costs, operating costs, fuel and decommissioning costs in bottom up methodology. The sixth section proposes alternative NACC configurations and scales (mobile, remote NACC) or alternative power cycles to the NACC that can be coupled to the FHR (supercritical carbon dioxide Brayton cycle).

Finally, the results of the dissertation are summarized and discussed in a concluding section.

2 NACC Design and Performance under Nominal Ambient Conditions

This chapter is an adapted version of the archival journal article "Reheat-Air Brayton Combined Cycle Power Conversion Design and Performance Under Nominal Ambient Conditions" by Andreades et al. [3]. *Full copyright permission for use in this dissertation has been granted by the American Society of Mechanical Engineers (ASME).*

2.1 Introduction

The possibility that nuclear reactors might be used to provide thermal power for air Brayton gas turbines (GTs) was first recognized in the 1950s and studied during the Aircraft Nuclear Propulsion (ANP) program [4]. The ANP studied direct heating of air with solid fuels, where neutron activation of air is a problem, and the more practical option of indirect heating of air with molten-salt fuel and sodium intermediate coolant. Because the military logic for nuclear-powered aircraft disappeared with the advent of intercontinental missiles, today's commercial nuclear power stations evolved instead from water-cooled submarine reactors where reactor mass and thermal efficiency were not design constraints as they were for the ANP application and for aircraft propulsion in general.

With the major advances in GT technology in the last 60 years, the potential to couple nuclear power and concentrating solar power (CSP) to air Brayton combined cycles merits reinvestigation. This chapter studies design options and presents two reference designs based on the GE 7FB and Alstom GT24 gas turbines for reheat-air Brayton combined cycle (RACC) power conversion. When coupled to nuclear reactors, this power conversion method can also be referred to as nuclear air Brayton combined cycle (NACC) power conversion.

Conventional light water nuclear power plants that were derived from early submarine reactors have core outlet temperatures around 320 °C and use steam-Rankine power conversion cycles with efficiency in the range of 32% to 37% [5]. By comparison, modern heavy-frame-type GTs with heat recovery steam generators (HRSGs) and steam bottoming cycles operate at combined cycle efficiencies approaching or exceeding 60%. The compressors in these large, stationary GTs (Table 2-1) achieve compression pressure ratios (PRs) ranging from 15 to 35, with compressor air outlet temperatures ranging from 350 °C to 580 °C. Fluoride-salt-cooled high-temperature reactors (FHRs), molten salt reactors (MSRs), and high-temperature CSP towers have the ability to deliver heat at temperatures above these compressor outlet temperatures, and, thus, as with the original ANP reactor designs, to provide heat to drive air Brayton power conversion.

With current ASME Boiler and Pressure Vessel Code certified materials, fluoride salts can be used as heat transfer fluids up to peak temperatures around 700 °C, which is the near-term design core outlet temperature for FHRs [6]. In a counterflow configuration in an external coiled-tube air heater (CTAH) with a pinch-point temperature difference of 30 °C, as discussed later, air could then be heated to a temperature of approximately 670 °C. Advanced materials now in

development for use with molten salt coolants could enable yet higher temperatures, potentially reaching 850 to 1000 °C [7].

In RACC power conversion, air is heated in an external CTAH to 670 °C or higher and is then expanded and reheated, as shown schematically in Figure 2-1. In general, it is optimal to expand the air to the pressure where its temperature is approximately equal to the outlet temperature of the compressor and then to reheat the air to the same turbine inlet temperature. While reheating is not required if cofiring with fuel is then used to further heat the air toward conventional gas turbine inlet temperatures [8], the major benefits of reheating are that it can double (single reheat stage) or triple (two reheat stages) the net thermal energy input from the external heat source and also increase significantly the cycle efficiency during operation without cofiring. Because external heating can utilize a low-carbon energy source, reheating increases the net low-carbon power output under base load, externally heated operation. Moreover, by injecting fuel downstream of the last reheater, net power production can be increased to provide peaking power.

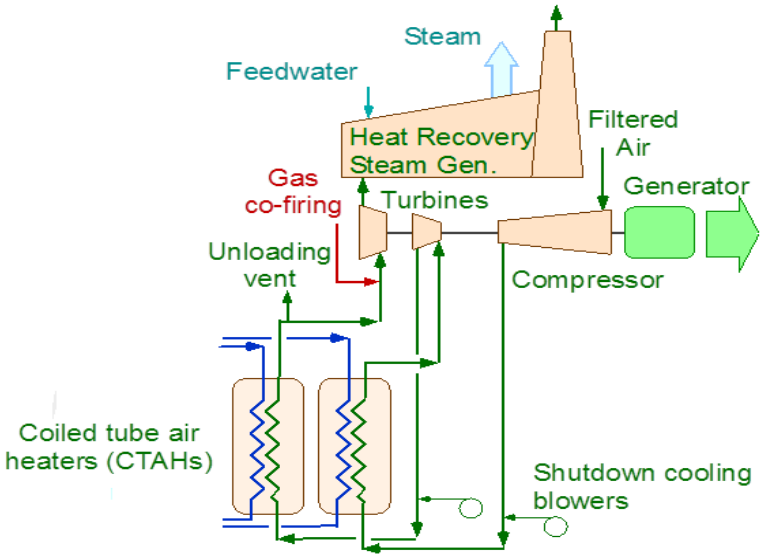

Figure 2-1. Flow schematic for a RACC power conversion system with a single stage of reheat.

This chapter examines issues and describes suggested modifications to conventional industrial gas turbines in order to accommodate external heating. It also presents two reference designs and performance results for operation under nominal ambient conditions.

2.1.1 Review of Nuclear Power Conversion and Open-Air Brayton Cycle Literature

A number of advanced power cycles for nuclear and CSP plants are currently under development and the applicability of each depends on the temperature range across which the low-carbon heat source delivers thermal energy to the power conversion system. Supercritical steam turbines are being investigated for light water and advanced reactors. Supercritical CO_2 turbines are being investigated for liquid metal reactors, whose peak coolant temperature is

550 °C. Helium Brayton cycles were investigated for helium-cooled reactors for which the peak coolant temperature can be as high as 900 °C and can also be used in multiple reheat configurations at lower temperatures [5]. The CO_2 and helium power cycles do not use off-the-shelf turbomachinery, operate with high pressures and large pressure differentials in the heat exchangers (100 to 200 bar), and significant technology development efforts are still needed before commercialization can be practical [9].

This chapter studies RACC power conversion systems that utilize off-the shelf GT compressors with turbine modifications that implement external air heating, a heating approach with important similarities to the external silo combustors used in some types of stationary GTs. In the electric power industry, GTs were initially used starting in the 1950s for peaking capacity because they had low efficiency but low capital cost and good starting reliability. Since then, GT efficiencies have drastically improved and today GTs are used for base load, spinning reserve, frequency control, and peaking services. They are also used for process heat cogeneration. Their combined cycle efficiency can approach or exceed 60%, depending on the firing temperature [10]

Open-air Brayton cycles have been previously proposed for solar thermal plants [11] and nuclear reactors [8]. For the solar application, with one reheat stage, compressor intercooling, and preheating of the air, this earlier work has estimated that power conversion efficiencies of 35% can be achieved [11].

2.1.2 Benefits of RACC Power Conversion.

One of the most attractive reasons for using an open-air Brayton cycle is that the major technology and components are commercially available and well developed for application to natural gas combined cycle (NGCC) power conversion. Additionally, due to the widespread adoption of conventional gas turbines the capability of nonoriginal-equipment manufacturers (non-OEM) third party service providers and part suppliers to re-engineer OEM products is quite well developed.

Another beneficial aspect of the open-air Brayton cycle is the feasibility to use a conventional combined cycle (CC) configuration with a Rankine bottoming cycle or other combined process heat application. The use of a bottoming cycle may enable RACC systems to produce low-carbon base load electricity at efficiencies above 40% in the near term and approaching 50% with advanced materials, some 20–40% greater than conventional light water nuclear reactors.

In combination with or in lieu of a steam bottoming cycle, the high-temperature exhaust of the gas turbine, ranging anywhere from 300 °C to 700 °C, can be used to provide process heat for steam production, distillation technology, hydrogen production, or other chemical processes. For example, low-temperature process heat can be used for thermal distillation of saline brines or seawater through advanced multi-effect distillation [12].

Furthermore, natural gas, hydrogen, or other fuels can be injected directly after the last external heater stage for cofiring, which yields increased temperatures and power output for

providing ancillary services as well as flexible capacity to the grid. Because peaking is initiated from a hot, spinning base-load condition, the efficiency penalties of maintaining the peaking capacity in standby condition are eliminated. Economically, a nuclear-gas or CSP-gas plant would have substantial latitude in exploiting variability in natural gas and electricity prices, as well as providing other grid support services such as spinning reserve. Load following ability offers insulation from volatile natural gas prices, while the ability to peak-on-demand would allow the plant to take advantage of high electricity spot prices [13].

While the flexibility of RACC power conversion allows it to provide a wide range of grid support and process heat services, to first order, the RACC design should be optimized around two primary revenue sources.

The first major RACC revenue source is the difference between nuclear or CSP fuel costs and electricity revenues during base-load operation, when typical electricity prices may be $0.04 to $0.08 per kilowatt-hour. Here, the most important design objective is to maximize low-carbon power production under base-load operation for a given gas turbine design to maximize net base-load electricity revenues. This focus on maximizing nuclear base-load output from a specific GT design is different from typical optimization of nuclear or CSP plants coupled to steam cycles, where the focus is on maximizing the net nuclear thermal power for a specific reactor design and the steam plant size is adjusted to match. For air cycles, the base-load thermal power rating of the GT system establishes the reactor thermal power, rather than the inverse. While the reactor power will be matched to a specific GT design, reactor power uprates can still be achieved by ganging up two or three GTs in 2×1 or 3×1 configurations with a single steam cycle plant, a practice widely adopted in conventional NGCC power plants.

The second major source of RACC revenue comes from operation during periods of peak electricity demand, when electricity prices may rise to $0.15 to $0.30 per kilowatt-hour or more. Here, the most important design objective is to maximize the total power output during peaking operation, which generally involves cofiring to bring the HRSG inlet (or possibly the turbine inlet) temperature to its maximum allowable limit. For peaking power production the efficiency for converting natural gas to electricity is a secondary metric. If the efficiency is higher than that of conventional NGCC power plants, then the RACC will be dispatched before these plants when base load electricity is needed. However, because the difference between fuel costs and electricity revenues will be relatively small during these periods, the contribution to net RACC revenues will be moderate (particularly compared to net RACC revenues from nuclear base-load generation), and this remains a secondary metric.

In brief, a NACC PCS coupled to an FHR, MSR, or CSP heat source may be attractive to electric utilities and independent system operators due to low fuel costs, low carbon emissions, high efficiency, and the capability to provide ancillary services such as peak power, spinning reserve, black-start, and the flexibility to provide a wide range of process heat services, such as desalination and other applications.

RACC power conversion does require two types of specialized equipment that are not currently commercially available. The first is a modified turbine system, which will enable external heating and one or more stages of reheat as well as the potential for fossil fuel cofiring. The GT modifications required to meet this functionality are the focus of this chapter. The second specialized equipment is the salt-to-air heat exchangers, for which a CTAH baseline design is proposed and briefly presented in the next section. Initial modeling structure is performed in a subsequent chapter.

This chapter presents the basic configuration options for RACC power conversion, some commercially available GT options currently available that are adaptable to RACC, and design challenges to implement RACC. To illustrate the design of a RACC power conversion system, a point design based upon the General Electric (GE) 7FB gas turbine and an advanced material design with higher salt temperatures based upon the Alstom GT24, both operating under nominal ambient conditions, are presented.

2.2 Commercially Available Gas Turbines

Gas turbines are ranked in classes depending on their firing temperature and power output. The latest generation GTs are the G/H class turbines; however, these GTs have features that make them less practical for near-term purposes, e.g., they require barge shipping. Conversely, near-term commercial FHR and CSP designs are expected to use rail transportable components, therefore limiting the maximum width of components to below 3.5 to 4 m. Gas turbine manufacturers offer two different frequency ratings for their machines to accommodate for the 60 Hz (North and South American markets, northern Japan, and a few other countries) and the 50 Hz (southern Japan, Asia, Africa, Europe, Oceania) markets. 60-Hz GTs are usually smaller than their counterpart large 50-Hz models and are rail transportable. This study considers the 60-Hz GT variants. The heaviest and bulkiest pieces for the PCS transportation are the gas turbine, the steam turbine, and the main step transformer. For technical and transportation purposes, F class GTs are well suited to the near-term RACC needs. The major manufacturers that provide F class GTs are Alstom, GE, Mitsubishi, and Siemens.

Table 2-1 reviews characteristics of their machines along with some G/H class turbines for comparison.

Table 2-1. Commercially available 60Hz F, G, and H class turbines. Power output is the rating for a simple combustion cycle.

Manufacturer	Model	Power output (MW)	Mass flow (kg/s)	PR	Compressor stages	Turbine stages	Exhaust temp (°C)
Alstom	GT11N2	115.4*	393	15.5	14	4	526
Alstom	GT24	218	494	35.4	22	4	597
GE	7FA.05	215	508	17.0	17	3	594
GE	7FB	186.6	445	18.5	17	3	626
GE	7H	400	565	23.0	18	4	566
Siemens	SGT6-5000F	208	503	17.4	16	4	582
Siemens	SGT6-8000H	274	600	20.0	13	4	620
Mitsubishi	M501F	185.4	459	16.0	16	4	613
Mitsubishi	M501G	272	599	20.0	17	4	614

*The GT11N2 also has a 50-Hz variant.

As is shown in the table, pressure ratios (PR) vary anywhere from 15.5:1 to 23:1, except for the Alstom GT24, which has a compression ratio of 35.4:1 and uses a single stage of reheat. With these pressure ratios, modern, large axial compressors have air outlet temperatures typically in the range of 350 °C to 580 °C, as shown in Figure 2-2, which are attractive temperatures to enter a salt-to-air heat exchanger since it allows for a reasonable log-mean temperature difference. Care must also be taken to assure that the compressor-outlet temperature is high enough to avoid freezing of the coolant salt, which may require some recycle of heated gas to the compressor inlet under low-ambient-temperature conditions.

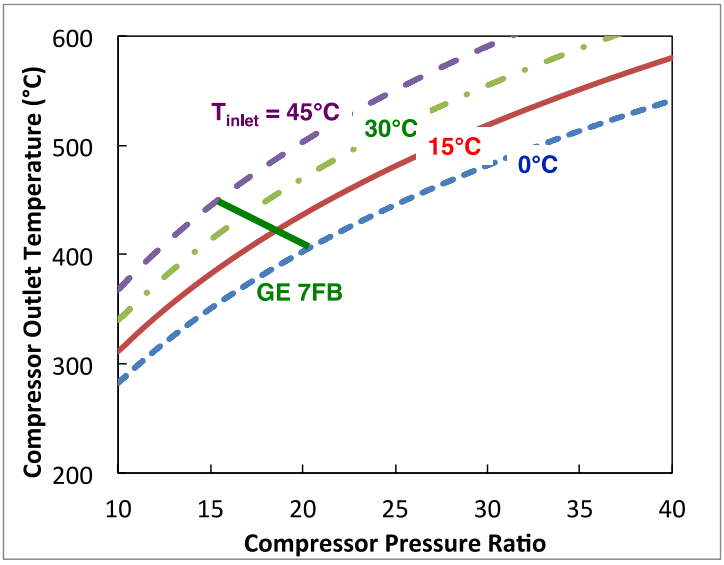

Figure 2-2. Compressor air outlet temperature as a function of inlet temperature and compression ratio, for a modern, large, high efficiency (89.4%) axial compressor.

2.3 Two Baseline Configurations

Air Brayton power cycles can be configured in simple cycles, recuperated cycles, or combined cycles. In practice, recuperation is only used with small GTs, for example, for mobile

applications. The combined cycle configuration is preferred for nuclear and CSP power application, due to its relatively high efficiency, and the decoupling of the salt-to-air heaters from the downstream use of the heated air, including the use of a heat recovery steam generator (HRSG) for either a Rankine bottoming cycle for extra power output or for steam supply to an industrial process or district heating system. Other potential options also include using the waste heat left in the air stream after the steam cycle for a distillation process or thermal desalination.

There also exists the possibility of creating a simple cycle configuration with an aeroderivative GT in the 10–20 MWth range for a scaled down version of the FHR, MSR, or CSP. Commonly, aeroderivative GTs are dual- or multi-shaft engines that would require a different design approach, but some smaller single-shaft GTs are also manufactured, such as the 11.25-MWe GE-10, that could be used for power conversion for low power applications. A brief description of such a system can be found in Chapter 6.2.

Here, the fluoride salt coolant inlet and outlet temperatures used for the RACC have been selected as 700 °C and 600 °C, respectively, limited by qualified materials selection for these coolants and the high freezing temperature of the reactor coolant. As such, the turbine inlet temperature for RACC base-load operation will be less than 700 °C. With these salt temperatures, appropriate air inlet temperatures to air heat exchangers are possible with compressors having compression ratios in the range 15 to 22 (Figure 2-2). With future advanced materials for nuclear reactors and CSP systems that might allow peak salt coolant temperatures in the range of 850 °C to 1000 °C, the increased compressor outlet temperatures provided by higher compression ratios, in the range of 30 to 40, would be attractive.

2.3.1 Two Baseline RACC Cycles.

One baseline for the RACC power cycle is presented based upon a modified GE 7FB GT shown in Figure 2-3, using a single stage of reheat with salt temperatures compatible with currently available materials (peak coolant temperature of 700 °C). Parameters for a second, advanced design, based upon a modified Alstom GT24 GT operating with higher temperature salt, are given in parentheses. The two reference designs are configured as follows:

(i) Air intake occurs through a filter bank, and the air is compressed to a pressure ratio of 18.5 (35.4). For a nominal 15 °C, 1.01 bar ambient condition the air exits the compressor at a temperature of 418 °C (560 °C).

(ii) After the GE 7FB (Alstom GT24) compressor outlet, the air passes through a high-pressure (HP) CTAH and is heated up to a turbine inlet temperature (TIT) of 670 °C (870 °C).

(iii) The air is then expanded to approximately the same temperature as the compressor outlet temperature, 418 °C (560 °C). This criterion determines the expansion ratio (ER) of the first expansion stage at design conditions.

(iv) The air is then reheated back up to 670 °C (870 °C) by passing through a second low-pressure (LP) CTAH. The design of this low-pressure external heating system to

minimize pressure drop is important to achieve acceptable circulating power loss and cycle efficiency.

(v) After the LP CTAH, the air is above the auto-ignition temperature of natural gas [14]. To provide power peaking, a fuel such as natural gas can be injected and burned to increase the turbine inlet temperature and the power output.

(vi) The heated air is then expanded down to nearly atmospheric pressure and 350–700 °C by passing through an additional set of turbine blades before entering the HRSG. The HRSG must be designed to accommodate a relatively wide range of air inlet temperatures due to the large change that occurs between low-carbon base-load operation and peak power operation with natural gas injection.

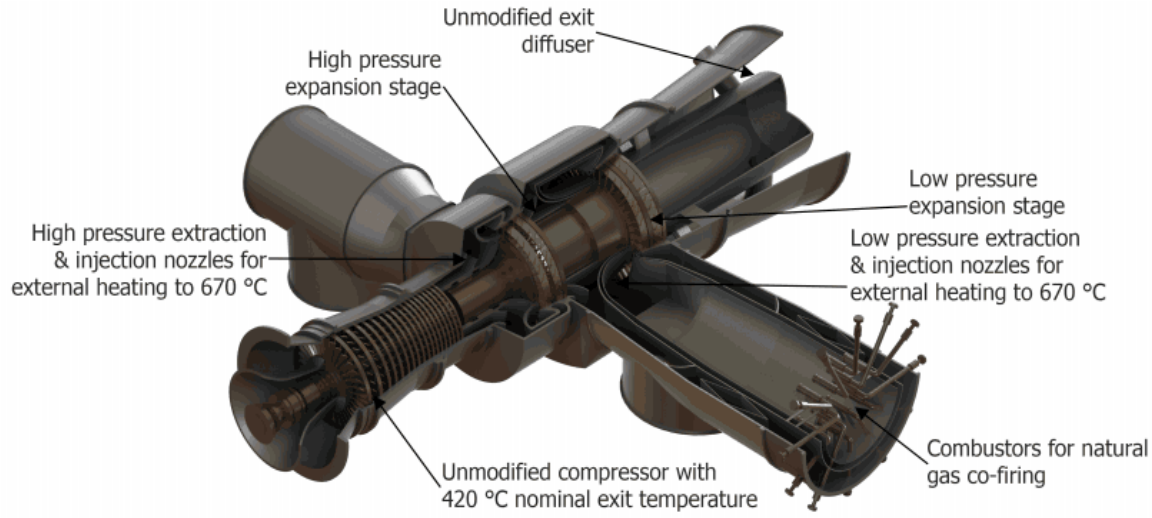

Figure 2-3. Computer-aided-design rendering of a baseline GE 7FB gas turbine modified to introduce external air heating and reheating, with cofiring.

There are several motivations for selecting this baseline configuration, with a single stage of reheat. First, an open cycle, and not a recuperated or closed cycle, was selected. For nuclear application during load rejection, one cannot rapidly shut down a reactor without causing a large thermal transient that places significant stress on primary system components. An open-air cycle with an unloading vent after the last CTAH, as shown in Figure 2-1, reduces the coupling between the reactor and the PCS. Opening the unloading vent allows the reactor and CTAHs to continue to operate at constant mass flow and temperature, while the flow through the last turbine expansion stage and HRSG can be reduced rapidly. Additionally, controlled venting in an open cycle allows for the reactor and the PCS to be ramped up or down at different rates, depending on operator needs.

The reference designs studied here, as shown in Figure 2-3, use a single stage of reheat as opposed to two or three stages of reheat. The primary reason for selecting one stage of reheat is the simplicity it introduces in the design due to the reduced amount of plumbing and modifications needed to the GT. Several other technical reasons also render this selection attractive. The surface area requirement of the CTAHs (A_{CTAH}) are significantly reduced by

allowing them to operate with a larger log-mean temperature difference (LMTD or ΔT_{LM}) due to the larger ER per stage and lower turbine exit temperatures (TET), than if more reheat stages were used:

$$A_{\mathrm{CTAH}} = \frac{\mathrm{Q}}{\varepsilon U \Delta T_{\mathrm{LM}}}. \qquad 2\text{-}1.$$

where Q is the net heat transfer in the CTAH, U the overall heat transfer coefficient, and ε the heat exchanger effectiveness.

Additionally, air circulating power requirements through the CTAHs are reduced due to smaller air pressure drops if the surface area requirements are smaller. Because the temperature change of the salt and air in each CTAH is nearly equal, the CTAHs have nearly the same size, simplifying their design, manufacturing, in-service inspection, and maintenance. Moreover, power output is distributed approximately in a 2:1 ratio between the air and steam cycles, as opposed to a more lopsided ratio for cases with dissimilar CTAH sizes or more than two CTAHs.

2.3.2 Rankine Cycle.

HRSGs and steam turbines are usually ordered tailored to the specific GT design, site, and needs, as opposed to GTs that are more or less ordered unmodified. Likewise, for nuclear and CSP applications, the steam cycle would require minor modification vis-à-vis one used for a conventional NGCC power plant, except to accommodate the relatively large variation in steam production and pressure that occurs with cofiring. Many appropriate HRSG designs are available "off-the-shelf," for example, GE's STAG or Alstom's KA24 pre-engineered systems.

The steam cycle may be set up in several different ways, depending on the desired output. Because the RACC PCS is intended to be a dual operation mode machine (base load and peaking) one needs to consider operation and design options for both modes [15].

Single, dual, and triple pressure HRSGs and steam turbine systems are available and are selected based on capital cost and HRSG inlet temperatures available from the GT exhaust. For RACC, a reasonable selection would use a triple pressure reheat HRSG and steam turbine assembly due to the wide range of HRSG air inlet temperatures compared to conventional natural gas combined cycle plants. The added combined cycle performance and output of a triple pressure steam cycle are significant when weighed against the increased capital cost from a single or dual pressure system, which is moderate relative to total plant cost. A triple pressure HRSG would be impractical to fit to the FHR in case of too low a GT exhaust temperatures during base-load operation. In the case of too low a temperature the flow in the low-pressure steam turbine is starved. The higher compressor PRs of the GE 7FB and Alstom GT24 allow for GT exhaust temperatures that do not run into this issue. GE suggests that a GT exhaust temperature of 593 °C or greater be available for coupling to its triple pressure HRSG [16]. In cofired operation the RACC GT exhaust exceeds this temperature and provides a significant increase in electric output compared to a dual pressure output. In terms of currently available technology, an HRSG

approach temperature of air/saturated steam of 15–25 °C pinch-point temperature difference is reasonable.

Overall, the RACC can be optimized based on the steam bottoming cycle. Many studies outline optimization techniques based on an exergy analysis and minimization of the various components of the Rankine cycle [17, 18]. This optimization can be performed once the baseline design for the RACC Brayton cycle is complete but has not been performed here.

Figure 2-4 shows a rendering of a potential plant layout using a NACC, with the HRSG, GT, generator, air ducts, two CTAHs, and an FHR reactor.

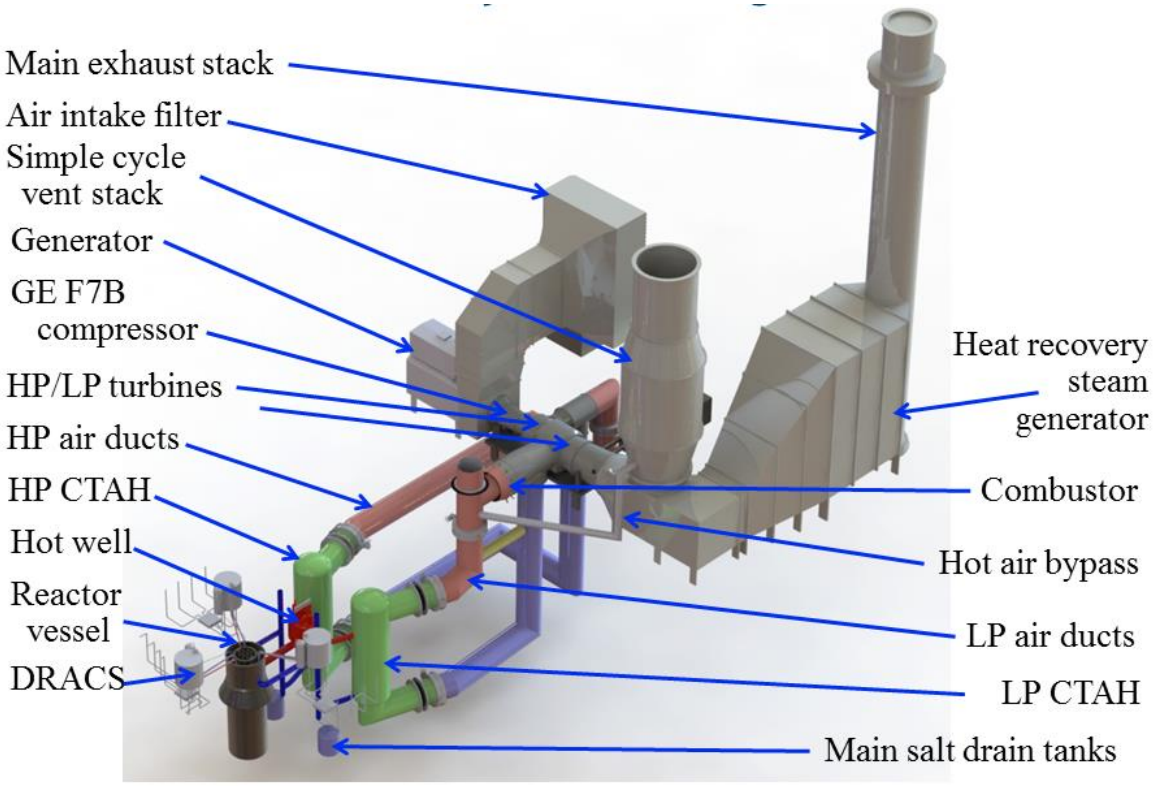

Figure 2-4. Mk1 FHR and NACC physical arrangement.

2.3.3 Base Load.

One major optimization goal for RACC power conversion is to maximize the net electrical power that can be produced from a given GT under low-carbon base-load operation. For a specific GT design, the use of reheat greatly increases the net base-load electrical power output. Because they operate at constant speed, large single-shaft GTs operate at a nearly constant air mass flow, while power output is varied by controlling the fuel injection rate, which in turn changes the turbine inlet temperature. Without reheat, the net thermal power that can be added with nuclear heating is limited by the difference between the compressor outlet temperature (Figure 2-2) and the maximum salt-to-air heater outlet temperature (perhaps 660 °C to 680 °C with current materials and 900 °C with advanced materials). If the air is then expanded partially,

additional thermal energy can be added using another salt-to-air heater operating at lower pressure.

Beyond greatly increasing the net nuclear or solar thermal power that can be added, reheat also increases the thermal efficiency of RACC base-load power conversion, counterbalanced partially by the increased circulating power to send lower-pressure air flow through the external ducting and reheat CTAH.

2.3.4 Cofiring.

Cofiring is attractive for RACC power conversion since the auto-ignition temperature of natural gas is 595 °C (lowest possible being 530 °C [14]), well below design CTAH air outlet temperatures of 660 °C to 680 °C. Cofiring capability is located after the final CTAH and before the final expansion stage inlet, as shown in Figure 2-3. The fuel injection system can use a similar design as for conventional external silo combustors, with the potential for simplification because the air enters above the auto-ignition temperature.

The major optimization goals for cofiring are to maximize peak power output, to maximize electricity revenues during periods of high electricity prices, and to enable rapid power ramping rates to increase the flexibility of NACC power conversion in providing spinning reserve and grid frequency control services. Issues associated with power ramping rates are studied in a subsequent chapter.

Two constraints limit the maximum peak power output of RACC power conversion: (a) the maximum turbine inlet temperature to the final expansion stage and (b) the maximum air temperature entering the HRSG.

By calculation one can determine the gas inlet temperature to each row of turbine blades and use those temperatures as the limit for cofiring operation in the RACC. If these temperatures, in combination with the optimized ER, yield an exhaust temperature above the typical 700 °C upper limit for conventional HRSGs then peak cofiring temperature will be limited by the HRSG instead (because RACC cofiring will have lower peak temperatures than conventional NGCC plants, this has positive implications for nitrous oxide emissions from RACC power conversion compared to conventional plants).

For modern GTs, optimal inlet temperatures into the HRSGs in terms of optimizing efficiency range between 580–640 °C (depending on the last stage ER) [17]. Maximum inlet temperatures for modern HRSGs are around 700 °C, where material constraints create limitations. Exceeding this limit is possible by adding a radiant section at the front end of the HRSG, which can push temperatures to 900–1000 °C, but adds a further complication to the design and is likely to not be compatible with effective RACC operation under base-load conditions.

Because the final expansion stage of RACC power conversion has a relatively low expansion ratio and under base-load operation has a relatively low turbine inlet temperature,

under base-load operation RACC power conversion has significantly lower HRSG air inlet temperatures than conventional NGCC plants. Under cofiring operation, boosting the HRSG inlet temperature to the 700 °C limit provides the highest bottoming cycle power and efficiency. Based on simulations presented later in this chapter, this requires cofiring with natural gas to achieve a TIT of 1070 °C for the GE 7FB and 1230 °C for the Alstom GT24.

An FHR NACC peaking unit with its steam bottoming cycle will be more efficient than simple air Brayton cycles. Initial estimates put the gas-to-electricity peaking efficiency of the FHR power conversion in the 54–70% range, where peaking efficiency is defined in equation 2-2 as the additional power generated from the additional heat input of natural gas. The top end CCGTs have plant efficiencies of 56–61%, but these efficiencies drop to 50–54% when run at intermediate loads so that peaking is possible.

$$\eta_{\text{peaking}} = \frac{P_{\text{peaking}} - P_{\text{baseload}}}{Q_{\text{peaking}} - Q_{\text{baseload}}}. \qquad 2\text{-}2.$$

The 7FB (GT24) baseline RACC power conversion design presented here is predicted to have a gas-to-electricity peaking efficiency of 66% (70%).

2.3.5 Coiled Tube Air Heaters (CTAHs):

NACC power conversion requires the use of air heaters that are external to the turbine casing. Relevant external heating experience exists with recuperator heat exchangers in smaller GT designs and with external silo combustors in small and large industrial GTs (such as the 115 MWe Alstom GT 11N2, Table 2-1). However, adapting this external-heating experience to large, stationary GTs with the relatively long air ducts required for NACC service introduces new issues.

A potential method to transfer heat from the salt coolant to air is using two CTAHs, consisting of a coiled bundle with a large number of small diameter tubes carrying salt in perpendicular flow. High-pressure air from the compressor diffuser is transferred to the CTAH through an internally insulated duct. The exterior pressure boundary of the duct is low carbon steel, providing leak tightness and structural strength, with a stainless steel hot duct liner to protect the insulation layer from the heated air flow. The duct operating temperatures are quite similar to those for HRSGs, where extensive experience exists, but the pressures are significantly higher. Thermal expansion of the internal liner is accommodated by having liner plates overlap each other, creating a sliding interface that minimizes pressure losses. The carbon steel ducts can use bellows to accommodate thermal expansion and also to simplify the gas flow path to and from the PCS. Elbows use miter joints with turning vanes, similar to those used in steam lines for low-pressure turbines. Appropriate high-temperature butterfly valves are also available for use to isolate CTAHs and to control bypass air flow around the CTAHs during start-up.

The basic design for the CTAHs was suggested originally by Gilli et al. [19], where coiled heat exchanger tubes form an annular bundle, with vertical manifold pipes outside the bundle providing flow to tubes that coil inward and downward, discharging their flow into vertical

manifold pipes inside the annulus where the coolant then flows downward and out of the CTAH vessel, as shown in Figure 2-5. Air enters the CTAH from the bottom, flows radially outward through the coiled tubes, and then exits upward and out the side of the CTAH vessel. Heat transfer coefficients on the coolant side, which has laminar flow inside the tubes, and on the air side, which has turbulent cross flow over the tubes, are comparable, so there are no benefits to adding surface enhancement to either side. The resulting simple tube geometry can use co-extruded tubes, so for NACC applications an alumina-forming alloy can be clad on the outside of the tubes to create a tritium diffusion barrier.

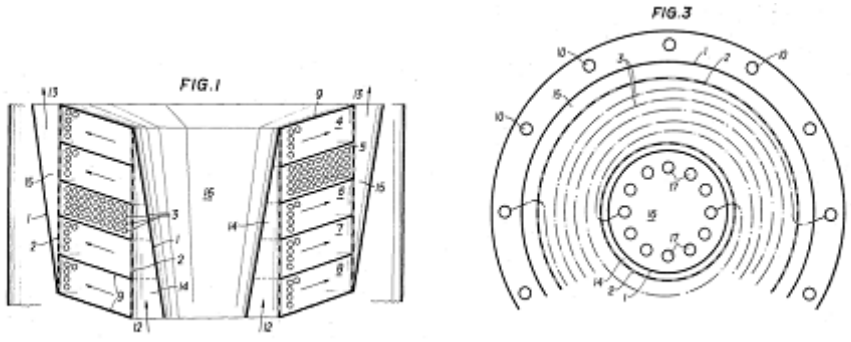

Figure 2-5. CTAH elevation and plan views, taken from Gilli et al. patent [19].

The physical arrangement and reactor design are simplified if both CTAHs have similar physical size and thermal loads so that each requires a similar salt flow rate. Table 2-2 provides key design parameters for CTAHs suitable for the reference RACC design presented here. Modeling results that study the tradeoffs described in this selection are given in a later section. Air temperature and flow parameters in Table 2-2 are slightly different from THERMOFLEX® model values in the "RACC Modeling and Optimization" section because they were calculated using a simplified spreadsheet model.

One more issue with the CTAHs is that the second, low-pressure air heater will dominate the circulating power losses. This is because for similar flow areas the air velocity depends inversely on the air density. Pressure loss depends upon the square of this velocity, and the circulating power depends upon the product of the pressure loss times the volumetric flow rate. So for similar flow areas, circulating power varies inversely with the cube of air density for a heater of fixed geometry. While in an optimized design the low-pressure CTAH ducting will have larger flow area, the low-pressure CTAH will still generate the dominant circulating power loss. The initial steps for a three dimensional performance model are outlined a later chapter.

Table 2-2. Key CTAH design parameters.

CTAH design summary results	HP CTAH	LP CTAH	
Thermal power	116.00	116.00	MW_t
Air mass flow	418.5	418.5	kg/s
Air pressure	18,760,000	499,000	Pa
Air heater inlet temp.	418.6	418.6	°C
Air heater outlet temp.	670.00	670.00	°C
Salt mass flow rate	480.2	480.2	kg/s
Salt volume flow rate	0.245	0.245	m^3/s
Salt inlet temp	700	700	°C
Salt outlet temp	600	600	°C
Heater ΔT_{LM}	84.14	84.14	°C
Air heat transfer coefficient	637.9	637.9	$W/m^2 \cdot °C$
Salt heat transfer coefficient	831.2	831.2	$W/m^2 \cdot °C$
Over heat transfer coefficient *U*	301.5	301.5	$W/m^2 \cdot °C$
Effectiveness	0.90	0.9	
Tube outside diameter	6.35	6.35	mm
Tube wall thickness	0.889	0.889	mm
Tube transverse (vertical) pitch *ST/D*	1.257	1.257	
Tube longitudinal (radial) pitch *ST/D*	1.400	1.400	
Diameter to middle of tube bank	1.96	1.96	m
Width of tube bank	0.64	0.64	m
Height of tube bank	5.92	5.92	m
Average cross-sectional area of bank	35.4	35.4	m^2
Total surface area	5041	5041	m^2
Total tube length	252,700	252,700	m
Number of loops per tube	3	3	
Tube length	18.47	18.47	m
Total number of tubes	13,680	13,680	
Salt velocity in tubes	1.09	1.09	m/s
Salt pressure drop	209,000	209,000	Pa
Tube bundle power density	5.15	5.15	MW_t/m^3
Total tube mass	31,750	31,750	kg/s
Air velocity between tubes	4.83	18.18	m/s
Air Reynolds number	7350	7350	
Air pressure drop across bundle	4100	11,500	Pa
Air circulating power across bundle	0.218	2.299	MW

2.4 Additional RACC Design Issues

The RACC will operate in a variety of conditions, including start-up, shutdown, power changes, steady state at part and full load, and peaking. Each mode of operation necessitates an understanding of phenomena that affect the performance and functionality of the turbomachinery. This chapter focuses on steady-state phenomena for nominal ambient conditions. Transient cases and off-nominal ambient conditions are studied in a subsequent chapter.

2.4.1 Turbine Blade and Nozzle Considerations.

Industrial GTs commonly use turbine blade and nozzle cooling to maintain material integrity at firing temperatures above approximately 980 °C (1800°F) [20]. This is accomplished by using specialized coatings on blades and nozzles and extracting air from various stages of the

compressor and feeding it to the turbine vanes, blades, and rotor; cooling the core of the blades; and, for the first stage, flowing out to create a small film of cooler air over the blade external surface. This feed is termed “chargeable air” [21]. It reduces mass flow and increases parasitic losses, while also requiring complex blades with high performance materials and coatings. The CTAH outlet temperatures are below 704 °C, where the onset of hot corrosion begins, a limiting factor in turbine blade performance [20]. During peaking operation blade temperatures for the low-pressure expansion stage will increase sufficiently that cooling is likely required for the first blade row in this last expansion stage. Under base-load operation the chargeable air flow to stator blades can be throttled or turned off to reduce parasitic losses.

In turbine design there are two types of turbines, namely impulse and reaction [20]. This refers to the split in pressure drop across the static nozzles and the rotating turbine blades. In impulse turbines, nearly the entire pressure drop takes place across the nozzle leading to high impact velocity on the blades and maximum power extraction per stage; however, impulse turbines are less efficient due to the high velocities creating drag losses. In reaction turbines, the pressure drop across the stage is split more uniformly between the nozzles and blades. The 50% reaction stage is the most efficient in power extraction.

In conventional GTs the first stage is usually an impulse turbine in order to take a large temperature drop across the stationary nozzle and reduce the gas temperature the rotating blades experience. Due to the relatively high pressure ratio across the stationary nozzle, this impulse stage also commonly operates in choked flow and, thus, limits and controls air flow through the GT. In RACC configuration, the low temperatures on the first expansion stage might not necessitate the use of an impulse type turbine. On the other hand, the second stage after the last CTAH and combustor might optimize to use an impulse turbine due to the high inlet temperature under cofired conditions, and the stationary nozzle for this stage may optimize to operate in choked flow.

2.4.2 Turbine Modification.

Implementing RACC power conversion with a commercial GT will require a certain amount of modification to render the two compatible. Turbine modification is primarily driven by the need to accommodate reheat. Moreover, one would want to modify the turbine section rather than the compressor because optimal compressor designs are challenging to develop as the compression stages operate with a reverse pressure gradient and a decelerating flow. Redesign or modification of the compressor, except to remove blade rows to reduce the compression ratio, would essentially nullify the “off-the-shelf” nature of the GT. To accommodate the air heaters, inlet/outlet diffusers, similar in concept to those used in large GTs with external combustors, as with the Alstom GT11N2 shown in Figure 2-6, can be used. The combustors for the NACC can be either of the “straight-flow” or silo variety, rather than reverse flow, to reduce pressure drops. Flame out is of reduced concern because the air temperature under base-load operation exceeds the auto-ignition temperature.

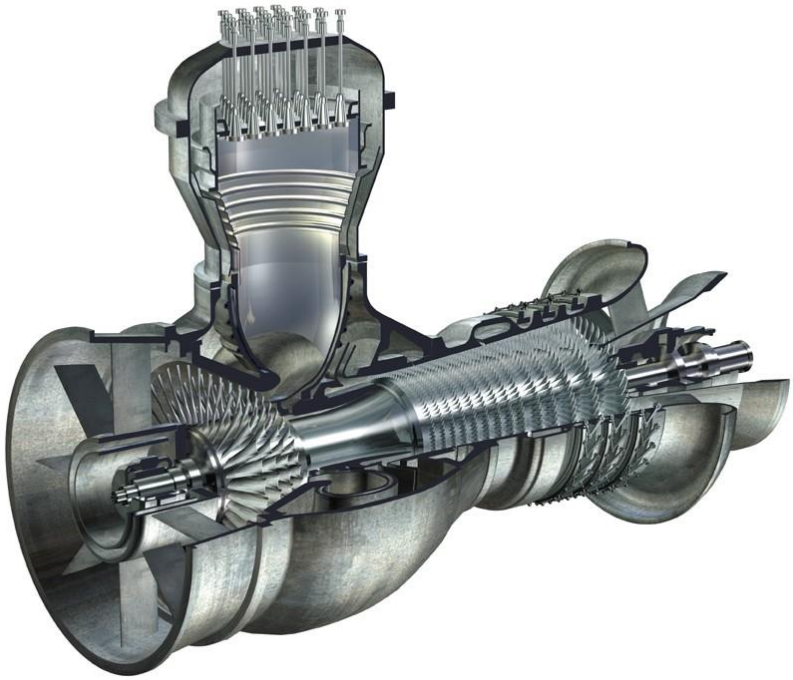

Figure 2-6. 113-MWe Alstom GT11N2 gas turbine with an external silo combustor [22].

The turbine can be modified in one of two ways. One option is to leave the existing number of blade rows and extend the shaft between them in the desired configuration. A second option is to add or remove blade rows to better optimize the pressure ratio of each expansion stage. An additional bearing can be added for flexural support, yielding a three bearing machine, similar to the GE 7EA. Overall, a substantially modified turbine casing will be needed. For the RACC baseline design, a single row of blades cannot provide sufficient pressure drop for the RACC expansion stage, so each stage needs at least two rows, for a total of at least four rows of blades.

2.4.3 RACC Turbine Orientation.

In Figure 2-4 the MK1 FHR and NACC physical are presented. The power train, including the gas turbine, is positioned parallel to the reactor containment structure boundary. For FHR and MSR applications, the proposed positioning allows the reactor containment structure to be easily demarcated from the nonnuclear equipment and to also reduce air duct lengths and resulting air circulating power. This arrangement does, however, raise the subject of turbine blade failure impact of the reactor containment.

Compressor and turbine blade failures can occur in gas turbines due to hot corrosion, cyclic and thermal fatigue, compressor surge, foreign object damage, and internal fires/explosions among other causes [23]. Generally, these events cause extensive internal damage to the turbine and its casing. In case of catastrophic failure or blade release, air flow stops rapidly and carryover of shrapnel is relatively small. The fact that blades are not ejected through the turbine casing is different than that for the much larger blades in low-pressure steam turbines. This allows the gas turbine to be oriented parallel to the reactor containment structure,

whereas for modern reactor designs steam turbines are normally oriented perpendicular. Both the CTAHs and their supply ducts are designed to minimize the risk of damage to tubes and salt leakage in the event of blade failure. The air supply duct system is designed to slow down and stop blade shrapnel. The miter-bend turning elbows and turning vanes act as filters to stop shrapnel from reaching the CTAHs.

2.5 RACC Modeling and Optimization

In order to model the RACC, the commercial code THERMOFLEX® was used. THERMOFLEX® is a fully flexible program for heat balance modeling and engineering with a graphical user interface [24]. The GT used as a baseline design case was the GE 7FB. A second design for high-temperature, advanced material operation with the Alstom GT24 is also presented. Several key assumptions are made in these simulations. Detailed performance maps for the GE 7FB were not available, but the THERMOFLEX® code includes internal models for specific GTs, such as the GE 7FB, and values for efficiency, PR, and mass flow derived from these THERMOFLEX® models were used in these simulations. Second, only first order estimates for piping losses and losses at duct elbow turning vanes, joints, valves, and other external air ducting are included. Due to its importance to net power production and cycle efficiency, a parametric study for the effect of low-pressure CTAH loop pressure loss on cycle efficiency was also performed. Third, all HRSG components are simulated using a one-dimensional thermodynamic model, without any detailed thermal hydraulics or heat exchanger layout. Instead, nominal pressure drops and heat losses are added across the HRSG. Finally, there is no dynamic simulation and, therefore, all results are steady state. Issues for transients are discussed in a subsequent chapter.

For baseline ambient conditions, the ISO 3977 standard was used (T_{amb} = 15 °C, p_{atm} = 1 atm, h = 0 m, RH = 60%), which is the standard environmental design point used in evaluating most GT systems [25]. This standard is divided into nine subsections and covers procurement, design requirements, installation, and reliability. Nearly equivalent performance and efficiency can also be obtained at higher ambient temperatures using compressor inlet water fogging.

The THERMOFLEX® model includes the primary salt loop, with the nuclear reactor core modeled as a dummy heat adder. The Brayton cycle is modeled as a compressor with no intercooling and the turbine has a single reheat stage (two expansion stages). The Brayton cycle exhaust goes into a triple pressure reheat HRSG before exhausting to the atmosphere. The Rankine cycle is a closed loop system and dumps heat to atmosphere through a wet cooling tower. The cofiring is modeled as a flow of natural gas into a combustor that raises the air temperature to 1070 °C (1230 °C) before the last expansion stage. A compressor efficiency of 88.7% and turbine efficiency of 91.5% were derived from the THERMOFLEX® GE 7FB GT model and used here for both the GE and Alstom GTs. The CTAH pressure losses were estimated using approximate assumptions for losses in the individual components, and a detailed calculation for pressure loss in the tube bundle, as discussed further below. An inlet fogger is added at the

compressor inlet for use when ambient air temperatures exceed 15 °C, operating at 95% effectiveness and with a small pressure drop. A maximum of 0.5% overspray of flow is injected [26]. Air mass flow is reduced by 5%, as opposed to a conventional 10% of the GE 7FB, to account for reduced blade cooling and chargeable air losses with the lower RACC TIT. Figure 2-7 and Figure 2-8 show schematics of the THERMOFLEX® model in base-load and peaking operation.

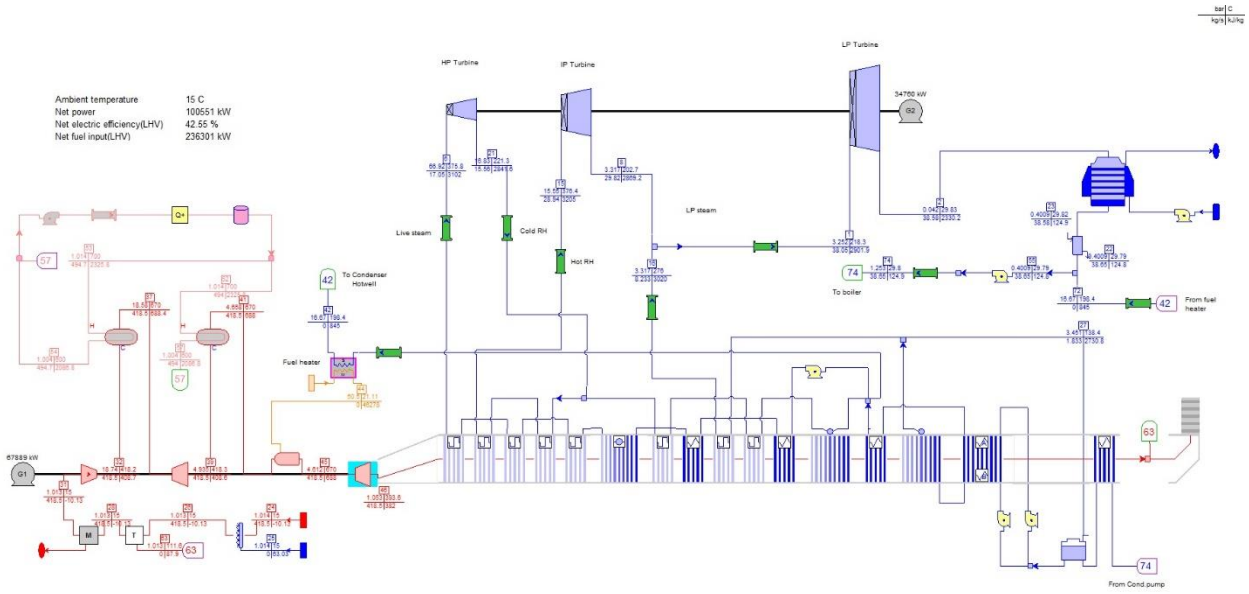

Figure 2-7. Base-load 100-MWe THERMOFLEX® power conversion system flow diagram.

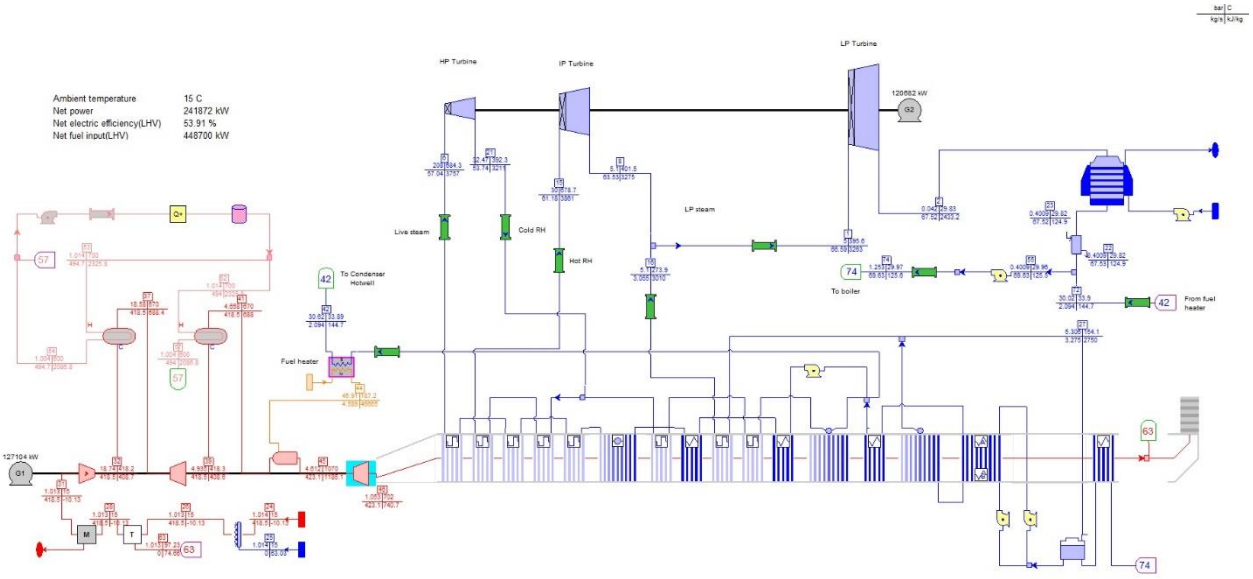

Figure 2-8. Peaking 241-MWe THERMOFLEX® power conversion system flow diagram.

2.5.1 Brayton Cycle Optimization.

Table 2-3 lists the GE 7FB and Alstom GT 24 design parameters for operation with NG firing. The GE 7FB compressor and turbine efficiencies were extracted from the THERMOFLEX® internal model for this GT. The Alstom values are assumed to be equal.

Table 2-3. GE 7FB and Alstom GT24 parameters for conventional natural gas firing.

GT	7FB	GT24	
PR	18.5	35.4	
Mass flow	440.4	494	kg/s
η_c	88.7	88.7	%
η_t	91.5	91.5	%
TIT	1371	–	°C
TET	626	597	°C
Simple cycle power	183.7	218.1	MW
Price	48.2	57.9	$MM

It is also necessary to estimate the pressure losses across the two CTAHs and ducting that routes the air from the GT to the CTAHs. Table 2-4 shows the expected losses through the two CTAHs and their associated ducting for the GE 7FB based RACC design.

Table 2-4. Ducting air pressure loss estimation for GE 7FB baseline design.

	HP CTAH	LP CTAH	
m_dot	418.5	418.5	kg/s
$A_{compexit}$	0.246	0.246	m^2
D_{duct}	1.50	2.00	m
A_{duct}	1.770	3.140	m^2
$V_{compexit}$	183.9	530.1	m/s
$V_{duct,\ C}$	25.6	41.5	m/s
$V_{duct,\ H}$	35.1	53.4	m/s
K_L	0.2	0.2	
Miter bends hot	3	2	
Miter bends cold	4	3	
ρ_H	6.76	1.89	kg/m^3
ρ_c	9.26	2.44	kg/m^3
L_H	30	35	m
L_c	38.5	43.5	m
f	0.015	0.015	
$\Delta p_{H,pipe}$	1245	708	Pa
$\Delta p_{C,pipe}$	1166	683	Pa
$\Delta p_{H,elbow}$	2490	1079	Pa
$\Delta p_{C,elbow}$	2423	1257	Pa
Δp_{CTAH}	9000	24,000	Pa
Δp_{Total}	16,300	27,700	Pa

By using relatively large diameter ducts and low air velocities, the pressure losses through the ducting and CTAHs are predicted to be moderate, approximately 16–28 kPa through each leg, and therefore, the total system efficiency penalty is not large. Because the net power production and cycle efficiency are particularly sensitive to the pressure loss in the LP-CTAH, a sensitivity study was also performed for the effects of this pressure loss.

An important design consideration for the RACC is the relative sizing of the two CTAHs, as mentioned in the earlier section, “Two Baseline RACC Cycles.” Having similar size CTAHs will

reduce manufacturing and maintenance complications, as well as simplify plant layout. To assess the best option in terms of relative CTAH sizes, the baseline performance characteristics of the GE 7FB at ISO 3977 conditions were used. The compressor PR was held constant while varying the first ER and having the second ER automatically adjust by setting it to "rubber" mode in THERMOFLEX®. Results are given in Table 2-5 and Figure 2-9, Figure 2-10, Figure 2-11, and Figure 2-12.

Table 2-5. Expansion ratio selection results.

INPUT									
ER_1		2	4	6	8	2	4	6	8
TIT	°C	670	670	670	670	1070	1070	1070	1070
OUTPUT									
η_{th}	%	40.59	42.56	42.11	41.36	54.34	53.75	50.46	41.32
P_{net}	kW	74,899	102,498	113,576	119,315	215,695	243,642	243,253	206,992
$P_{Brayton}$	kW	60,855	67,715	62,427	53,930	141,802	124,670	103,283	82,408
P_{Steam}	kW	15,563	36,944	53,819	68,557	78,437	125,052	146,820	129,759
Net fuel input(*LHV*)	kW	184,526	240,858	269,711	288,512	396,946	453,256	482,101	500,889
Q_{FHR}	kW	184,526	240,858	269,711	288,512	184,526	240,858	269,711	288,512
η_{cofire}	%					66.28	66.45	61.06	41.28
PR		18.5	18.5	18.5	18.5	18.5	18.5	18.5	18.5
$T_{comp,out}$	°C	418.2	418.2	418.2	418.2	418.2	418.2	418.2	418.2
ER_1		2	4	6	8	2	4	6	8
$T_{turb1,out}$	°C	530.3	408.3	344.5	302.3	530.3	408.3	344.5	302.3
ER_2		8.477	4.108	2.652	1.924	8.477	4.108	2.652	1.928
$T_{exhaust}$	°C	294.2	404	478.7	537.7	567	716	816.1	894.1
$Q_{SAHX,1}$	kW	117,057	117,057	117,057	117,057	117,057	117,057	117,057	117,057
$Q_{SAHX,2}$	kW	65,643	121,418	149,985	168,601	65,644	121,418	149,985	168,601
$Q_{SAHX,1}/QSAHX,2$		1.78	0.96	0.78	0.69	1.78	0.96	0.78	0.69
$ER1/ER_2$		0.24	0.97	2.26	4.16	0.24	0.97	2.26	4.15

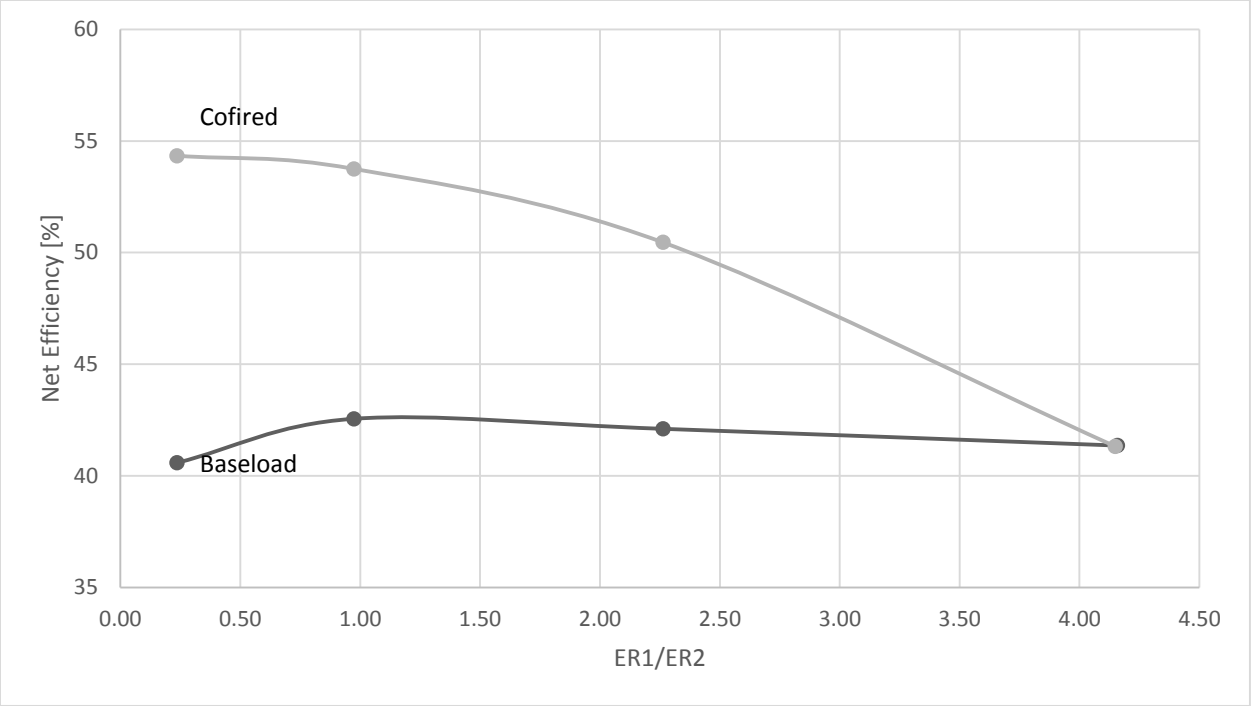

Figure 2-9. Net efficiency vs. ER for GE 7FB baseline.

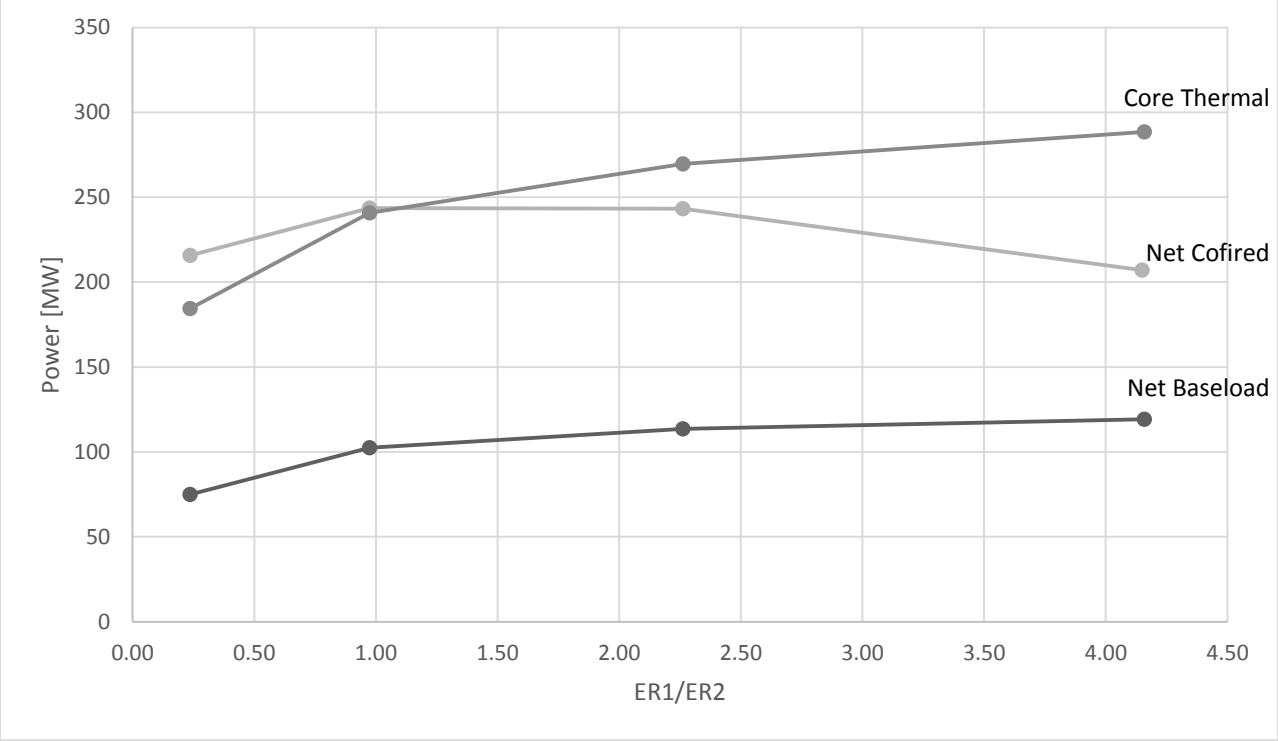

Figure 2-10. Power vs. ER for GE 7FB baseline.

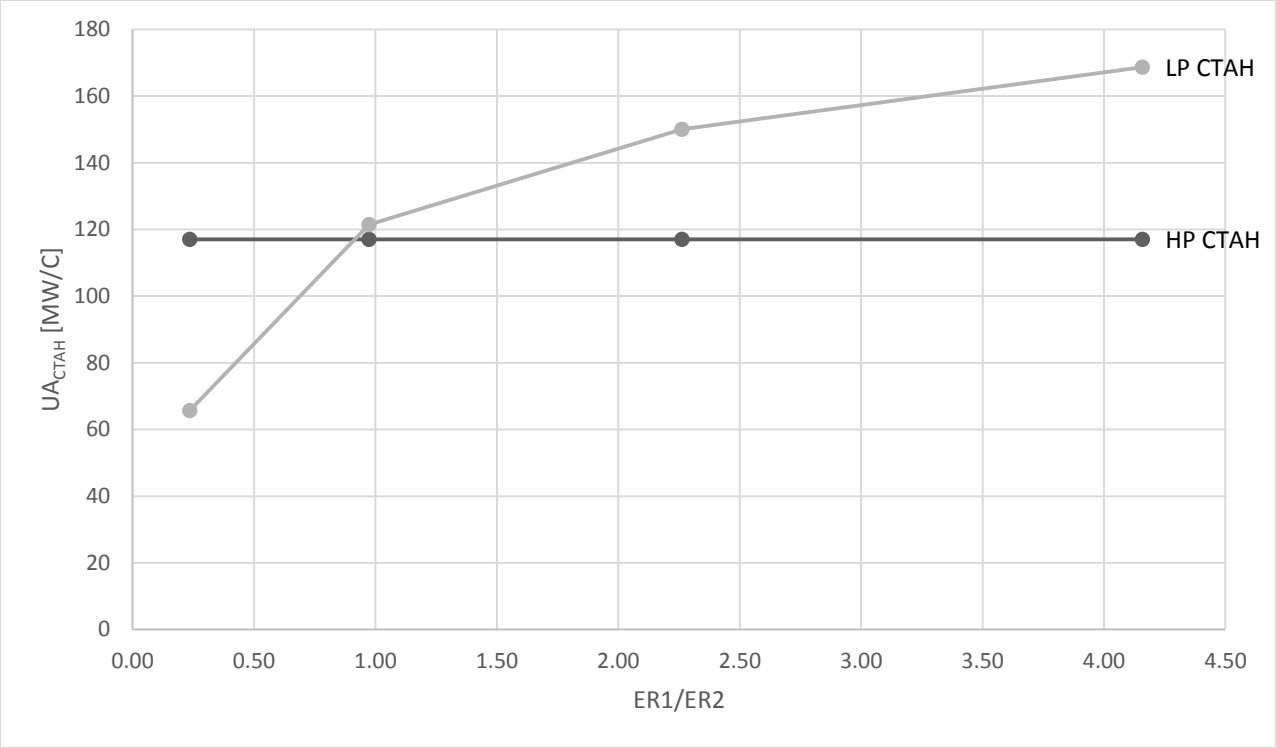

Figure 2-11. CTAH Size vs. ER for GE 7FB baseline.

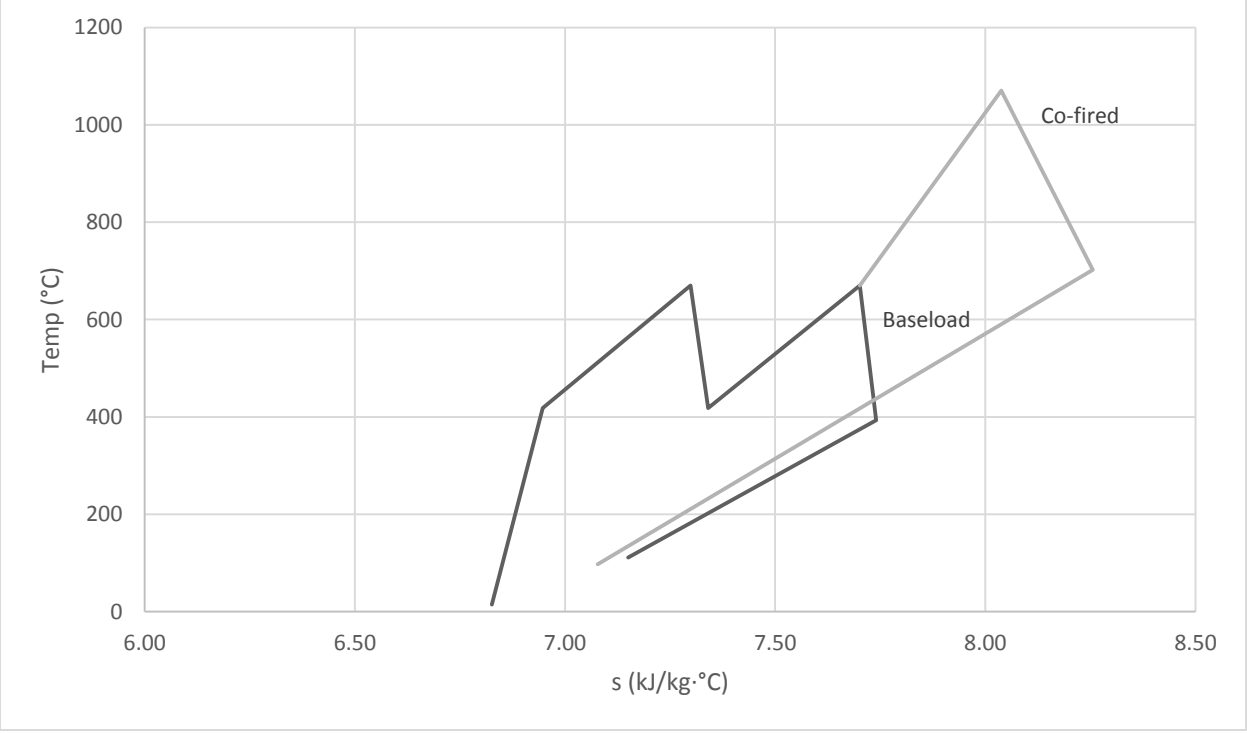

Figure 2-12. NACC T-s diagram for GE 7FB baseline.

Reviewing the figures, a peak in efficiency is evident when the CTAH sizes are similar. Increasing the second CTAH size allows more thermal and electric power to be extracted from

the FHR but less efficiently. Moreover, cofiring efficiency suffers substantially because the smaller second stage expansion ratio cannot extract enough power from the natural-gas-heated fluid stream. Therefore, the optimal ER ratio between the two expansion stages is the one that gives approximately the same CTAH size between the two air heaters.

The parameters shown in Table 2-3 and Table 2-4 were selected for the Brayton cycle, except for the reduced air mass flow to account for the reduced blade cooling requirements. The overall optimized RACC for the GE 7FB design has a net electric efficiency of 42.5%, a net power output of 100 MWe, and an FHR core thermal requirement of 236 MWt. Peaking output is 241.8 MW, with a peaking efficiency of 66.4%, as defined by equation 2-2. Finally, Figure 2-12 provides a T-s diagram for the open-air Brayton cycle.

A sensitivity study was also performed to assess the effect of the uncertainty of the pressure losses through the air ducts. The pressure drop through the LP ducting and CTAH were varied from the calculated value of 27,700 Pa up to 100,000 Pa for both base-load and cofired operation. The results are displayed in Figure 2-13. LP pressure losses versus net power are shown in Figure 2-14. As is observed, power and efficiency variations are not substantial in either case even in the high pressure loss scenario, with a decrease of no more than 3% in efficiency for base load (1.5% for cofired net) and 6 MW in electric output. The cofiring efficiency as defined by equation 2-2 does not vary with LP duct losses and remains high because the power extraction happens after the LP ducts. The higher pressure losses in the LP ducting are also counteracted by a higher turbine exhaust temperature, allowing for a partial power recovery in the steam bottoming cycle.

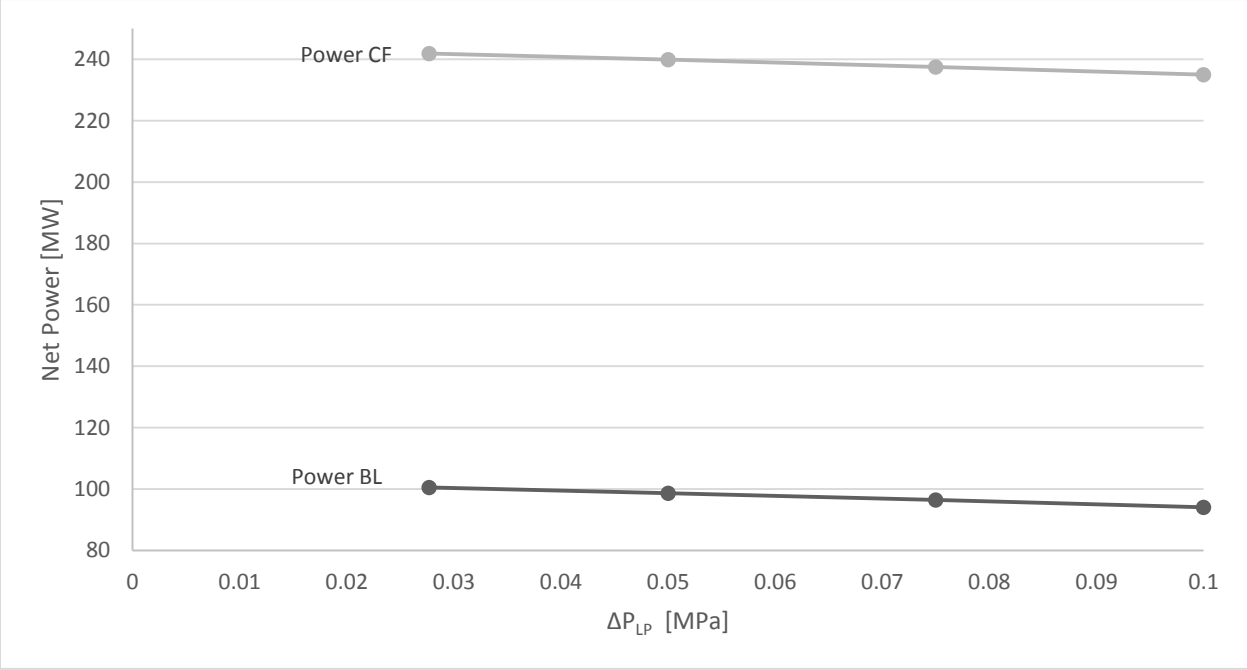

Figure 2-13. LP pressure losses vs. net power.

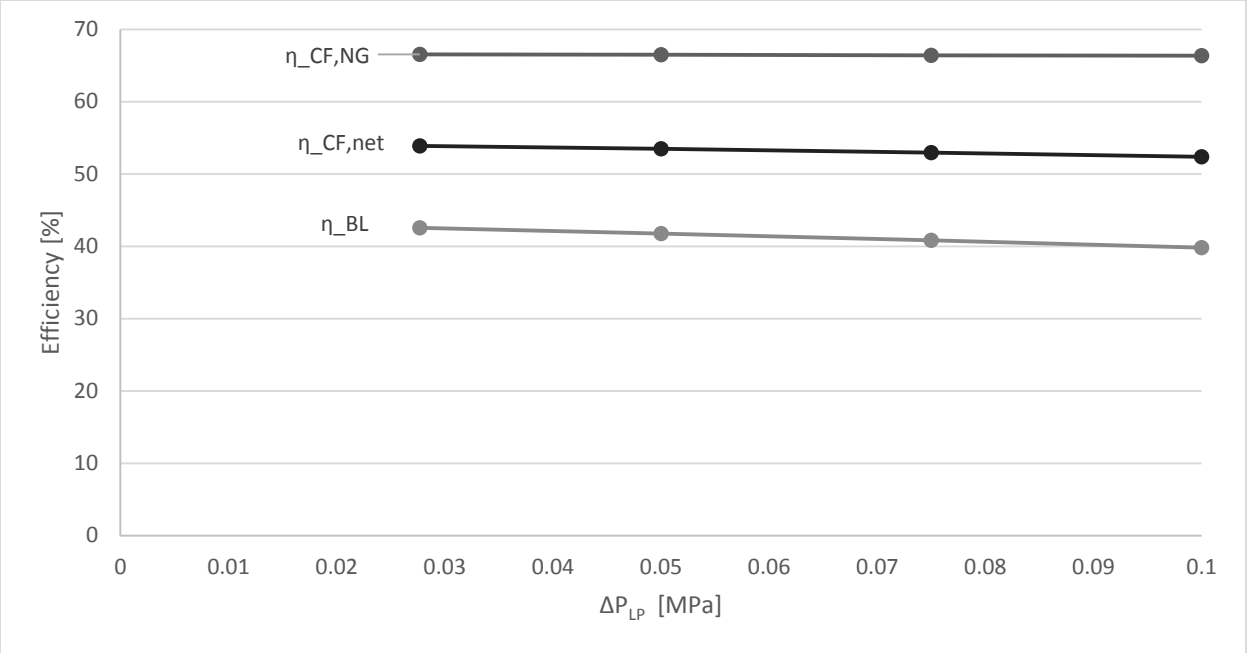

Figure 2-14. LP pressure losses vs. net efficiency.

2.5.2 Rankine Cycle Optimization.

The steam cycle pressures were optimized iteratively for best efficiency in base-load and cofiring applications by keeping the HRSG inlet temperature and the intermediate pressure fixed and varying the high pressure and then keeping the best value for high pressure fixed while varying the intermediate pressure. A caveat in the optimization of the steam cycle is the fact that the large increase in HRSG inlet temperature due to cofiring causes a substantial increase in the predicted pressure and mass flow in the steam turbine (ST) if modeled in sliding pressure mode, in turn causing an incompatibility between calculations for the two operating modes. A way to overcome this in the THERMOFLEX® model is to size the ST and HRSG for cofiring operation and then use a control valve on the ST to keep to the optimized base-load pressure in off-design mode by setting a "low-flow set point pressure." Table 2-6 provides the selected pressures for the steam cycles for the GE 7FB and Alstom GT24 designs.

Table 2-6. Steam cycle pressure selection.

	GE 7FB		Alstom GT24		
	Base-load	**Cofired**	**Base-load**	**Cofired**	
High pressure	6.0	20.8	1.13	20.65	MPa
Intermediate pressure	1.5	3.0	1.8	2.4	MPa
Low pressure	0.25	0.5	0.22	0.25	MPa

2.5.3 Alstom GT24.

A similar configuration and optimization study was performed for the Alstom GT24 as was described above for the GE 7FB. The TIT was increased by 200 °C, from 670 °C to 870 °C. This

resulted in a log-mean temperature difference across the two CTAHs of 100.9 °C, compared to 84.2 °C for the GE 7FB CTAHs. Assuming the same effectiveness and overall heat transfer coefficient, the CTAHs for the advanced material high-temperature configuration need to be approximately 20% larger due to the larger thermal power. Additionally, to reach the targeted 700 °C HRSG inlet temperature, a cofired TIT of 1230 °C is necessary. The resulting power under base-load operation is 178 MW with a core thermal power of 348 MW, giving a base-load efficiency of 51%, and a cofiring output of 324.6 MW with a cofiring efficiency (gas-to-electricity) of 70%.

2.6 Discussion

The combination of a FHR, MSR, or CSP heat source with RACC power conversion could enable the production of both base-load electrical power as well as ancillary services, such as peaking, load following, spinning reserve, and black start capability, previously not possible by commercial nuclear reactors or CSP facilities. This is possible due to the high-temperature, low-pressure heat delivered by these sources. Table 2-7 summarizes key design parameters for the proposed RACC configurations.

Table 2-7. Key RACC design parameters.

	GE 7FB	**Alstom GT24**
Nominal ambient temperature	15 °C	15 °C
Elevation	Sea level	Sea level
Compression ratio	18.52	35.4
Compressor outlet pressure	1,858,000 Pa	3,587,000 Pa
Compressor outlet temperature	418.7 °C	560.4 °C
Compressor outlet mass flow(total flow is 440.4 kg/s; conventional 7FB design uses balance for turbine blade cooling)	418.5 kg/sec	469.3 kg/sec
CTAH outlet temperature	670 °C	870 °C
Base-load net electrical power output	100 MW_e	178 MW_e
Base-load thermal efficiency	42.5%	51.2%
Cofiring turbine inlet temperature	1065 °C	1230 °C
Cofiring net electrical power output	241.8 MW_e	324.6 MW_e
Cofiring efficiency (gas-to-peak-power)	66.4%	70%

The earlier modular SmAHTR FHR design considered both steam and supercritical CO2 as power conversion fluids, which are predicted to give thermal efficiencies of approximately 45% and 48%, respectively [4]. This is greater than the 42.5% base-load efficiency predicted for the GE 7FB based power conversion system that operates at similar temperature, but the capability of the NACC system to also generate large amounts of peak power using cofiring generates additional revenues that would greatly exceed those from these larger base-load thermal efficiencies.

This chapter surveyed currently available commercial GTs, examined several parameters that are important in coupling a commercial GT to non-fossil, external heat sources, and

suggested a possible set up to achieve it. Important operating scenarios, such as salt freeze, condensation of ducting, turbine modification, and ambient conditions are reviewed in the following chapter.

3 Nuclear Air-Brayton Combined Cycle Power Conversion Off-Nominal and Transient Performance

This chapter is an adapted version of the archival journal article "Reheat Air-Brayton Combined Cycle Power Conversion Off-Nominal and Transient Performance" by Andreades et al. [27]. *Full copyright permission for use in this dissertation has been granted by the American Society of Mechanical Engineers (ASME).*

3.1 Introduction

The ability of molten-salt coolants to deliver heat in the temperature range between 600 °C and 700 °C with currently available materials, and higher temperatures with advanced materials, opens the possibility of adapting modern air Brayton combined cycle technology to use heat from nuclear and concentrating solar power sources. Research at U.C. Berkeley, sponsored by the U.S. Department of Energy, has identified approaches to achieve net thermal efficiency above 40% with heat provided by fluoride-salt-cooled, high temperature reactors (FHRs), molten salt reactors (MSRs), and high-temperature concentrating solar power (CSP) heat sources. This nuclear air combined cycle (NACC), described in the previous chapter more generally as RACC, uses external heating of the air, with a single stage or two stages of reheat. The injection of natural gas or other fuels after the last reheat stage can be used to boost power output, to provide peaking power and to provide other grid reliability and support services such as frequency regulation.

Open air Brayton power cycles have substantially greater sensitivity to external ambient conditions (air temperature, barometric pressure, and humidity) than typical closed steam and gas power cycles. Brayton power cycles also typically have more flexible transient response but suffer from significant efficiency penalties when run at part load. Procedures for start-up and shutdown also differ from closed cycles.

While the RACC power conversion system (PCS) based upon molten-salt external heating appears to have attractive characteristics, it is important to understand its operation under off-nominal ambient conditions as well as under start-up, shut down, and operational transients including ramp up and ramp down. This chapter discusses these topics. RACC power conversion must also be analyzed for accidents, including consideration of natural gas safety. All of these off-nominal conditions need to be managed safely and effectively. During RACC transients, phenomena such as heat soakage, blade tip clearance changes, control system delays and lags, and heat transfer within multistage components need to be considered [28].

Extensive experience exists for these questions for conventional natural gas combined cycle (NGCC) power plants. Beyond operational industry experience, several publications and books outline performance, monitoring, and diagnostics of gas turbines (GTs) under transient conditions. GT performance under off-nominal ambient conditions has been described in detail in textbooks and handbooks [28, 29]. Mitigating techniques and performance enhancement under off-nominal ambient conditions have been outlined in other review articles [15, 30] while

performance and mechanical transient analysis techniques for GT problem troubleshooting are also well understood [31]. Compressor operation, maintenance, surge, and diagnosis are additional topics that have been studied extensively [32, 33]. All of this experience provides a strong foundation for the development of RACC power conversion.

This chapter focuses on issues unique to RACC power conversion coupled to nuclear and solar heat sources. The RACC configuration used as the reference for this study is compatible with current material temperature constraints. This reference design draws in ambient air, compresses it, routes it through high pressure external ducting to a coiled tube air heater (CTAH) in which air is heated to 670 °C by a molten-salt heat source and is then routed back to the turbine and expanded down to compressor discharge temperature. This expanded air is then routed to and reheated to 670 °C in a second similar-sized low-pressure CTAH and then re-expanded through a second turbine stage. An option to inject and burn natural gas after the last reheat stage and increase the turbine inlet temperature (TIT) allows for a boost and quick ramp in power. Finally, turbine exhaust is routed to a heat recovery steam generator (HRSG) in which additional power is extracted from a steam bottoming cycle; therefore, waste of available energy is minimized. The option of cofiring air with natural gas (NG) can allow the RACC to provide ancillary services to the grid, including spinning reserves, black start services, peaking power, etc.

In order to model the performance of the RACC in off-nominal conditions, a flexible thermodynamic modeling program with a graphical user interface named THERMOFLEX® was used [24]. THERMOFLEX® does not have transient performance analysis, so quasi-steady results are predicted that are relevant to understanding operation under off-nominal conditions.

3.2 Baseline Design Selection

The General Electric (GE) 7FB gas turbine was used as the reference RACC technology. Similar gas turbines are available from multiple vendors, including Alstom, Mitsubishi, and Siemens. The GE 7FB has a higher pressure ratio (PR) compared to its sister 7FA.05 machine, which gives it a higher compressor discharge temperature, reducing the thermal power required from the CTAH. It also allows for a more efficient power extraction due to its higher PR. The modifications made to the base GE 7FB to accommodate external heating included a heavily modified casing, an extended shaft between expansion stages to allow for reheat, removal of can-annular combustors and replacement with a silo type combustor on the low pressure extraction stage, use of four rows of turbine blades divided into two expansion stages of two rows each, modified and reduced blade cooling patterns, and a reduced firing temperature (limited by HRSG inlet temperature). The turbine exhaust is routed to an HRSG with a triple pressure steam bottoming cycle. The above modifications are discussed in detail in the previous chapter. The design-point (International Organization of Standards (ISO) conditions) performance characteristics of the RACC are shown in Table 3-1.

Table 3-1. Key RACC design parameters based on the GE 7FB.

Nominal ambient temperature	15 °C
Elevation	Sea level
Compression ratio	18.52
Compressor outlet pressure	1,858,000 Pa
Compressor outlet temperature	418.7 °C
Compressor outlet mass flow (total flow is 440.4 kg/s; conventional 7FB design uses the balance for turbine blade cooling)	418.5 kg/s
CTAH outlet temperature	670 °C
Baseload thermal power output	236 MWth
Baseload net electrical power output	100 MW_e
Baseload thermal efficiency	42.5%
Cofiring turbine inlet temperature	1065 °C
Cofiring net electrical power output	241.8 MW_e
Cofiring efficiency (gas-to-peak-power)[a]	66.4%
a. Cofiring efficiency is defined as the additional net power output over baseload divided by the additional heat input of the fossil fuel/natural gas. It is a measure of conversion efficiency of natural gas to electricity calculated on a lower heating value basis.	

3.3 Off Nominal Ambient Conditions

Open air Brayton cycles are more sensitive to ambient air conditions than closed Rankine and Brayton cycles. Temperature, barometric pressure/altitude, and relative humidity all affect the efficiency and power output of the power cycle. The parameters with the most dramatic effects are ambient temperature and altitude. On the other hand, the PCS is not too sensitive to relative humidity and its performance varies by approximately 1% between 0% and 100% relative humidity [34].

For the RACC model, best estimates of the duct losses and CTAH parameters were used. Initially, the point design involved optimization of the expansion ratios (ER) of the two expansion stages and of the steam cycle pressures under ISO conditions. The resulting ISO performance figures are outlined in Table 3-1.

The off-nominal conditions of interest for the RACC are varying ambient conditions, as well as decoupling the GT and ST cycles by partially venting turbine exhaust air to atmosphere in order to gauge the initial response to increased and decreased load demand. Increased altitude has a similar but relatively modest effect on cycle performance as increased ambient temperature but can be managed using a relatively small power derating or adjusting downward the threshold temperature for inlet fogging. A detailed study of relative humidity effects is omitted in this chapter, as the variations in cycle performance are very small compared to temperature and altitude.

3.3.1 Off-Nominal Ambient Temperature.

When operating a nuclear reactor at its maximum licensed power to produce base-load power, maintaining a constant core thermal power across a range of outside ambient conditions is important for economically optimal performance. Changing the ambient air temperature from the nominal design value has two significant effects: varying both the compressor outlet

temperature and density. Density changes are important because for electricity generation stationary, single-shaft GTs are usually operated at constant speed and, thus, are constant volume-flow machines. Varying density due to changing ambient temperature changes the machine's mass flow rate and, in turn, the machine's power output. At higher ambient temperatures, air is less dense; hence, there is less air passing through the air heaters, reducing the amount of power extracted from the reactor core. Under the opposite condition, when ambient temperature decreases, the thermal input, power output, and thermal efficiency increase.

The second effect of varying ambient temperature is on the compressor outlet temperature. A higher ambient temperature results in a higher compressor outlet temperature, consequently, reducing the temperature rise and heat input necessary to achieve the desired CTAH outlet temperature. Reduced ambient temperature has the opposite effect.

These effects of ambient temperature are important for nuclear reactors and CSP systems because the low cost of nuclear and solar fuel makes it desirable to maintain power output at the maximum allowable value under variable ambient temperature conditions.

Technical methods have been developed and used commercially to manage high and low ambient temperatures in GTs, which can be adapted to RACC use. For higher ambient temperatures, one can use compressor inlet air cooling, a widely accepted practice for natural gas GTs. Several technologies exist, including air fogging (wet compression), inlet air chilling, and evaporative cooling [15]. Air fogging and evaporative cooling reduce the inlet air temperature by extracting heat from it to evaporate water. They also increase the fluid density and, therefore, compensate for the density reduction caused by high ambient air temperature. Air fogging uses more compact equipment and has a negligible pressure drop on the inlet stream; however, water quality requirements are higher than evaporative cooling, necessitating use of demineralized water. Neither technology has a pronounced effect on long term material degradation and both are easily installed [30].

At colder ambient temperatures, warm air from the compressor, turbine, or HRSG exhaust can be mixed with the inlet air to increase its temperature and reduce its density. In commercial GTs, compressor discharge air is commonly bled back to the inlet to heat up cold inlet air to prevent icing. Additionally, for RACC power conversion warm HRSG exhaust air can be recycled back to the inlet during base-load operation to increase compressor inlet air temperature. During cofired operation, this approach may need to be avoided to prevent flue gas contaminants causing corrosion in the compressor. If required, PCS mass flow can also be reduced to best match reactor output by using the variable inlet guide vanes on the compressor.

The baseline RACC design considered here selects 15 °C, sea-level elevation, and 60% relative humidity as the nominal ambient operating conditions. These are standard ISO 3997 conditions widely used by the gas and oil industry to report performance and are, therefore, similarly used for RACC performance reporting. Moreover, a 15 °C ambient design temperature

is a reasonable threshold to select between low ambient temperatures, where there is a risk of freezing of the primary salt in the CTAHs and corrosion, as well as stack condensation, and higher ambient temperatures, where the reduced power output increases the construction cost per unit power output without providing any significant performance benefits.

The first step to performing off-nominal modeling of the RACC is to understand the performance variation of the unmodified GT itself. To this end, operating characteristics of a GE 7FB model included in THERMOFLEX® were back-calculated at various ambient conditions. Table 3-2 presents results from these calculations.

Table 3-2. GE 7FB operating characteristics at varying ambient conditions.

T (°C)	PR	$m_{comp,in}$ (kg/s)	$m_{charg,air}$ (kg/s)	m_{RACC} (kg/s)	$T_{comp,out}$ (°C)
0	19.18	457.1	47.7	434.2	409.3
5	18.99	452.1	47.2	429.5	412.5
10	18.77	446.2	46.6	423.9	415.9
15	18.52	440.4	46.0	418.4	418.7
20	18.08	429.8	44.9	408.3	420.7
25	17.64	419.3	43.8	398.4	422.5
30	17.19	408.5	42.6	388.2	425.1
35	16.74	397.6	41.5	377.8	427.8
40	16.24	386.1	40.3	366.9	429.4

The column m_{RACC} denotes the reduced mass flow of the RACC to account for chargeable air losses. Rather than using the full 10% chargeable air, only 5% was used to account for the reduced nozzle and blade cooling requirements for RACC service, where the TIT is lower because temperature limits are established by the HRSG and where the chargeable air can be withdrawn from the compressor at a lower pressure and temperature because the cooled blades are in the second, low-pressure expansion stage of the turbine. The effects of varying ambient conditions were studied on a RACC cycle without mitigating measures and compared with an RACC with (1) wet compression for warm ambient temperature conditions, (2) stack discharge recirculation in baseload under cold ambient conditions, and (3) compressor bleed heat in cofired mode for cold ambient conditions. Figure 3-1 through Figure 3-3 illustrate selected cases. Figure 3-1 shows the baseline base-load RACC under nominal 15 °C ambient ISO conditions with no varying ambient mitigation equipment. Figure 3-2 shows the 0 °C low ambient case with stack recycle, and Figure 3-3 shows the 40 °C high ambient case with inlet air fogging. In these cases, the flow rate of stack recycle and the flow rate for fogging, respectively, are adjusted to maintain a constant thermal power load on the molten salt heat source. For the ISO nominal ambient case (Figure 3-1), the PR, m_{RACC}, and $T_{comp,out}$ are taken from Table 3-2.

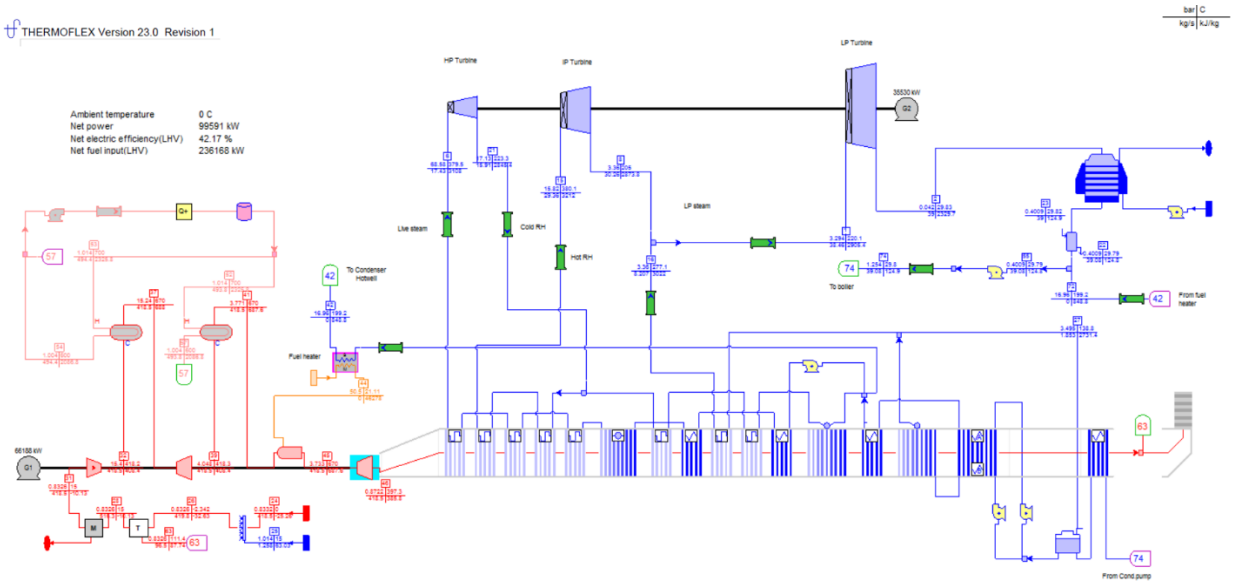

Figure 3-1. Reference THERMOFLEX® power conversion system flow diagram for base-load, 15°C nominal ambient conditions.

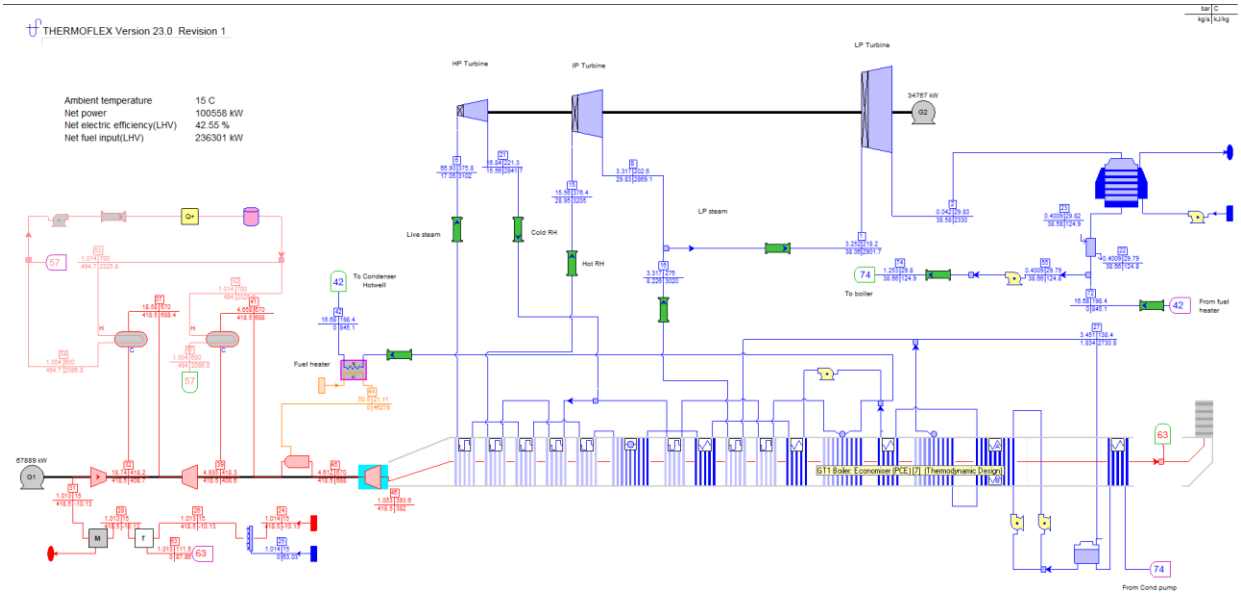

Figure 3-2. THERMOFLEX® power conversion system flow diagram for 0°C cold ambient conditions with stack recirculation.

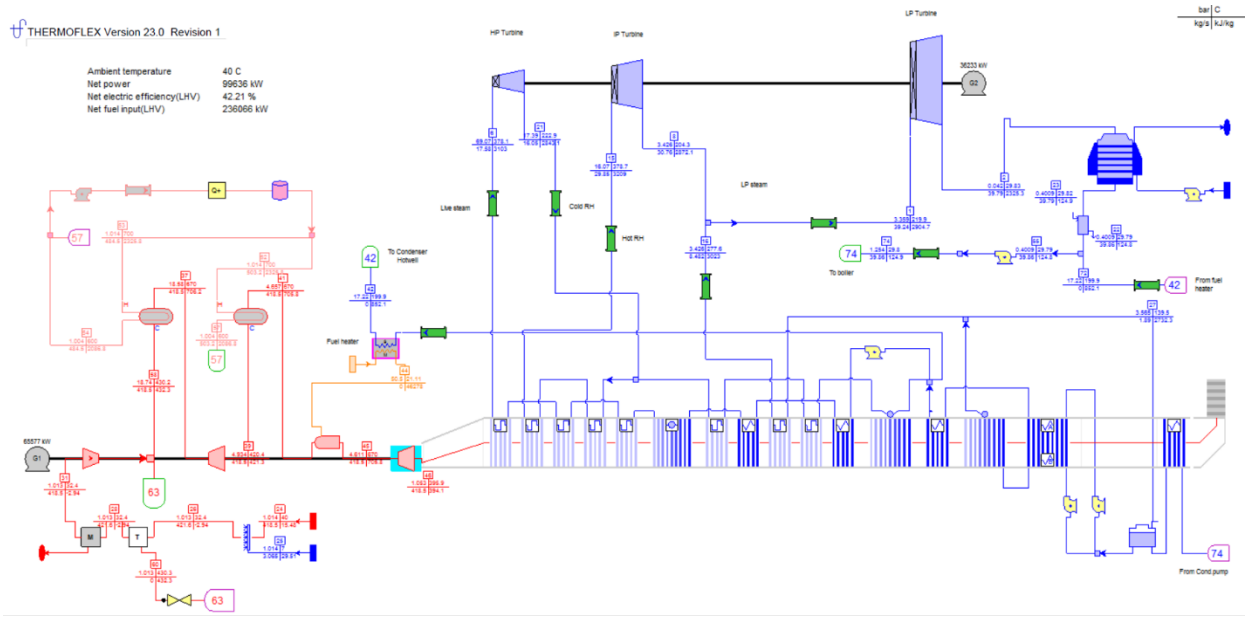

Figure 3-3. THERMOFLEX® power conversion system flow diagram for 40°C warm ambient conditions with compressor inlet fogging.

Figure 3-4 through Figure 3-9 present results from a parametric study across a range of ambient temperatures, for base-load and cofired operation of the reference RACC system. Observing the figures, it is apparent that if no compressor inlet control is used for varying ambient conditions, then the power output, net heat input, efficiency, and CTAH thermal requirements vary considerably with changing ambient temperature. By using compressor heat bleed or warm stack air recirculation in cold ambient conditions and inlet fogging during warm conditions, all parameters can be controlled to nearly match the nominal ISO condition values while maintaining a constant thermal power load on the molten salt heat source (Figure 3-4). With inlet control, relative CTAH heat transfer requirements remain constant and equal while with no inlet control there is approximately a 20 MW swing in thermal power requirement in high pressure (HP) CTAH. The low pressure (LP) CTAH thermal power requirement remains constant since the inlet and outlet temperatures remain constant as well.

In Figure 3-8, net cofiring power increases with ambient temperature. This is caused by the fact that at cold ambient conditions, warm air is recirculated from the compressor discharge (approximately 9.3 kg/s with a resulting 9 °C compressor inlet temperature), thus, cannibalizing some power from the cycle but counteracting with a lower compressor inlet temperature; at warm conditions, the denser mist that is injected (about 3 kg/s at 7 °C, 0.43% overspray) boosts power output. At baseload conditions approximately 65 kg/s of stack exhaust air needs to be mixed with compressor inlet air to maintain constant power at cold ambient conditions. Figure 3-9 shows cofiring efficiency remaining high in all scenarios.

For warm ambient conditions where inlet air cooling is required, the rate of water consumption is an important consideration since water may be scarce in many deployment

regions. Wet compression requires highly purified water compared to evaporative coolers [15]. However, water consumption for the proposed method of inlet air cooling is remarkably small at 3.07 kg/s for the 40 °C ambient case, which can be compared to the bottoming steam cycle condenser cooling tower's 2790 kg/s water circulation with a make-up of 33.5 kg/s.

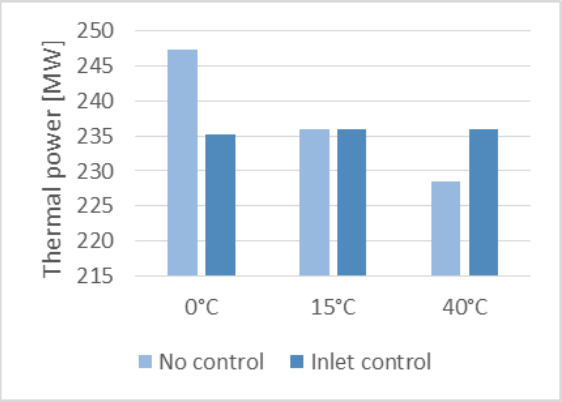

Figure 3-4. Net FHR thermal power at different ambients, with and without GT inlet control.

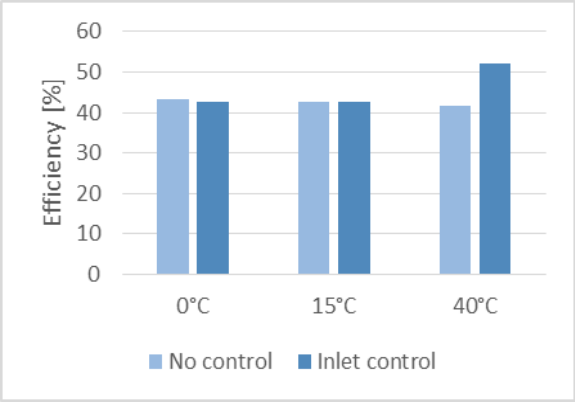

Figure 3-7. Net baseload efficiency at different ambients, with and without GT inlet control.

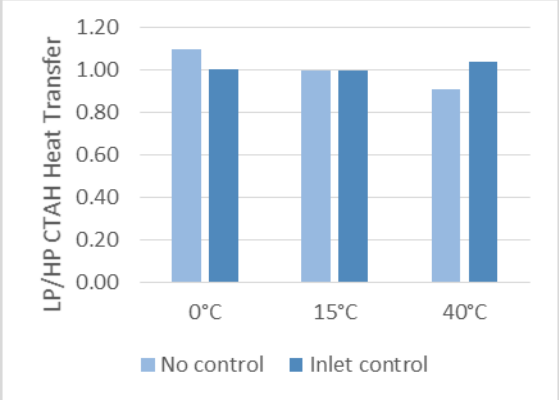

Figure 3-5. LP/HP CTAH heat transfer ratio at different ambients, with and without GT inlet control.

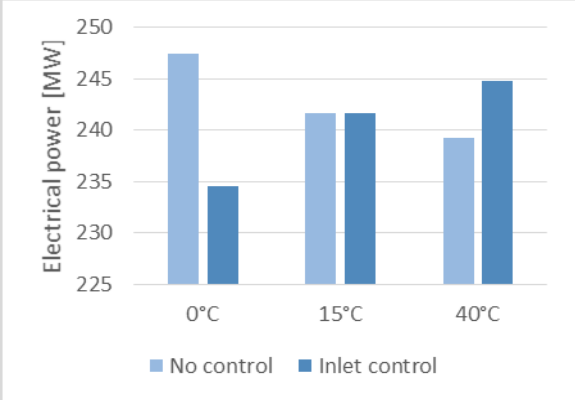

Figure 3-8. Net co-firing electrical power at different ambients, with and without GT inlet control.

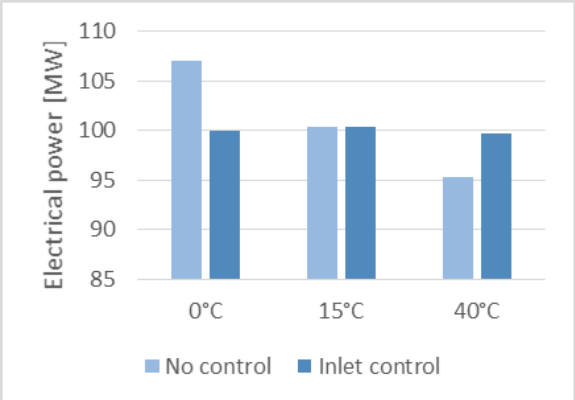

Figure 3-6. Net baseload electrical power at different ambients, with and without GT inlet control.

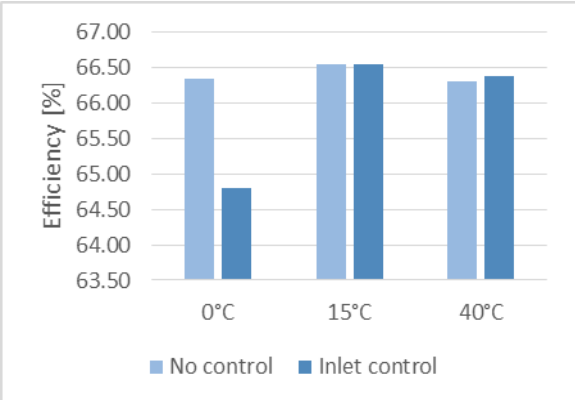

Figure 3-9. Net co-firing efficiency at different ambients, with and without GT inlet control.

For practical, esthetic, and public relations purposes, stack condensation should be avoided. Condensation is more likely in colder climates. In all ambient conditions and operating modes, including cofired operation at 0 °C, THERMOFLEX® predicts that the HRSG exhaust stack produces an invisible plume. Condensation can have HRSG corrosion repercussions but can also be a public perception issue for pollution and freezing of surrounding soil. Typical ways to avoid or reduce condensation include plume eliminators among others.

3.3.2 Off-Nominal Elevation.

At higher altitudes, the reduced barometric pressure results in lower ambient air density and reduced GT air mass flow rate and thermal power. Since the capital cost of a plant does not change greatly, reduced power output would have an economic penalty. To model the performance variation and possible mitigating techniques, Denver, CO was used as a reference city with an elevation of 1625 m and average high temperature of 31 °C.

To increase the density of the air flowing into the compressor, which at these conditions is about 82% of its sea-level value, wet compression can be initiated at a lower temperature than the 15 °C threshold used in the reference, sea-level design. For colder temperatures at increased elevation, a combination of wet compression (if sufficiently above freezing) with warm air recirculation can stabilize inlet air temperature/density. Alternatively, an inlet air blower might be used to increase the air supply pressure, although this is not a conventional commercial technology for large GTs. The results are displayed in Figure 3-10 through Figure 3-13 and Table 3-3.

Table 3-3. RACC performance at sea level and Denver, CO.

	Sea level-no control		Alt-no control		Alt-contol		Unit
T_{amb}	0	31	0	31	0	31	°C
Elevation	0	0	1625	1625	1625	1625	m
Recirc	0	0	0	0	65.0	0	kg/s
Overspray	0	0	0	0	0	1.98	kg/s
TIT,CF	1070	1070	1070	1058	1061	1058	°C
P_{net}	108.8	92.5	108.0	92.1	99.2	99.3	MW
η_{net}	43.4	41.6	43.1	41.2	42.2	42.0	%
Q_{FHR}	250.6	222.5	250.8	223.5	235.4	236.5	MW
P_{CF}	249.4	235.3	248.7	231.3	237.7	238.4	MW
Q_{CF}	462.1	437.2	462.4	433.2	444.2	446.2	MW
η_{CF}	66.5	66.5	66.5	66.4	66.3	66.3	%
$Q_{CTAH,1}$	131.6	102.6	131.7	103.3	117.5	115.9	MW
$Q_{CTAH,2}$	116.6	117.7	116.6	118.0	116.8	118.3	MW
$Q_{CTAH,1}/Q_{CTAH,2}$	1.13	0.87	1.13	0.88	1.01	0.98	

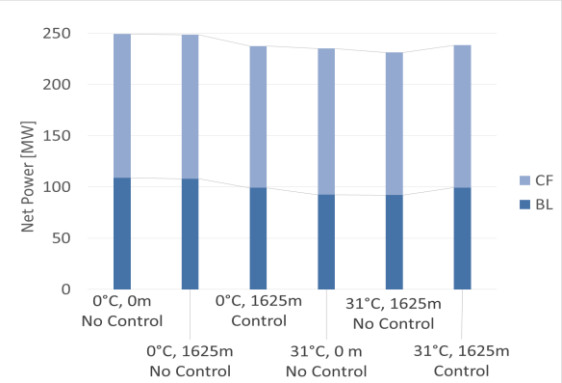

Figure 3-10. Net Power (base load, BL, and co-fired, CF) at varying ambient conditions for 0 m and 1625 m elevations.

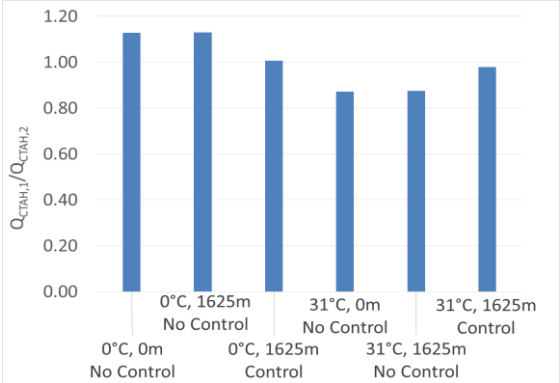

Figure 3-12. Relative CTAH sizes at varying ambient conditions for 0 m and 1625 m elevations.

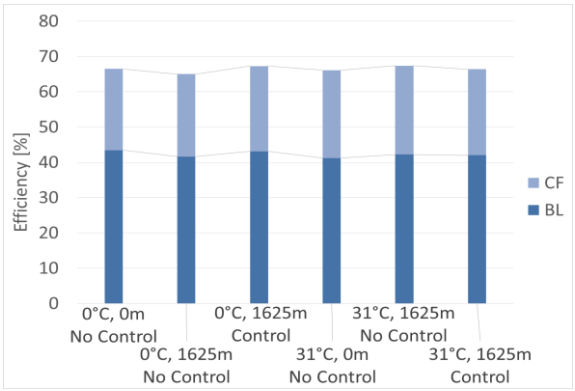

Figure 3-11. Efficiency (base load, BL, and co-fired, CF) at varying ambient conditions for 0 m and 1625 m elevations.

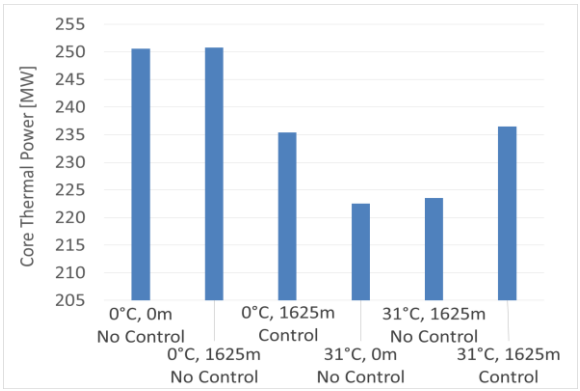

Figure 3-13. Core thermal power at varying ambient conditions for 0 m and 1625 m elevations.

From the figures, it is observed that both at sea level and at high altitude the variations in the uncontrolled cases are similar and are not too significant. When inlet air control is added at high altitude, the major parameters, including core thermal power, are maintained nearly constant as at the ISO conditions design point. Additionally, cofiring efficiency remains rather constant regardless of conditions due to the fact that it happens after the last point of contact with the salt loop and the fact that the turbine exhaust temperature is maintained at approximately 700 °C (reason for TIT variation in Table 3-3).

Taking into account the above results, an important consideration is whether to derate the machine or to use a different design point for compressor inlet control, other than the standard ISO conditions. The answer will invariably be dependent on location, licensing, and economic factors, but altitude is not expected to have a major impact on RACC economics.

3.4 Start-Up

The start-up of RACC PCSs involves some differences from conventional GTs because the thermal power comes from an external heat source. As with conventional GTs, normal start-up of a RACC GT involves motoring the generator using a static start system, which provides variable frequency voltage and current, to crank the shaft until it is self-sustaining. For black start capabilities, diesel powered or small gas-turbine generators can be used to provide power to motor the GT. In the RACC, each hot and warm air duct has a bypass line between the ducts, which allows flow to be bypassed around the CTAHs during start-up, as shown schematically in Figure 3-14. Each of the two bypass lines has a butterfly valve to control the bypass flow rate, and the CTAH hot and warm air ducts also have butterfly isolation valves to isolate the CTAHs during shutdown and to control flow through the CTAHs during start-up. These bypass lines are used to prevent overcooling of the CTAHs with the CTAH isolation valves initially closed. Air bleed valves, which bypass air from the compressor around the turbine directly to exhaust, are positioned fully open at start-up to prevent compressor surge, and variable inlet guide vanes (VIGV) are in their fully shut position to reduce air flow.

At start-up, the CTAHs are in standby, in a nearly isothermal condition (~600 °C), and are isolated by butterfly valves from the air ducts. When used with a nuclear reactor, the CTAHs may be used for normal shutdown cooling to remove decay heat, with a separate air blower system to provide low flow rates of ambient air for cooling. When a CTAH is used for shutdown cooling, its main salt pump operates at approximately 10% of its normal flow rate to remove reactor decay heat (0.3–4% of normal full power), so the temperature drop from the inlet to the outlet of the CTAHs is a few degrees centigrade.

Due to the high freezing temperatures of the fluoride salts, ranging from 350 °C to 460 °C, the control of freezing in the CTAHs is a key design issue. Under power operation, thermal analysis for temperature and pressure drop along the length of the CTAHs shows that freezing is readily prevented due to the high temperature of the air entering the CTAHs (~420 °C). Under start-up, shutdown, and operational transients, however, air entering the CTAHs can have lower

flow rates and significantly lower temperatures. The CTAHs may also be used for normal shutdown cooling, in which case freezing must be prevented when atmospheric, ambient temperature air is blown through the CTAHs. Specific methods to control CTAH freezing under start-up, such as using a recirculation blower to mix hot outlet air with inlet air, fall outside the scope of this dissertation.

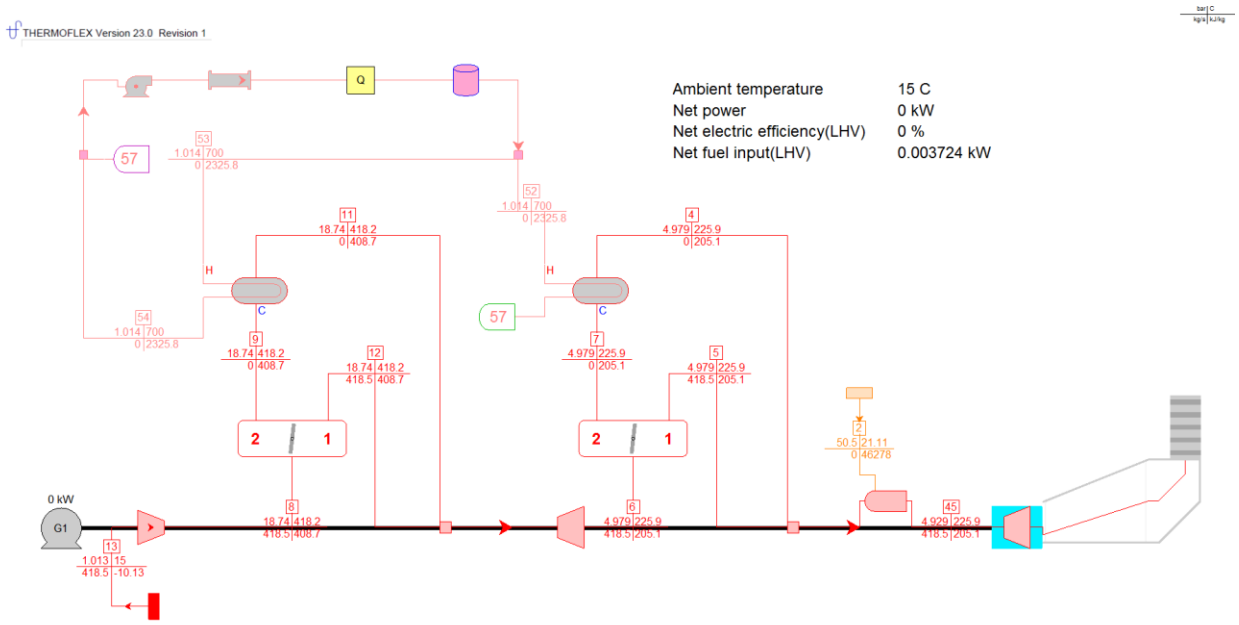

Figure 3-14. THERMOFLEX® power conversion system flow diagram for start-up.

For start-up of RACC systems, the compressor is motored at part speed. The turbine inlet temperature is increased by gradually opening the CTAH isolation valves and closing the bypass valves. The fraction of the air flow that goes through the CTAH is heated and is then mixed with the bypass air. For conventional combined cycle plants at 25–30% speed, approximately 7–10 times the volume of the machine needs to pass through for several minutes to purge any fuel gas that remains and avoid combustion downstream of the combustor [28]. This step can be reduced or avoided for RACC start-up with nuclear heat. For conventional combined cycle plants, the rotor is then normally coasted down to 15% speed to allow for turbine firing to begin. This can be omitted in RACC configuration. Alternatively, if NG firing is desired to assist in start-up, this step must be maintained. The optimal approach to balancing heat addition between the HP and LP CTAHs will depend upon the specific approach used to control freezing and upon other operational requirements, such as keeping the salt outlet temperature difference between CTAHs below some defined limit. At 40–90% speed, the start-up power source is decoupled from the shaft once the machine becomes self-sustaining. Once full air flow has been established, the compressor outlet temperature rapidly approaches its nominal value (418 °C in the baseline design).

Additional operational actions should be similar to those for conventional combined cycle plants. Once the machine reaches synchronous speed, the main breaker is closed. Throughout

this process, inlet bleed valves are closed and at about 80% speed VIGVs are gradually opened halfway and held there until load builds up. For combined cycle (CC) configuration, they may then closed back down to allow the pressure to build up in the steam cycle.

The reactor control system (RCS) or solar thermal storage control system responds automatically to the increased thermal load from the RACC PCS. For a RCS, the primary control functions are to maintain the core inlet temperature at the nominal design value (600 °C) to minimize transient thermal stresses in the primary system including the reactor vessel, to prevent the core bulk outlet temperature from exceeding its maximum design value (700 °C), and to maintain the temperature difference for the outlet salt from the two CTAHs below a defined threshold to minimize thermal stresses in the region where these two flows mix before entering the core inlet. The RCS controls three parameters—control rod position, speed of the HP salt circulating pump, and speed of the LP salt pump—to control these three variables. The optimal control algorithm will depend upon methods used to control freezing in the CTAHs and will also depend upon nuclear safety requirements for the reactor start-up.

To study the start-up system for the RACC and estimate the turbine speed where the PCS can become self-sustaining using nuclear heat, a quasi-transient analysis was performed using THERMOFLEX®, using several set point conditions for the flow schematic shown in Figure 3-14. The steam cycle was omitted to simplify the modeling.

In addition to the reactor power, which is controlled by control rods, and the HP and LP CTAH salt pump speeds, the PCS control system adjusts the HP and LP CTAH air bypass ratio and the compressor bypass flow rate to control CTAH freezing and compressor operational stability. For the part-load calculations performed here, it is assumed that mass flow and pressure ratio/expansion ratios are linearly proportional to shaft speed down to 0 rpm. Turbomachinery efficiency is assumed to have a lower bounding value of 40% and have a parabolic relationship to shaft speed. The reason for the parabolic relationship between turbomachinery efficiency and shaft speed is to restrict the compressor discharge temperature at part load below the full operating compressor discharge temperature. If a linear relationship is used between the two, compressor discharge temperature at part load exceeds its full load value due to the low compressor efficiency and gives erroneous results. Finding the optimum start-up procedure involves an optimization of the adjustable start-up parameters to reduce the cranking power requirement.

The bounding limit for cranking power is the full speed no heat (FSNH) condition where both CTAHs are isolated from the air stream. From this condition, bypass air and primary salt temperature can be regulated to minimize cranking power required for start-up and reduce the difference of heat delivery and salt outlet temperatures for the two CTAHs. Figure 3-15 displays the net shaft power, as a function of shaft speed, for four start-up configurations: (1) a TIT of 570 °C throughout start-up with no air-bypass through the HP CTAH, (2) a TIT of 670 °C throughout start-up with no air-bypass through the HP CTAH, (3) no air-bypass though either CTAH with a TIT of 670 °C, and (4) no heat input.

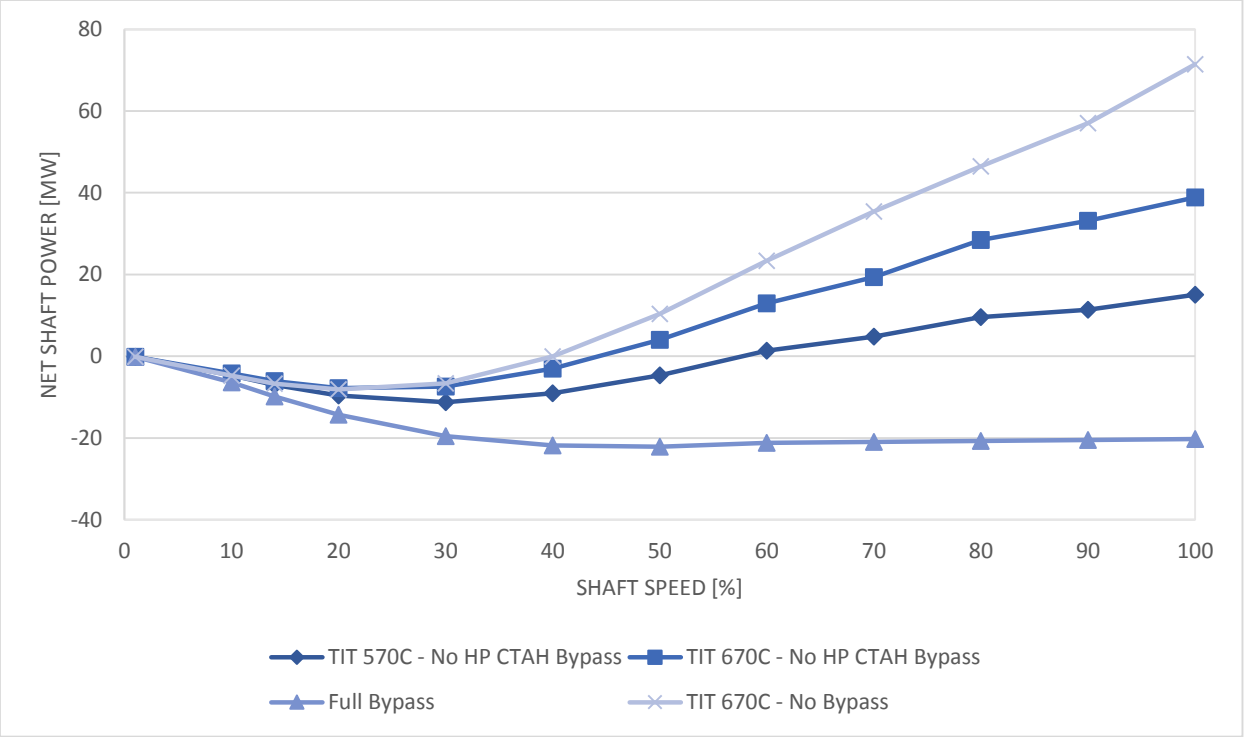

Figure 3-15. Net shaft power versus shaft speed.

From observation, it is noticed that the RACC can become self-sustaining at as low of a shaft speed as 40% in an ideal situation and requires a minimum cranking power of approximately 7.8 MW. The FSNH condition requires a bounding cranking power of 22.1 MW. Additionally, there is approximately a 4 MW difference in cranking power requirement between the low and high TIT scenarios, which in turn suggests that primary salt temperature should be brought up (by increasing reactor power while maintaining lower salt flow rates) during the early phase of start-up, while the turbine is coasting during its "purge" period in order to reduce the cranking power requirement. Figure 3-16 shows normalized values for several start-up parameters versus shaft speed for a potential start-up procedure that provides a relatively low maximum cranking power requirement and difference between HP and LP CTAH thermal power and the CTAH outlet salt temperatures.

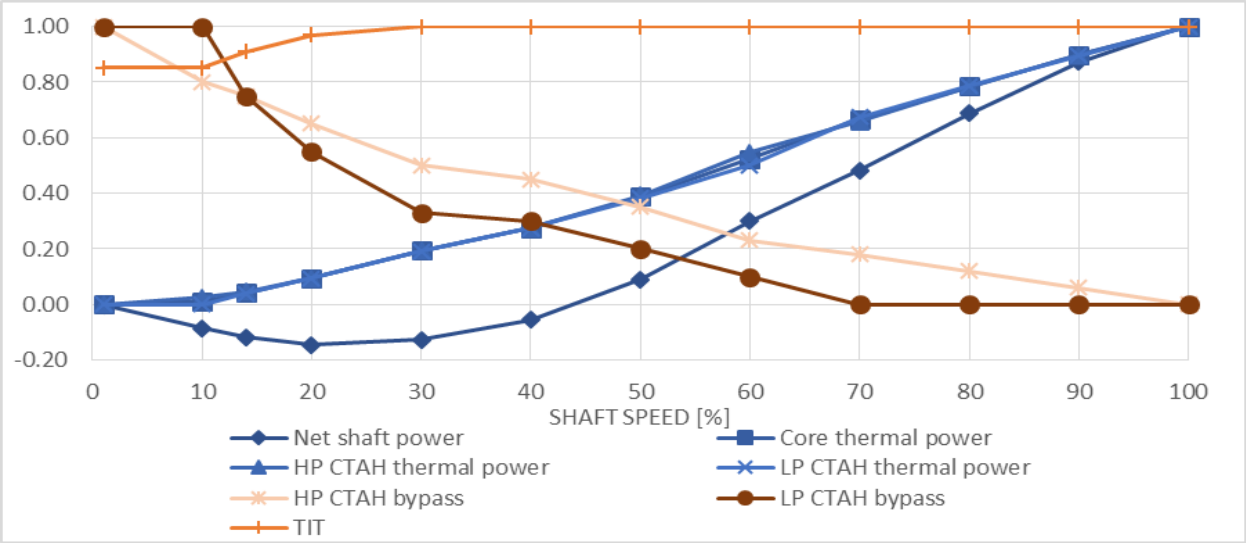

Figure 3-16. Normalized start-up parameters versus shaft speed.

Figure 3-16 depicts the early rise in TIT necessary to reduce cranking power requirements and the smaller amount of LP air-bypass necessary to maintain a similar thermal power for the two CTAHs, which simplifies control to maintain equal HP and LP salt outlet temperatures. Peak cranking power is approximately 10.2 MW at 20% speed and the RACC becomes self-sustaining at about 44% speed.

It may be possible to further reduce the maximum cranking power required for start-up by using cofiring or by using steam in the HRSG to generate additional electrical power using the bottoming steam turbine.

The start-up power requirements for the RACC system are sufficiently low, so they can, if desired, be provided by on-site diesel generators or small gas turbines if black-start capability is desired for the station.

3.5 Shutdown

The primary differences between shutting down a RACC PCS compared to a conventional combined cycle plant involve managing heat removal from the CTAHs to control the thermal transient delivered to the heaters and their heat source. To facilitate control of this thermal transient, RACC PCSs have an LP turbine bypass line that allows air exiting the LP CTAH to be vented to the bypass stack and, thus, to reduce power output from the LP turbine and steam generation in the HRSG.

While detailed assessment of shutdown control has not been performed and an appropriate shutdown power ramp rate has not been defined, RACC shutdown is still expected to share significant similarities with shutdown of conventional combined cycle plants. Once a shutdown signal is received, if the PCS is in cofired mode, fuel injection is reduced until the base-load power level is reached. From baseload power, the turbine inlet temperatures are then reduced by initiating bypass of air around the CTAHs. The specific balance between the HP and

LP CTAH bypass flows will depend upon the methods used to control freezing. At the same time, the compressor air bleed valves are opened as power is reduced.

When at minimum load, main and field breakers are tripped while the heat source continues to provide sufficient thermal power to motor the GT at full speed. Thermal power input can then be reduced, in the inverse of the start-up process, to slow the turbine to its minimum self-sustaining speed. At this point, the reactor may be tripped, CTAH isolation valves closed, and normal shutdown cooling initiated. VIGVs will ramp to full closed position as a function of temperature corrected speed [35]. Once the rotor is coasted down to 15% speed, the turning gear is engaged. The turning gear needs to keep rotating the shaft at slow speed even after shutdown to relieve thermal stresses and prevent the rotor from bowing. Also, the lube oil system needs to be kept on for 30–60 min after shutdown to cool equipment [36].

If the need to restart within a 48 h time period is anticipated by the grid operator, it is preferable to maintain the reactor at significantly higher thermal power to control xenon build up, and to use LP turbine bypass valve to unload the generator, so the main and field breakers can be tripped and the unit disconnected from the grid.

3.6 Load Rejection

Grid disturbances and blackouts can result in the need to abruptly reduce power generation to avoid a unit trip. For RACC systems, abrupt reduction in generator load is achieved by isolating the gas supply (if cofiring) and opening the LP turbine bypass valve to vent heated air from the outlet of the LP CTAH to the bypass stack to prevent turbine over speed and a turbine trip.

Reactors using RACC can operate at full power with LP turbine bypass in order to be capable of rapidly ramping power back up if the grid operator expects transmission to be restored in a short period of time, or power can be reduced using the normal shutdown sequence. When venting to atmosphere, discharged bypass air needs to be silenced and mixed with cold air for safety reasons.

3.7 Unit Trips

A unit trip can be generated by the various protection systems, which monitor parameters important to plant safety and reliability. The most important goal during a unit trip is to bring the gas turbine and its heat source (reactor or CSP) to a safe shutdown state while minimizing stresses imposed on equipment to acceptable values.

The detailed approach to controlling equipment during unit trips initiated by plant protection systems will depend upon the design of the unit heat source. For reactor heat sources, a unit trip will generate a reactor scram. CTAH isolation valves will fail closed, and CTAH bypass valves will fail open to protect the CTAHs from overcooling during the gas turbine coast down. Depending on the nature, severity, and rate of the trip, the GT will be coasted down to zero power at a parts life penalty from normal shutdown. For GT equipment

protection, the lube oil system will keep running after shutdown to provide cooling to the bearings, and the turning gear will be engaged on slow roll to relieve thermal stresses and prevent rotor bow as described in the “Shutdown” section above.

3.8 Power Ramping and Cofiring

A frequently anticipated mode of operation of the RACC is ramping up and down between base-load and peak power levels, using cofiring to increase and decrease the LP TIT. Because the air inlet temperature to the LP turbine is above the fuel auto-ignition temperature, RACC has no combustor limits on the temperature ramp rate. Achieving a high power ramping rate is desirable to increase RACC electricity generation revenues. However, a question that emerges is whether the LP inlet nozzle and first turbine blade state and the HRSG can tolerate a rapid ramp in the air inlet temperature. Moreover, additional requirements, tolerances, and operating limits must be laid out to better define the cofiring capability.

Cofiring initiation in the RACC can be seen as equivalent to the light off in a conventional GT, except that the air temperature entering the combustor will be above the auto-ignition temperature. Fuel nozzle placement and design should be investigated in order to assure appropriate natural-gas/air mixing and ignition at different cofired loads.

Power ramping for the GT, which produces about 2/3 of the total RACC power output, can be rapid, so using the GT to provide grid support services, such as frequency regulation, can be considered. The HRSG and steam systems must be ramped more slowly. For normal steam-systems power ramping a steady ramp of 5%/min is typical over a large increase in load, with up to 10%/min for smaller changes, typically for the first 50 °C change in gas temperature entering the HRSG. The limiting factors are how quickly steam temperatures are allowed to change and how quickly the HRSG can adjust to the new load without subjecting the components to excessive thermal stress and low cycle fatigue.

For rapid power ramps between base-load and peak power levels, the GT and steam turbines (ST) can be decoupled by bypassing air from the HRSG and venting directly to atmosphere. An attemperation water spray system in the HRSG superheater will be used to limit the initial steam temperature rise, then, under the influence of the control system, allow a slow ramp up to the new steady state conditions. Care must also be taken to ensure a uniform temperature profile across the HRSG inlet to avoid hot spots and localized overheating. The addition of ST inlet throttle valves can maintain a minimum pressure and actively control HRSG pressure during load transitions to mitigate the effects of large load changes.

Rapid ramping of the GT power between zero and base-load power levels is also possible using LP turbine bypass. In this case, reactor power is increased while the generator load is maintained at a reduced level by bypassing air past the LP turbine. This type of rapid power ramp may be applied, for example, when a RACC system is used to restore power to a black grid to maintain generator voltage during the rapid increase in current. This type of rapid power ramp using LP turbine bypass requires protection of the steam system using the same approach as used

for rapid GT ramps with cofiring. A quantitative estimation of the RACC power ramp rate is performed in the next chapter.

3.9 Service Life and Maintenance

The modified operating conditions of the RACC GT compared to the conventional NG configuration will have an impact on the service life and maintenance program for the machine. Depending on frequency and amount of cycling between baseload and cofired mode, maintenance schedules will vary. Maintenance requirements might also change based on the selected GT materials for the RACC. Key factors affecting service life for GTs are cyclic effects, firing temperatures, fuel, steam/water injection, and site environment [29]. The RACC is expected to have a cyclic duty application; therefore, the main causes of wear are expected to be thermal mechanical fatigue, high cycle fatigue, and rubs.

GT manufacturers have two ways of scheduling service outages: (1) by using both the number of starts and hours of operation combined into an equivalent number of operating hours and (2) by considering the number of starts and operating hours separately and using whichever one reaches a set number first as the limiting factor. GTs usually have three planned service intervals, with the following typical values: combustion inspection at 12,000 factored hours or 450 factored starts (which may or may not be warranted for the RACC depending on the amount of cofiring), hot gas path inspection at 24,000 factored hours or 900 factored starts, and major inspection at 48,000 factored hours or 2400 factored starts. The number of hours and starts are also modified by factors depending on operation deviating from a base case. Sample equations for calculation of service intervals and part replacement intervals for the GE 7FB can be found in Balevic et al. [37].

For the RACC, the lower firing temperatures should increase parts' lives while the fact that the majority of cycling happens when the machine is already warm should also decrease the maintenance factors. An alternate view is to treat the RACC as running in frequency regulation mode, where turbines are dispatched to run at part load on stand-by and pick up load rapidly when there is a frequency disturbance. Such operating conditions can yield sub-10 second responses [28].

The desire to maintain a constant reactor thermal power introduces the use of inlet air cooling during warm ambient conditions. This might also have an insignificant to a small increased wear effect on the GT because the increased humidity of the air increases the heat transfer coefficient and, in turn, the metal temperatures. This might be partially mitigated by the substantially lower firing temperature used by the RACC.

A clear quantitative assessment of service factors and intervals for the RACC is premature at this point. A major consideration for optimizing maintenance intervals, and making economic decisions about the frequency and rate of power ramping, is to coordinate scheduled maintenance periods for the heat source (reactor or CSP) with maintenance for the RACC system. A brief discussion on economic impacts of power ramping is provided in a later chapter.

3.10 Blade Failures

Compressor and turbine blade failures can occur in gas turbines. Generally, these events cause extensive damage to the turbine and its casing, but air flow stops rapidly and carryover of shrapnel is relatively small. The fact that blades are not ejected through the turbine casing of large, stationary GTs is different than for the yet larger blades used in low-pressure steam turbines, so a RACC gas turbine can be oriented parallel to a reactor containment structure, whereas steam turbines should be oriented perpendicular. Both the CTAHs and their supply ducts are designed to minimize the risk of damage to tubes and of salt leakage in the event of blade failure. The air supply duct system is designed to slow down and stop blade shrapnel, with the miter-bend turning elbows and turning vanes acting as filters to stop shrapnel from reaching the CTAHs.

3.11 Natural Gas Safety

NG provides a source of stored energy, which must be considered for the safety and security design of the plant, particularly for nuclear reactors. Widespread experience exists with operation and handling of NG and NG systems. For RACC systems, hazardous area regulations, standard NG plant safety features, and additional safety and security measures will be combined to prevent and mitigate leaks and explosions.

High pressure NG pipe lines are generally robust and low hazard in the absence of flanges and fitting, thus, making their minimal use important for the RACC. The NG supply system also has a double block and bleed system to prevent uncontrolled release into equipment. These valves are designated with fail positions, along with position feedback, that assure redundancy and safety.

The RACC operates at base-load using external heat, meaning that it is hot, spinning, and at pressure when NG is injected. Having the RACC run on external heat for a while prior to injecting NG for cofiring ensures that the system is fully purged and ventilated. Any unburned NG downstream of the combustors or in the HRSG can cause combustion and overheat or damage parts of the turbine and HRSG. In order to allow for NG injection, the gas supply control system verifies that the PCS is at full base load power and that the combustor temperature is above auto-ignition temperature. The stack gases leaving the HRSG are monitored to detect any unburned NG. Additionally, as an early warning that a block valve has failed or is improperly sealing, gas flow through the vent lines is also monitored.

The RACC LP air duct also has a back-flow damper with position feedback between the LP CTAH and combustor, which closes on low flow. During coast down and cool down, the backflow damper prevents residual NG from flowing back through the GT to the LP CTAH when air flow ceases. It also protects the LP CTAH from overpressure in case of an explosion in the combustor system. If necessary, gas concentration monitoring, back-up fans, and sparking elements to prevent explosive NG concentrations can be provided.

To protect the NG supply system from external events and to enhance physical security, the NG supply skid may be placed in below-grade vaults with an independent ventilation system and access control systems to prevent unauthorized entry. The high pressure gas line that supplies gas to the supply skid is buried and extends to a master isolation valve system located within the plant owner controlled area at a sufficient distance from the plant to provide secure isolation for all site NG piping in an emergency. The baseline design of RACC is located outdoors; however, the sound and insulation enclosure around the GT is actively ventilated to prevent NG accumulation. The air ducts and vaults are also designed to relieve overpressure with rupture disks and blow-out panels.

3.12 Discussion

Various off-nominal ambient and transient scenarios need to be considered for RACC operation. In order for the RACC cycle to provide economic and system benefits to both plant operators and the electricity grid, such as peaking power, spinning reserves, black start services, and frequency regulation, it must be able to accommodate these off-nominal and transient conditions successfully. This chapter has proposed qualitative methods for the RACC to meet safety and reliability performance requirements while maximizing the use of standard gas turbine and combined cycle components wherever possible. A numerical study of the RACC performance under different ambient and off-nominal conditions was also performed.

4 NACC Power Ramp Rate Calculation

This section is an adapted version of the stimulated summary "Nuclear Air Brayton Combined Cycle (NACC) Power Ramp Rate" by Andreades et al. [38]. *Copyright granted 24 April, 2015 by the American Nuclear Society, La Grange Park, Illinois.*

The large scale introduction and adoption of intermittent renewable energy sources (RES) has necessitated careful consideration for their integration into the electric grid. As an ever-increasing capacity of RES is introduced, transmission system operators need to guarantee the stability and security of the grid. A problem facing transmission system operators is the so called scenario of the duck-curve, under which a large amount of RES capacity goes offline during a short period of time in the early evening during sundown, reducing supply, and people returning to their homes, increasing demand. Although the installed capacity might be available in absolute terms, the physical constraints of fossil backup resources do not allow for a quick enough ramp rate within that short period of time, leading to potential brown-outs/black-outs.

The Nuclear Air-Brayton Combined Cycle (NACC) is a hybrid nuclear-natural gas (NG) power conversion system, designed to be coupled to the Mk1 fluoride-salt-cooled High-Temperature Reactor (FHR), currently under development at UC Berkeley, MIT, and UW-Madison [2, 39, 40]. The NACC operates in two modes, namely baseload, under which all heat input is provided through nuclear heat, and cofired operation, under which NG is injected into the air stream to boost power. The NACC can provide a quick ramp rate for the output coming from the gas turbine (GT) and a more moderate ramp rate for the power output of the steam turbine. The important issue is to try and estimate how quickly one can provide the additional power from the GT, which can provide flexible capacity in a highly intermittent renewable integrated grid. This is the focus of this chapter.

4.1 Methodology

Under baseload operation the net power output is 100 MWe, split between 66.3 MWe from the gas turbine and 33.7 MWe from the steam turbine, with a turbine inlet temperature (TIT) of 670°C for the GT. Under cofired operation the net power output is 242 MWe, split between 124.1 MWe from the gas turbine and 117.9 MWe from the steam turbine, with a turbine inlet temperature (TIT) of 1070°C for the GT. The performance characteristics of the NACC are summarized in Table 4-1.

Table 4-1. NACC performance characteristics.

Description	Value	Units
$P_{BL,net}$	100	MW_e
$P_{BL,GT}$	66.3	MW_e
$P_{BL,ST}$	33.7	MW_e
$P_{CF,net}$	242	MW_e
$P_{CF,GT}$	124.1	MW_e
$P_{CF,ST}$	117.9	MW_e
ΔP_{GT}	57.8	MW_e
ΔP_{ST}	84.2	MW_e
$TIT_{BL,GT}$	670	°C
$TIT_{BL,GT}$	1070	°C
ΔTIT_{GT}	400	°C

In order to arrive to a final load ramp rate for the NACC, conventional GT ramping had to be understood, followed by back-calculation of conventional TIT as function of turbine exhaust temperature (TET), and finally applied to the NACC's operating characteristics.

4.2 Data and analysis

When commercial GTs typically change their load, they change the air mass flow through various techniques, such as variable geometry or bypass air flow. The firing temperature or TIT is ramped quickly initially and once it reaches its design value, it does not vary significantly. This is a different approach from the NACC in which under baseload operation and cofired operation the air mass flow remains the same. The parameter that is altered instead to change power output for the NACC is the TIT. Thus, the primary indicator to understanding the ramp rate of the NACC is the rate of change of TIT for a conventional GT. This operation occurs during the startup phase of a conventional GT and leads to the examination of the startup process as depicted in Figure 4-1.

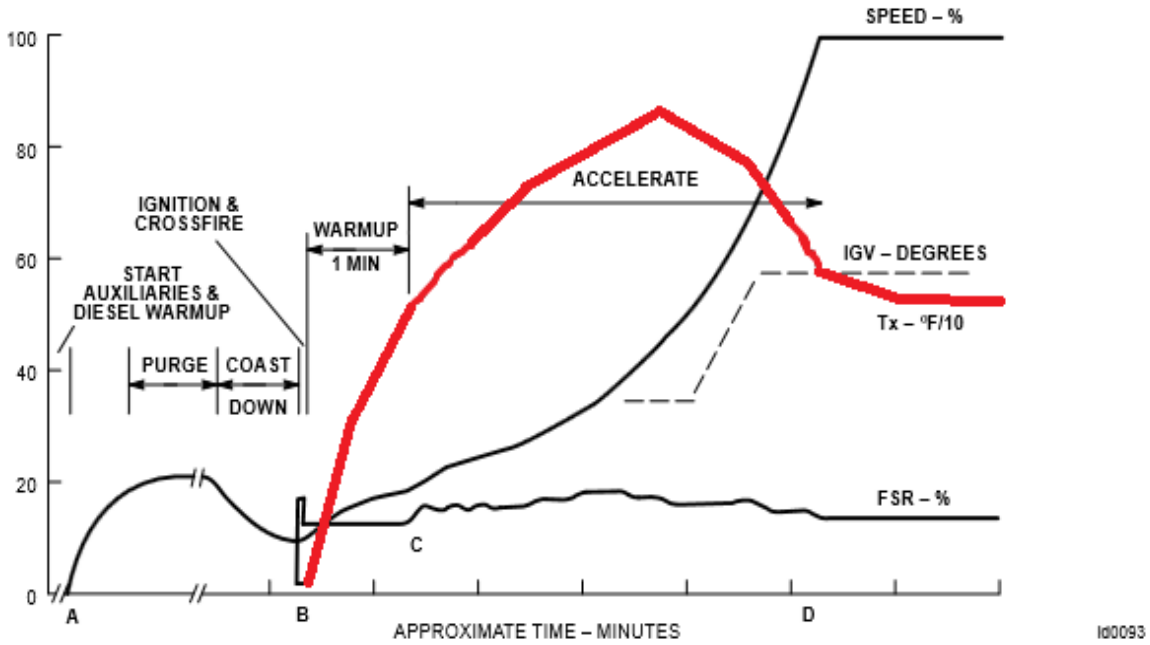

Figure 4-1. Typical startup curve for a GT [41].

The curve of interest is the one in red, which is the TET, Tx. There are two parts to the curve in which temperature rises at a significant rate: (a) the warm-up period and (b) the acceleration period. The TET was related to TIT through the following thermodynamic relation:

$$\eta_t = \frac{TIT - TET}{TIT \cdot \left(1 - \frac{1}{ER^{\gamma-1/\gamma}}\right)}. \qquad 4\text{-}1.$$

Which in turn reduces to:

$$TIT = \frac{\mathrm{TET}}{1 - \eta_t \cdot (1 - 1/\mathrm{ER}^{\gamma - 1/\gamma})}. \quad 4\text{-}2.$$

Where η_t is the turbine efficiency, ER the expansion ratio of the turbine, and γ the specific heat capacity ratio. Before calculating the TIT a relationship between TET, ER, γ, and η_t had to be established.

A simple THERMOFLEX® [42] model of the GE 7FB in simple cycle, depicted in Figure 4-2, was created in order to back calculate turbine expansion ratio, turbine efficiency, and specific heat capacity ratio from given state points. The power output was varied from 0% (also known as full speed no load – FSNL) up to 100% (full power). The results are displayed in Table 4-2.

Table 4-2. GE 7FB state points as a function of power.

Power	TIT (°C)	P_3 (MPa)	h_3 (kJ/kg)	s_3 (kJ/kg°C)	TET (°C)	P_4 (MPa)	h_{4s} (kJ/kg)	h_4 (kJ/kg)	η_t (%)	ER	γ_{avg}
0%	758	0.7213	1208.5	4.6248	469.5	0.1018	752.66	885.78	70.80	7.09	1.34715
5%	820.6	0.744	1280.7	4.6839	497.6	0.1018	790.24	916.37	74.28	7.31	1.3435
10%	899	0.7717	1372	4.754	533.9	0.1018	837.61	956.16	77.82	7.58	1.3393
15%	979.5	0.7994	1466.7	4.822	572.3	0.1018	886.6	998.58	80.70	7.85	1.33525
20%	1058.9	0.8262	1561	4.8855	611.3	0.1018	935.21	1042	82.94	8.12	1.33165
25%	1135	0.8536	1652.1	4.9426	649.1	0.1018	981.4	1084.4	84.64	8.39	1.32845
30%	1164.6	0.9163	1687.7	4.9472	649.1	0.1018	985.22	1084.4	85.88	9.00	1.3279
35%	1191.2	0.9778	1719.8	4.9507	649.1	0.1018	988.14	1084.4	86.84	9.61	1.32745
40%	1215.4	1.038	1749.1	4.9533	649.1	0.1018	990.32	1084.4	87.60	10.20	1.327
45%	1237.5	1.098	1775.9	4.955	649.1	0.1018	991.75	1084.4	88.18	10.79	1.32665
50%	1257.9	1.157	1800.7	4.9563	649.1	0.1018	992.84	1084.4	88.67	11.37	1.32635
55%	1276.6	1.215	1823.5	4.957	649.1	0.1018	993.43	1084.4	89.04	11.94	1.32605
60%	1294	1.274	1844.7	4.9569	649.1	0.1018	993.34	1084.4	89.30	12.51	1.3258
65%	1310.1	1.331	1864.3	4.9568	649.1	0.1018	993.26	1084.4	89.54	13.07	1.32555
70%	1335.2	1.389	1895	4.9637	649.1	0.1018	999.08	1084.4	90.48	13.64	1.3252
75%	1339.3	1.446	1900	4.9553	649.1	0.1018	992	1084.4	89.82	14.20	1.32515
80%	1352.5	1.503	1916.2	4.9541	649.1	0.1018	990.99	1084.4	89.90	14.76	1.32495
85%	1364.7	1.56	1931.2	4.9526	649	0.1018	989.73	1084.3	89.96	15.32	1.3248
90%	1367.5	1.627	1934.6	4.9426	642.3	0.1018	981.4	1076.7	90.00	15.98	1.325
95%	1369.4	1.695	1937	4.9323	635.5	0.1018	972.89	1069.1	90.02	16.65	1.32525
100%	1370.4	1.763	1938.3	4.9217	628.5	0.1018	964.21	1061.3	90.03	17.32	1.32555

Thermodynamic properties of air were obtained through REFROP Mini [43]. The turbine efficiency was calculated according to the following relation:

$$\eta_t = \frac{h_3 - h_4}{h_3 - h_{4s}}. \qquad 4\text{-}3.$$

State point 3 is the turbine inlet, whereas state point 4 is the turbine exhaust, and h denotes the enthalpy at each point.

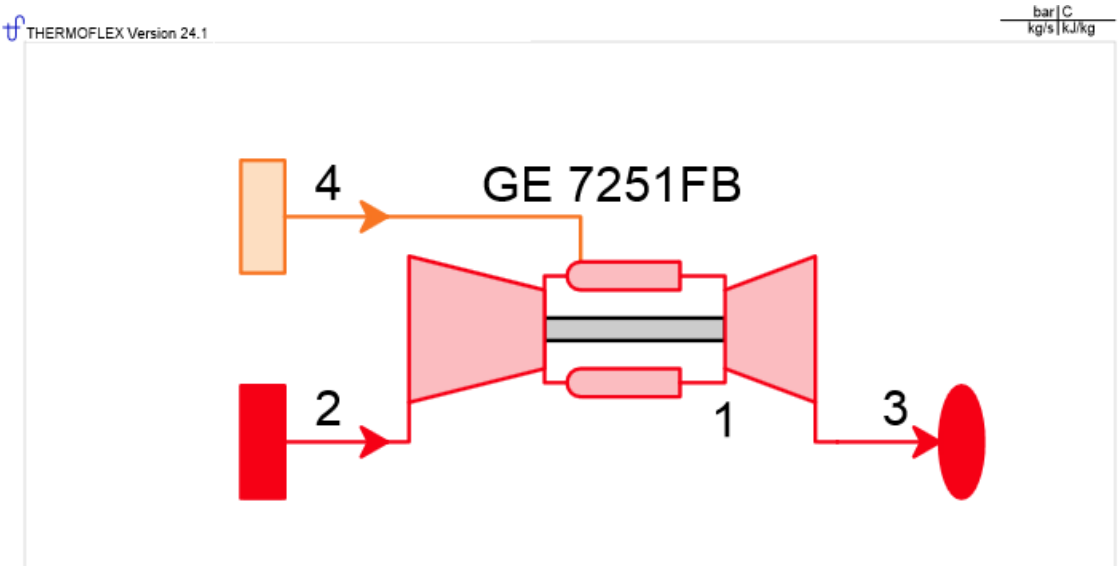

Figure 4-2. THERMOFLEX® schematic of GE 7FB simple cycle.

By observation of the values in Table 4-2 it was noted that TET stopped increasing after a certain point and TIT varied slightly. Thus a range of interest for back calculation from 0 to 25% power was selected, in which temperatures varied significantly. To get to TETs below the FSNL condition, relationships between ER, η_t, and γ to TET had to be established through polynomial trendlines. At the same time reasonable intercepts had to be selected to bind the trendlines. Limiting values for ER of 1, η_t of 45% and γ of 1.4 were selected at a TET 15°C. The results are displayed in Figure 4-3 through Figure 4-5.

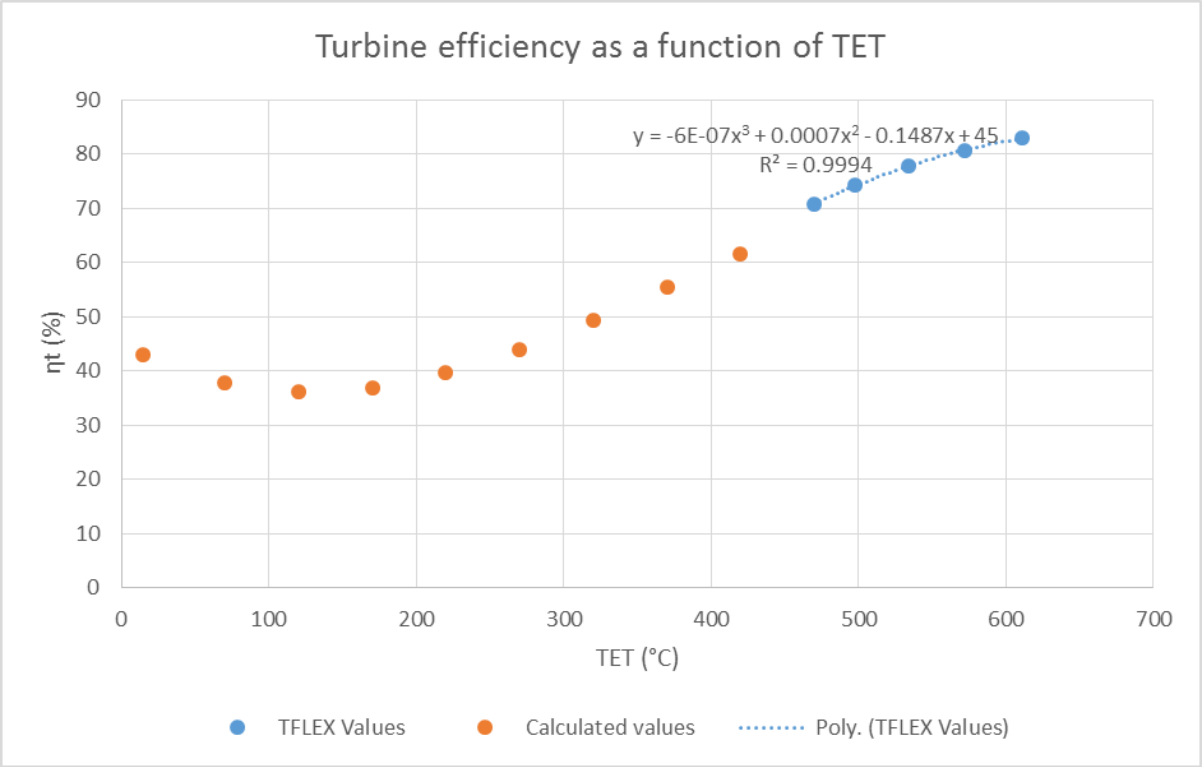

Figure 4-3. Turbine efficiency as a function of TET.

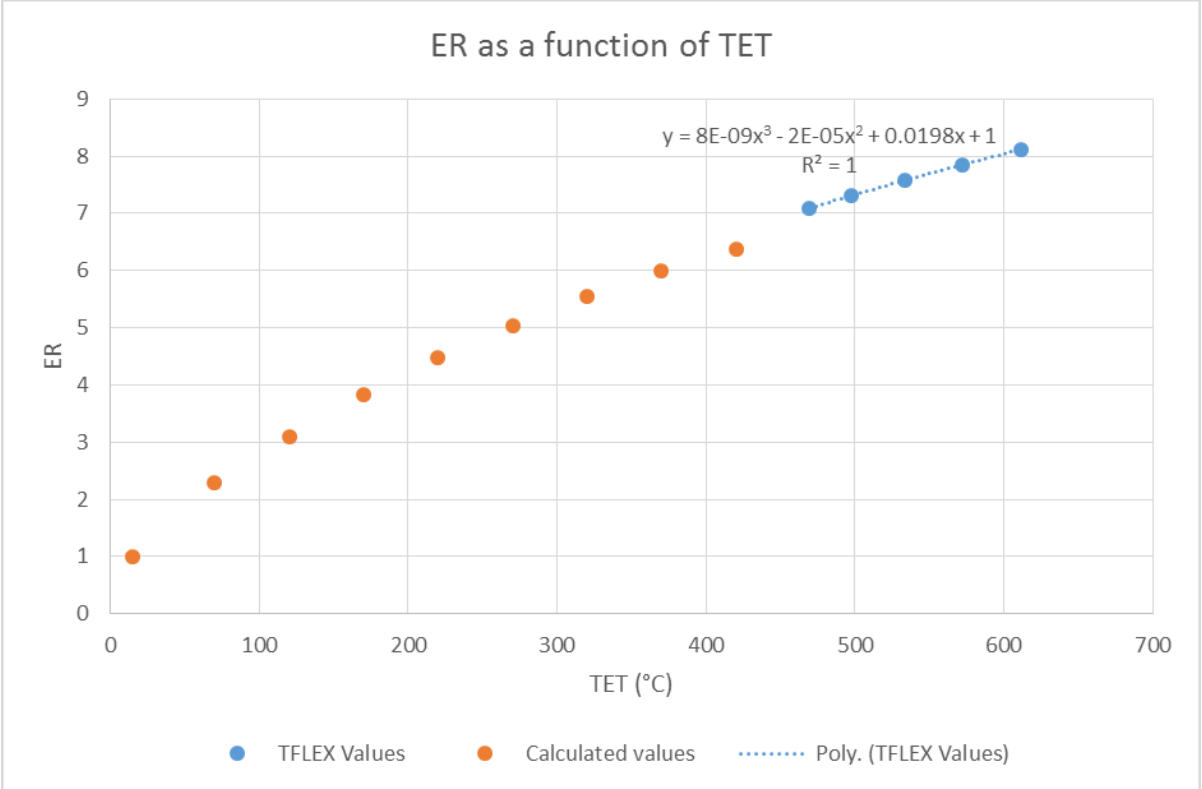

Figure 4-4. ER as a function of TET.

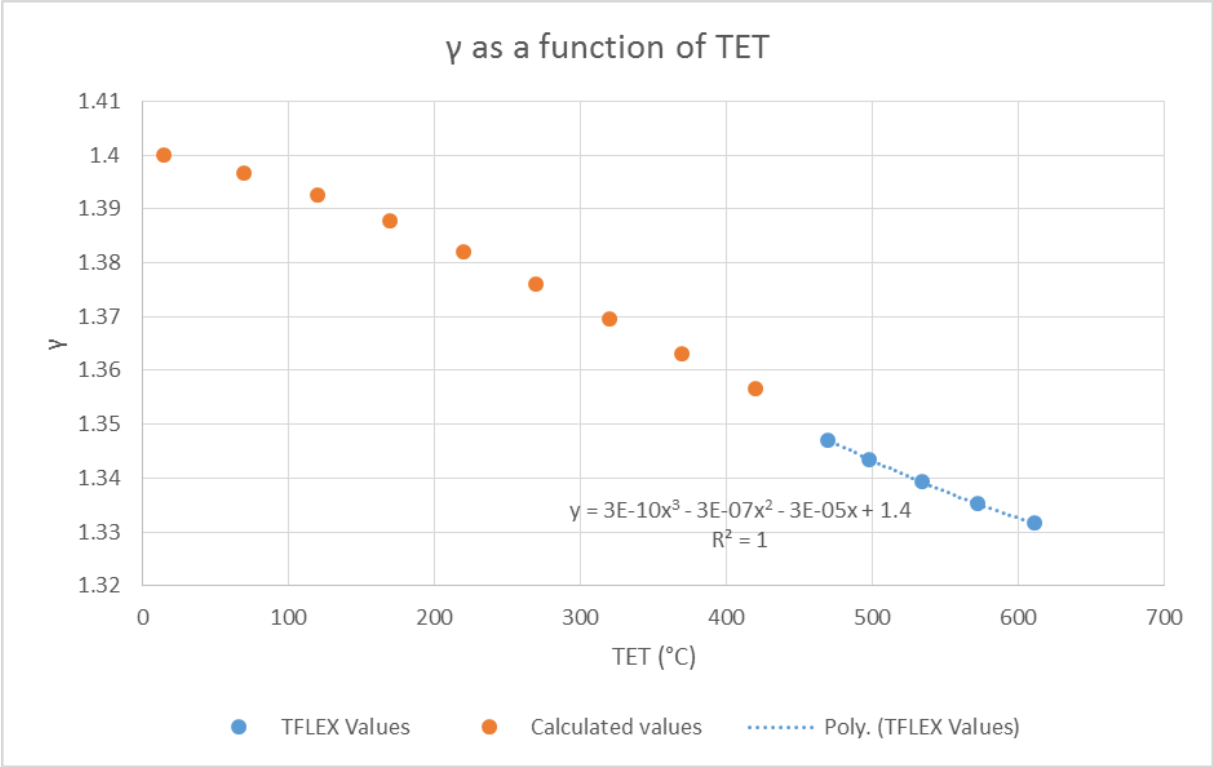

Figure 4-5. γ as a function of TET.

Using the developed relations for the variables and plugging into equation 2-2, TIT was correlated to TETs below FSNL. The results are displayed in Figure 4-6.

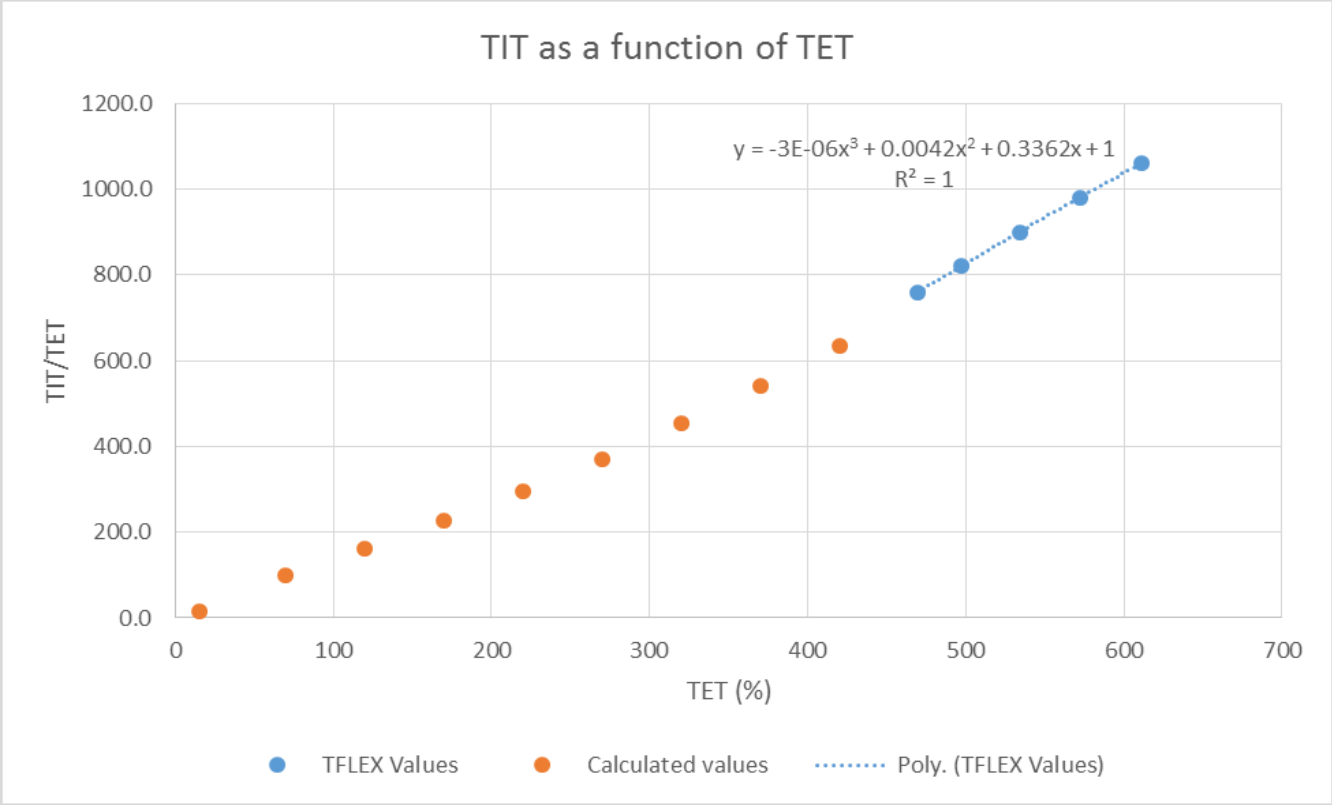

Figure 4-6. TET as a function of TET.

The next step involved normalizing TET to a maximum value of 649.1°C from .

Table 4-2 and then establishing absolute values to Figure 4-1 and in turn superimposing TIT on the graph using the relationship from Figure 4-6. The results are displayed in Table 4-3, Table 4-4, and Figure 4-7.

Table 4-3. GE 7FB operating startup and low power operating point estimations.

TET (°C)	η_t (%)	γ_{avg}	ER	TIT (°C)	TET (%)
15	42.92	1.4	1	15.0	0.023
70	37.82	1.397	2.29	99.6	0.108
120	36.20	1.393	3.10	163.2	0.185
170	37.00	1.388	3.83	228.0	0.262
220	39.78	1.382	4.47	296.9	0.339
270	44.07	1.376	5.05	371.5	0.416
320	49.44	1.369	5.55	452.9	0.493
370	55.42	1.363	5.99	541.2	0.570
420	61.57	1.357	6.38	635.9	0.647
469.5	70.8	1.347	7.09	759.2	0.723
497.6	74.28	1.344	7.31	821.8	0.767
533.9	77.82	1.339	7.58	900.5	0.823
572.3	80.70	1.335	7.85	981.2	0.882

611.3	82.94	1.332	8.12	1060.9	0.942
628.5	90.03	1.326	17.31	1376.2	0.968

Table 4-4. GE 7FB ramp rates during startup.

TET (%)	TET (°C)	t (min)	TIT (%)	TIT (°C)	ΔTIT/Δt (°C/min)
2.4	15.6	0	0.5	6.3	0.0
31.2	202.5	0.46	15.8	216.6	458.7
51.2	332.3	1	34.1	467.4	463.0
72	467.4	2.25	56.3	770.9	242.8
84.8	550.4	3.5	70.1	960.3	151.6

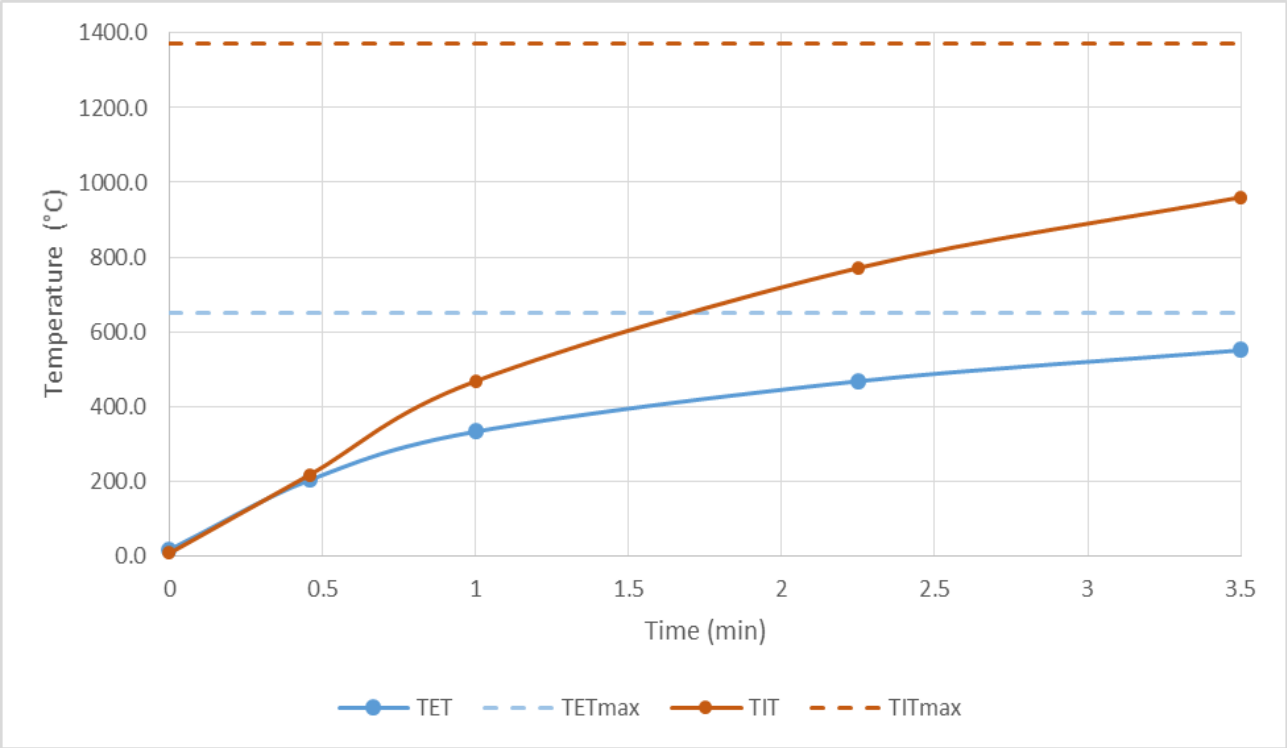

Figure 4-7. GE 7FB ramp rates during startup.

During the initial warm-up phase of startup a TIT ramp rate of approximately 460°C/min was calculated, whereas during the acceleration phase a lower TIT ramp rate between 150 and 240°C/min was calculated. As the full power TIT is approached the TIT ramp rate is reduced accordingly. Regarding the NACC, one can assume that a TIT ramp rate of anywhere between 150-460°C/min is reasonable which in turn yields a power ramp rate from the Brayton cycle of 21.7 MW/min to 66.5 MW/min, by interpolating between the values in Table 4-1. Typical ramp rates for conventional gas turbine are around 8 MW/min, but can be ramped to a maximum of 8 times faster during emergency startups. The maximum calculated ramp rate for the NACC thus appears to fall within maximum ramp rates of conventional gas turbines. The slower ramp rate of the steam turbine, also had to be taken into account, and was subsequently added to the above power ramp rates. Assuming a 30 minute ramp time for the steam cycle yields a 2.8

MW/min ramp rate. Adding this to the gas turbine ramp rate yields an overall ramp rate for the NACC of 24.5 MW/min to 69.3 MW/min.

4.3 Discussion

Such large power ramp rates can prove critically important during situations such solar eclipses, or during early evening hours when renewable generation stops being produced in large capacities within short time intervals. When selecting a ramp rate between the calculated values one has to balance potential material degradation, shortening of maintenance intervals, and added operating and maintenance costs to the added revenue generated from providing flexible capacity to the grid. Additionally, one has to take into account that although the TIT at baseload is above autoignition temperature of NG, the full air mass flow is running through the nozzles, in turn necessitating careful nozzle placement and design for the establishment of a steady flame.

5 Mk1 FHR Cost Estimation

5.1 Introduction

This chapter provides an initial study for costs of fluoride salt cooled high temperature reactors, with a focus on the Mk1 PB-FHR design. Understanding the costs of any engineered system is vital to in turn understanding whether or not such a system merits being constructed and will ultimately be profitable for the manufacturer and end user. When speaking of costs, one needs to recognize that costs are split into different categories, and within those categories into smaller sub-categories. Typically, one separates costs into capital and construction costs that are usually upfront costs, and operating and maintenance (O&M) costs that occur once the system is operational. O&M costs can be further broken down into fixed and variable, depending on whether they accrue regardless of production or not.

Determining the costs of the Mk1 PB-FHR nuclear air combined cycle (NACC) by itself, independent of its heat source, is not a necessarily useful or particularly insightful exercise. It can be considered as simply estimating and scaling the cost of a conventional combined cycle power plant, something that is relatively well understood as a low capital cost/volatile fuel and operating cost system. On the other hand, nuclear plants are generally known to be capital intensive systems with low operating costs. The NACC needs to be studied in unison with its heat source, in this instance the Mk1 PB-FHR, in order to give a true sense of its overall costs. For the following two chapters the combination of a NACC power conversion system with a Mk1 PB-FHR will simply be referenced as the Mk1.

Developing an appropriate cost estimation methodology considering the lack of any manufacturing data for the NACC required obtaining information from various sources and combining them appropriately according to best judgment. There are two methodologies to estimate costs, namely bottom up and top down approaches. In a bottom up approach one estimates costs based on primary inputs, such as amounts of materials, amount of labor required, etc. In a top down approach one inputs system parameters into cost models based on historical trends and data, such as the one suggested in Rothwell et al. [44]. For the Mk1 cost study presented here, a mixture of both top down and bottom up cost estimations was used depending on the type of cost considered. The mixing of cost estimation methodologies was necessary since the last U.S. nuclear plant to be connected to the grid was Watts Bar-1 in 1996 [45], therefore making most of the reactor cost data outdated. Furthermore, since the proposed technology is a combination of two different technologies, i.e. nuclear and NGCC, a mix or average of each technology's economic and operating characteristics was used.

The cost study separated costs into four broad categories, which are the capital/construction costs, operations and maintenance (O&M) costs, fuel costs and decommissioning costs. Carbon tax costs are discussed in the next chapter. All costs are assumed

for an N^{th} of a kind (NOAK)[1] plant unless otherwise stated. All costs have been adjusted to 2014 US dollars.

As a disclaimer, it is understood by the author that costs represented in this chapter might be underestimated due to the early design stage of the proposed system and the possible unintentional omission of unanticipated costs. This is in additional problem associated with a lack of historical costs for FHRs and the continuously changing construction, manufacturing, and project financing industry.

5.2 Construction Costs

Construction costs are split into several categories, including preconstruction costs, direct costs, and indirect costs. Each one was studied in sequence.

5.2.1 Preconstruction Costs

Preconstruction costs are all the costs that accrue prior to any physical construction work (e.g. site clearing, excavation, etc.). The main preconstruction costs when building a nuclear plant are the land and land rights, and the licensing and application fees. The input cost figures were taken from Gandrik et al. [46], based on NGNP Program Planning Bases for the Schedule and Cost Estimates [47].

The land rights are based on the Mk1 twelve unit (1200 MW_e) physical site arrangement presented in Andreades et al. [48]. It occupies a 950m by 751m owner-controlled area, which corresponds to 176.3 acres. Although overly simplistic, it was assumed that each single unit uses a twelfth of the land for the purpose of this study. The preconstruction costs for a single unit Mk1 (100 MW_e) include pre-application, early site permit and combined operating license application and review by NRC, state and local permitting, and support of construction and initial operation, and are presented in Table 5-1.

Table 5-1. Preconstruction costs for a single unit Mk1.

Description	Value	Unit	Reference
Licensing	78,864,500	$	[46], pg 11
Site Area	14.7	acres	
Land Cost	110,300	$/acre	[46], pg 11
Land and Land Rights	1,620,491	$	
Preconstruction Costs	80,484,991	$	

An important issue to note is that licensing fees dominate preconstruction costs. Licensing fees do not scale linearly with number of units, but rather increase marginally with added units. This is a potential drawback in building single unit plants, as the entire cost of licensing has to be borne by the single unit, rather than be split among several others. This effect

[1] NOAK is usually understood to mean the plant number at which point the benefits and cost reductions due to experience become relatively minor. The first plant of a product learning curve is termed First of a Kind (FOAK).

is demonstrated in Figure 5-1. Licensing costs increase from $78.8M for a single unit to $244.2M for a twelve unit site, whereas land and land rights correspondingly increase from $1.6M to $19.5M. The preconstruction costs per unit fall from $80.5M/unit for a single unit to $22M/unit for a "twelve pack."

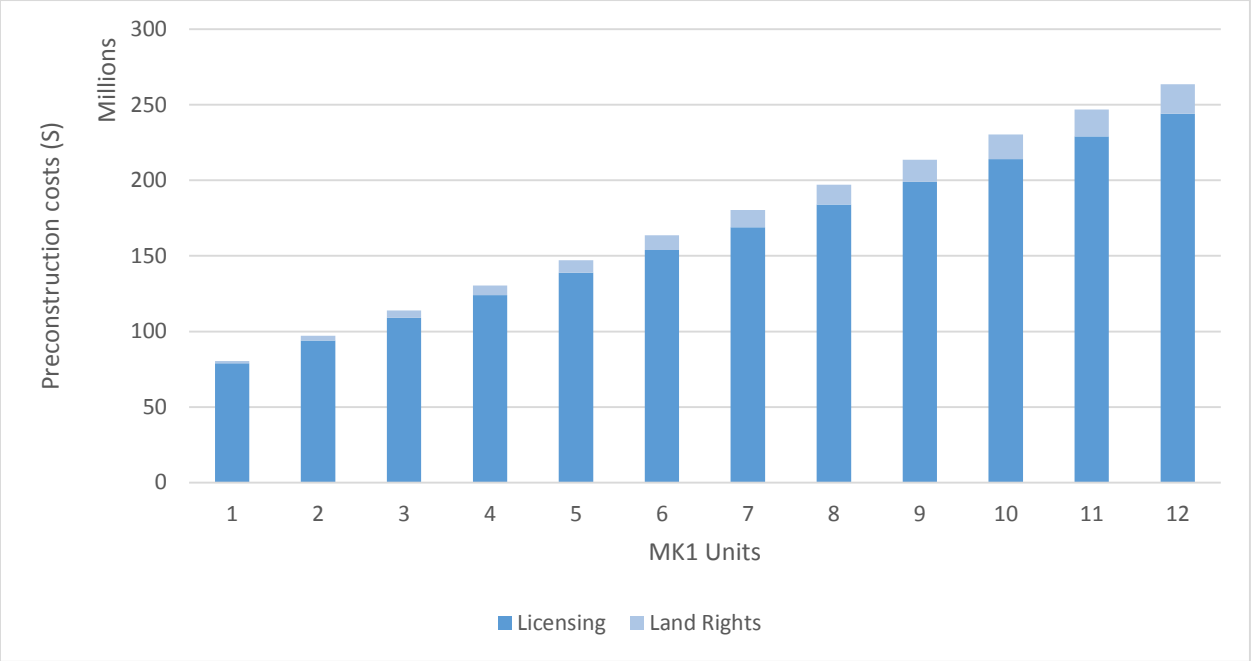

Figure 5-1. Preconstruction costs as a function of units on site

5.2.2 Direct Costs

The capital costs were estimated using a bottom up approach. The first step to understanding the Mk1's capital costs involved creating a materials inventory list. To estimate the capital/construction costs major classes of material used in plant construction were estimated from a combination of information from computer assisted design (CAD) software – Solidworks – and engineering estimates from THERMOFLEX/PEACE. The resulting material inventories along with material prices are displayed in Table 5-2. A more detailed breakdown of each category can be found in Zweibaum et al. [49].

Table 5-2. Mk1 material inventory and costs.

Material	Mass (MT)	Price ($/MT) [9]	Cost ($)
316 Stainless Steel	238.42	3,700	882,154
High-Alloy Steel	797.8	1,000	797,800
Carbon Steel	6,987.10	622	4,345,976
Concrete	42,508.30	42	1,785,349
Graphite	49.25	17,700	871,725
Flibe	91.9[2]	176,000	16,174,400
Total			24,857,404

The total cost of simply multiplying raw material prices with material quantities is around one and half orders of magnitude below anticipated and general historical costs of reactor construction and cannot be considered an accurate method of cost estimation, as also concluded by Peterson et al. [50]. The fact that fabrication, machining, transportation, assembly, construction, engineering, quality assurance and other costs aren't included in the raw materials prices explains this discrepancy. On the other hand, it also points out that construction costs should be relatively insensitive to raw material price variations.

A second approach to construction cost estimation was to use the cost of an existing and known technology, i.e. NGCC, and by analogy scale the Mk1 materials and costs to the NGCC costs. This analysis was performed by setting up a conventional 4x1 NGCC unit similar to the Mk1 NACC in THEFRMOFLEX using a GE 7FB gas turbine, as depicted in Figure 5-2**.**

[2] Flibe costs are estimated from the major constituents of flibe, beryllium ($770/kg) and lithium ($63/kg), or resulting in $79/kg for flibe [73]. Added to it is the cost of enriching lithium to 99.995% ^{7}Li with 0.97 SWU/kg at a cost of $100/SWU [48].

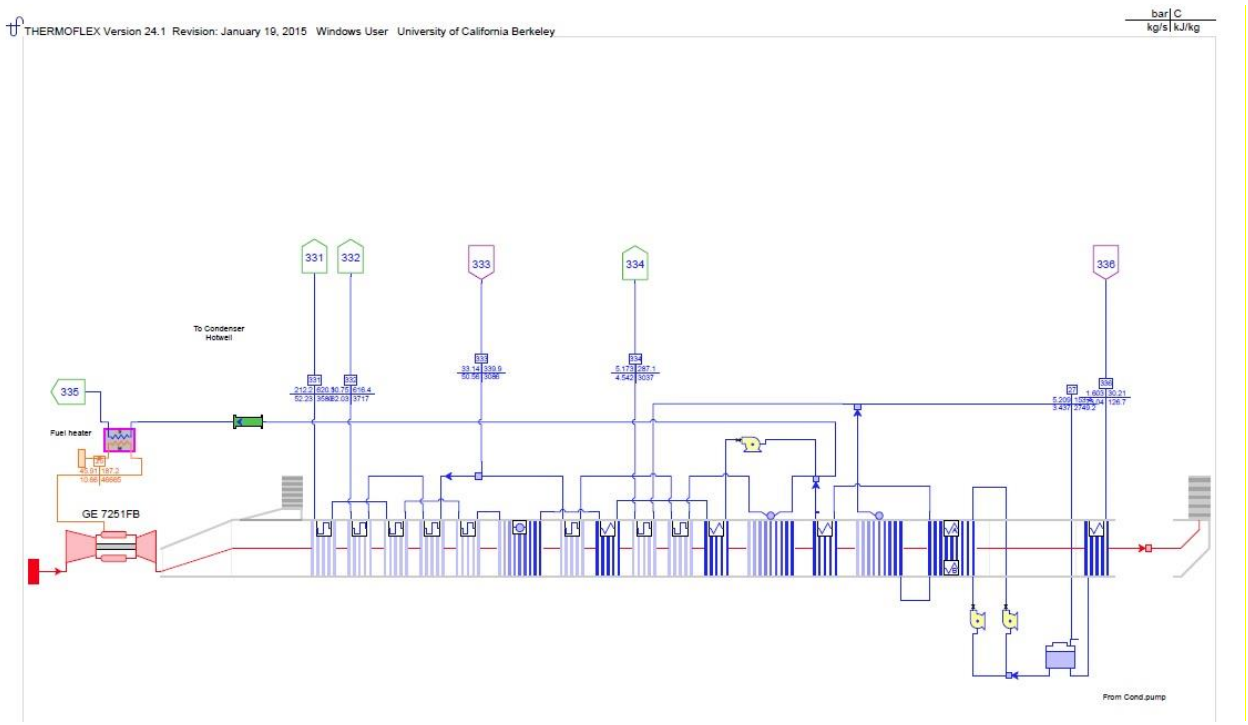

Figure 5-2. GE 7FB CC THERMOFLEX schematic flow diagram.

Material inventory numbers from PEACE listed costs for concrete volumes and masses, including the civil labor, excavation, etc. as well as steel masses for the HRSG and steam turbine assembly. PEACE also estimated additional costs, such as owner soft costs and profit margins among others. These were not included in the cost scaling to the Mk1 for direct costs, as they were accounted for later in the analysis. The resulting numbers are displayed in Table 5-3**.**

Table 5-3. GE 7FB CC material inventory and prices.

		Mass (MT)	Cost ($)	Price ($/MT)
ST	Steel	1153	77,667,764	67,361
	Concrete	3912	4,709,236	1,204
HRSG	Steel	2170	32,966,000	15,192
	Concrete	5568	3,859,000	693
Turbine	316SS	80	54,900,000	686,250

PEACE's concrete volumes were converted to masses using a concrete density of 2400 kg/m^3. Additionally, for Mk1 scaling purposes HRSG steel numbers were considered to be carbon steel, whereas steam turbine steel was considered to be 316SS. In order to estimate a high alloy steel price, an interpolation between the PEACE carbon steel and 316SS prices was performed based on Table 5-2 prices. The graphite price was also multiplied by a factor of 21.7 to account for manufacturing, transportation, and installation, according to the average of raw material to installed cost of other material categories. The resulting scaling from the GE 7FB to the Mk1 is displayed in Table 5-4.

Table 5-4. Single unit Mk1 material inventory and scaled direct costs.

Material	Mass (1000 kg)	Price ($/1000 kg)	Cost ($)
316 Stainless Steel	238.4	67,361	16,058,972
High-Alloy Steel	797.8	21,599	17,231,297
Carbon Steel	6987.1	15,192	106,145,962
Concrete	42508.3	948	40,316,148
Graphite	49.25	384,134	18,918,600
Flibe	91.9	176,000	16,174,400
SUM			**214,845,380**

From the above table it becomes apparent that carbon steel dominates the overall direct costs due to its sheer quantity (found in rebar, HRSG, ducting, etc.). The second contributor to direct costs is concrete; even though its per unit cost is an order of magnitude lower than the rest of the materials, its sheer volume makes up for it. An additional insight from the above table is the fact that no single material is a negligible cost contributor. This might signify that replacement of 316SS with a more exotic material, say Hastelloy N, might have a substantive impact on the overall direct costs.

A final remark to be made is that the direct costs presented in Table 5-4 lack several other classes of materials that there is no estimate for, such as copper, paint, cabling, etc., and might therefore be on the low side. Looking into material inventories of a typical 1000 MW_e LWR, displayed in Table 5-5, it is evident that materials other than concrete and steel are found in smaller quantities and their omission in this study should not have a significant impact on the overall capital cost. Copper is mainly found in the power conversion system, which THERMOFLEX/PEACE already accounts for in its cost estimation.

Table 5-5. Estimated quantities of composite materials contained in a typical 1000 MW_e PWR power plant, including field construction materials consumed [51].

Material	Total estimated quantity
Aluminum, metric tons	18
Babbit metal, metric tons	<1
Brass, metric tons	10
Bronze, metric tons	25
Carbon steel, metric tons	32,731
Concrete, yd3	98,130
Copper, metric tons	694
Galvanized iron, metric tons	1,257
Inconel, metric tons	124
Insulation (thermal), metric tons	922
Lead, metric tons	46
Nickel, metric tons	1
Paint, gal	17,500
Silver, metric tons	<1
Stainless steel, metric tons	2,080
Wood, bd ft	4.8×10^6

5.2.3 Indirect Costs and Project Contingency

Indirect costs are costs not involved with the direct construction costs of the project. These costs can include home and field office engineering services, construction managements, scheduling, quality inspections, site safety, general and administrative expenses, etc. These costs were estimated as a percentage of direct costs, in line with previous supplier estimates and historical LWR costs. Gandrik et al. [46] estimate an indirect cost of 57% based on the previously mentioned sources. Indirect costs, which include a final design fee for an NOAK unit, are presented in Table 5-6.

Table 5-6. Total indirect cost for a single unit Mk1.

Description	Value	Unit	Reference
Final Design	20,000,000	$	[46], pg. 17
% of Total Direct Cost	57	%	[46], pg. 17
Indirect Cost	**142,462,635**	$	

Additionally, a project contingency of 20% was added to the overall capital cost. The total capital investment for a single and twelve unit Mk1 FHR power plant is presented in Table 5-7.

Table 5-7. Total capital cost for a single unit Mk1 FHR.

Description	Single Unit	12 Unit	
Preconstruction Costs			
Licensing	78,864,500	244,176,625	$
Site Area	14.7	176.3	acres
Land Cost	110,300	110,300	$/acre
Land and Land Rights	1,620,491	19,445,890	$
Preconstruction Costs	80,484,991	263,622,515	$
Direct Costs			
Total Direct Cost	214,846,727	2,578,160,727	$
Indirect Costs			
Final Design	20,000,000	240,000,000	$
% of Total Direct Cost	57	57	%
Indirect Cost	142,462,635	1,709,551,614	$
Project Contingency			
Contingency	20	20	%
Total Contingency	71,461,872	857,542,468	$
Total Capital Investment	**509,256,225**	**5,408,877,325**	$
Specific Capital Investment (Nuclear)	**5,093**	**4,507**	$/kW
Specific Capital Investment (CF)	**2,133**	**1,870**	$/kW

The total specific cost ranged from $4,500-5,100/kW depending on the number of units at the plant site. Two specific costs are provided, one taking into account only the 100 MW nuclear output provided by the Mk1 and one taking into account the added 142 MW output from the NACC's cofiring capability. An important point to clarify is that the Mk1 should be compared in terms of economics to a combination of a standalone nuclear and NGCC rather than with each one separately.

5.3 Operation and Maintenance Costs

The previous section dealt with capital costs. Capital costs are generally paid upfront and are amortized over the lifetime of the reactor. On the other hand, operation and maintenance (O&M) costs are incurred during the lifetime of the reactor and are associated with its continued operation. Furthermore, O&M costs are generally split into fixed and variable. Fixed O&M costs are incurred regardless of whether the system is producing any output or not, such as license fees and payroll, whereas variable costs depend on the amount of output produced by the system.

There are different ways to calculate O&M costs, whether it be a bottom up approach as outlined in Gandrik et al. [46], a top down approach outlined in Rothwell and Ganda [44], or by interpolating available numbers in historical series provided by various agencies, such as the U.S. Energy Information Administration (EIA) [52]. The preferred method for this chapter was the

former, since it provides a look into details of O&M costs. The latter two methods will be used as a comparison in future work.

The initial step to estimating O&M costs was to figure out the overall plant payroll. Payroll has two components, namely the amount of labor and the price of that labor. Staffing estimations were taken directly from Gandrik et al. [46] for a single unit and for each additional unit. The cost of staffing was estimated by multiplying the amount of staffing by the average electric power worker compensation for 2014 [53], adjusted upward by 61.7% to account for overtime (7.5%), retirement benefits (38.5%), bonus and incentives (8%), and payroll taxes (7.7%) [54].

Overhead and fees are based on numbers presented in the INL report [46], whereas outage costs are scaled to an assumed outage cost of \$12M/year for 1,200MW_e LWR [54]. The results are presented in Table 5-8.

Table 5-8. Annual O&M costs for Mk1.

Description			Unit	Source
Total Plant Staff	382	382		[46], pg. 39
Staff per Additional Unit	71	71		[46], pg. 39
Total Units	1	12		
Average Base Salary	72,800	72,800	$	[53]
Total Benefits	61.7	61.7	%	[46], pg. 37
Total Salary	117,718	117,718	$	
Total Payroll	44,968,123	136,905,569	$	
Overhead and Fees	17,118,560	17,118,560	$	[46], pg. 37
Overhead and Fees per Additional Unit	14,327,970	14,327,970	$	[46], pg. 37
Total Annual O&M	62,086,683	311,631,799	$	
Specific Annual O&M	70.88	29.65	$/MWh	

Similar to preconstruction costs, adding more units to the power plant site spread the fixed O&M costs and reduced the overall specific annual O&M. A discrepancy in staffing levels was found in the INL report with the design supplier providing a lower estimate than the report authors. The discrepancy has a significant effect on annual O&M costs when there is a small number of units on site, but nearly levels out once the Mk1 site has twelve units. Both effects are demonstrated in Figure 5-3.

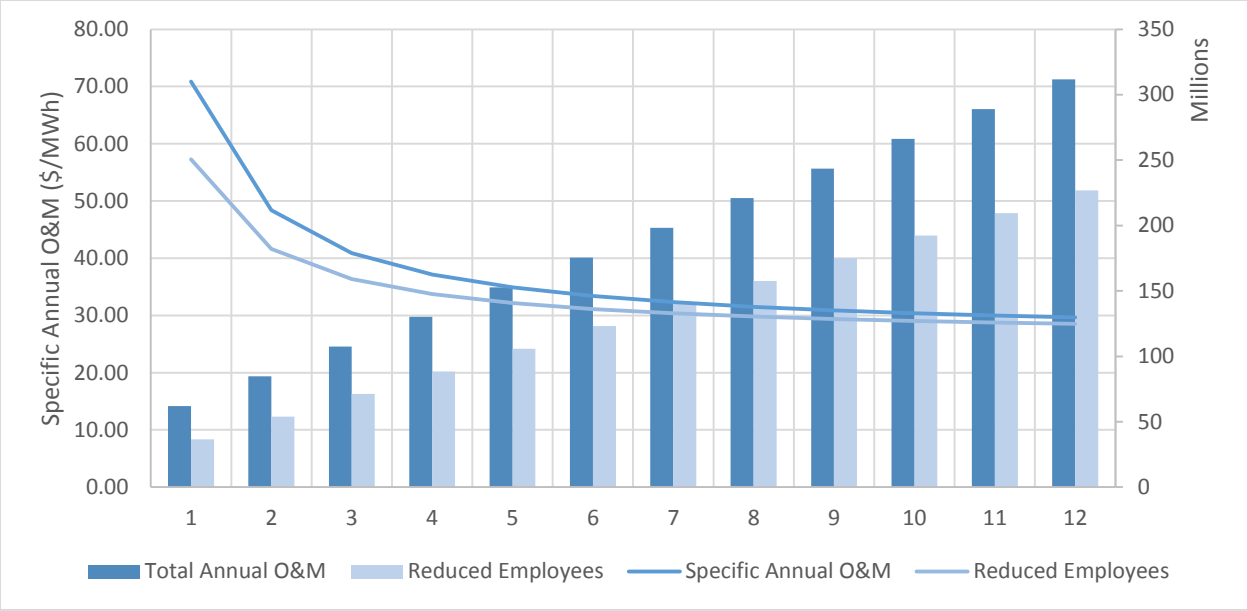

Figure 5-3. Annual O&M Costs as a Function of FHR Units.

There are two sources of variable O&M costs for the Mk1, one from the nuclear component and the other from the NG component of the NACC. Nuclear variable O&M costs are estimated based on fuel and decommissioning costs presented in the next section. NG variable O&M costs are based primarily on NG price and are simply estimated at 3.37 $/MWh using the numbers from the EIA report [52] and are displayed in Table 5-9. An important note to make is that the EIA's numbers didn't necessarily take into account the two-shift operation of the advanced CC that is becoming quite common now due to the deregulated nature of electricity markets. This type of cycling imposes additional costs on top of those stated above and are displayed alongside the EIA numbers [55]. The cycling costs are dependent upon the type of load change (i.e. hot/warm/cold start or load following) and are multiplied by a factor of 1.2 to 4 according to the speed of the ramp rate compared to normal (1.1 to 2x). More details on the cycling costs can be found in Kumar et al. [55].

Table 5-9. Estimates of Advanced NGCC operating costs (2014$) [52, 55].

Description	Value	Unit
Capacity	400	MW
Fixed O&M Cost	15.85	$/kW-yr
Variable O&M Cost	3.37	$/MWh
Startup Cost	1.00	$/MW cap
C&M Cost Startup	29-106	$/MW cap
C&M Cost Load Follow	0.32-0.78	$/MW cap

The Mk1 has the capability for significant rather than shallow load following, and its charges were considered to fall under the hot start regime. For these reasons the lowest C&M

costs of an advanced CC were added and adjusted with a fast ramp rate multiplication factor of 2. The physical effects due to higher cycling are discussed in a previous chapter.

5.4 Fuel Costs

The fuel costs were estimated using the basic design parameters for the Mk1 fuel presented by Andreades et al. [48] and the methodology presented by Gandrik et al. [46]. All fuel costs were estimated for a single unit Mk1 plant. For a twelve unit Mk1 power plant requirements are multiplied twelvefold. The fuel design parameters are given in Table 5-10.

Table 5-10. Mk1 fuel design parameters.

Description	Symbol	Value	Units	Reference
Number of fuel pebbles	Pebbles	470,000		[48], Table 2.1
Average Uranium Loading	Loading	0.0015	kg/pebble	[48], Table 2.1
Average Fuel Enrichment	x_P	19.9	%	[48], Table 2.1
Fuel Cycle Length	FCL	16.8	months	[48], Table 2.1
Mass of Heavy Metals per Refueling Segment	P	705	kg	

In order to estimate the annual uranium product requirements, M_P, from the above table the number of pebbles per core multiplied by their uranium content, yields the product P, which is then scaled by the fuel cycle length, FCL. Mathematically:

$$M_P = \text{Pebbles} \cdot Loading \cdot \frac{12}{FCL} \tag{5-1.}$$

Using basic mass balances for product, feed, and tailings as described in Lamarsh and Barata [56], the separative work unit (SWU) requirements were estimated using equations 5-2 through 5-5, and are presented in Table 5-11.

$$M_F = M_P + M_T \tag{5-2.}$$

$$x_F \cdot M_F = x_P \cdot M_P + x_T \cdot M_T \tag{5-3.}$$

$$SWU = M_P \cdot V(x_P) + M_T \cdot V(x_T) - M_F \cdot V(x_F) \tag{5-4.}$$

$$V(x) = (1 - 2x) \cdot \ln\left(\frac{1-x}{x}\right) \tag{5-5.}$$

Table 5-11. Annual uranium requirements for Mk1 core.

Description	Symbol	Value	Units	Reference
Uranium in Tailings	x_T	0.3	%	
U235 in Natural Uranium	x_F	0.72	%	
Uranium in U3O8	U/U3O8	85	%	
Uranium Product	M_P	504	kg	[46], pg. 40
Uranium Feed	M_F	19,078	kg	[46], pg. 40
U3O8 Feed		22,444	kg	[46], pg. 40
Tailings	M_T	18,574	kg	[46], pg 40
Separative Work Units	SWU	22,722	kg-SWU	[46], pg 40

Having obtained physical annual uranium feed and product requirements for the Mk1, the next step involved calculating the cost of core refueling. Uranium ore, conversion and enrichment costs were obtained from the Ux Consulting Company, LLC (UxC) [57]. Fuel fabrication costs vary from approximately $275/kg for LWRs [58] to the estimated $10,609/kg from Gandrik et al [46], based on the Advanced Fuel Cycle Cost Basis [59]. An intermediate value of $5,000/kg was used. Spent fuel storage and disposal costs were obtained from the Nuclear Energy Agency fuel cycle report [58]. The results are presented in Table 5-12.

Table 5-12. Annual fuel costs for a single unit Mk1 FHR.

Reactor Phase Description	Symbol	Annual Usage (kg)	Unit Cost ($/kg)	Annual Cost
Uranium Ore (U3O8)		22,444	111	$2,499,473
Uranium Conversion	M_F	19,078	8	$152,621
Uranium Enrichment	SWU	22,722	90	$2,045,006
Tails Disposal	M_T	18,574	12	$225,359
Fuel Fabrication	M_P	504	5,000	$2,517,857
Spent Fuel Storage		705	140	$98,700
Spent Fuel Disposal		705	300	$211,500
Total - Annual Cost				$7,750,516
$/MW$_e$-hr				$9.67

Initial core fuel loading cost for a single and twelve unit Mk1 power plant would be $10.9M and $130.2M respectively. LWRs generally have fuel costs of around $6/MWh. The main driver in the price difference between the Mk1 fuel and LWR fuel is the higher enrichment of the FHR pebble fuel of 19.9% compared to approximately 3% for LWRs, and the shorter fuel cycle length of 16.8 months (FHR) compared to 36 months (LWR). Additionally, the higher assumed fuel fabrication costs compared to conventional LWR fuel also increase the price of Mk1 fuel. A caveat to mention is the wide range of unit costs in literature which creates uncertainty in estimating fuel prices for the Mk1. A range of $6.49/MWh on the low side to $16.91/MWh on the high side was estimated.

5.5 Decommissioning Costs

The Nuclear Regulatory Commission (NRC) provides a report that outlines a methodology for estimating the minimum required decommissioning fund that needs to be available for a power plant. All of the information is based on conventional PWRs and BWRs, but it is assumed here that one can extrapolate to other reactor types. The decommissioning costs were thus estimated using the methodology presented in NUREG 1307, Rev. 15 [60].

The basic formula for estimating the minimum decommissioning fund is presented below.

$$EstimatedCost(YearX) = [1986\$Cost] \cdot (A \cdot L_x + B \cdot E_x + C \cdot B_x) \quad 5\text{-}6.$$

Where the estimated decommissioning costs in year X dollars are estimated using the 1986 estimated decommissioning costs adjusted by the labor, materials, and services fraction (A) multiplied by a labor, materials, and services cost adjustment (L_x), the energy and transportation fraction (B) multiplied by an energy and waste transportation cost adjustment (E_x), and the waste burial fraction (C) multiplied by a low level waste burial cost adjustment (B_x). The results are displayed in Table 5-13.

Table 5-13. Estimated specific decommissioning costs.

Item	Value	Unit	Reference
C1986	118,425,000	$	NUREG-1307 v15, pg 6
A	0.65		NUREG-1307 v15, pg 5
B	0.13		NUREG-1307 v15, pg. 5
C	0.22		NUREG-1307 v15, pg. 5
L_x	2.40		NUREG-1307 v15, pg.7
E_x	2.75		NUREG-1307 v15, pg. 8
B_x	28.80		NUREG-1307 v15, pg. 4
Estimated Cost	1,007,829,568	$	NUREG-1307 v15, pg.3
Power	3400.00	MW_{th}	
Specific Cost	296,420	$/$MW_{th}$	

The specific cost is estimated to be approximately \$296,420/MW_t. The decommissioning costs for a single unit and twelve unit Mk1 are shown in Table 5-14.

Table 5-14. Estimated decommissioning costs for a single and twelve unit Mk1.

Mk1 Units	Thermal Output [MW_{th}]	Decommissioning Cost [$]	Specific Cost [$/MWh]
1	236	69,955,229	1.33
12	2832	839,462,746	1.33

As shown, decommissioning costs were estimated to be insignificant over the anticipated 60 year operating lifetime of the Mk1.

5.6 Discussion

Estimating the cost structure of a system is a vitally important part of assessing its overall profitability. This chapter tries to quantify the costs of a Mk1 using a combination of top down and bottom up approaches. Capital costs were estimated using an inventory of major classes of materials and scaling their cost to those of known conventional systems. An overall capital cost of $4,500-$5,093/kW base load was estimated depending on the number of units, ranging from one to twelve, present at the power plant site. Having more units on site spreads out fixed costs and reduces the specific cost. When comparing the Mk1 to other plants it is important to take into account its ability to produce added electricity at essentially no additional capital cost, since all infrastructure required is already present and accounted for, which reduces the specific capital to $1,870-2,133/kW base load plus peaking. These numbers should be compared to capacity weighted average capital costs of a NGCC and a conventional nuclear power plant, rather than each separately. O&M costs, along with fuel and decommissioning costs, which together constitute the marginal cost of electricity production for the baseload nuclear output were also estimated. The marginal cost of production for the peaking output is simply the cost of NG, which is not considered here due to its highly volatile price. Similar to capital construction costs, O&M costs drop from $81.05/MWh (¢8.1/kWh) to $39.82/MWh (¢3.98/kWh) as the number of units per site increase from one to twelve. The overall results are demonstrated in Table 5-15.

Table 5-15. Overview of Mk1 costs.

Description	Single Unit	12 Unit	
Capital Construction Costs			
Preconstruction Costs	80,484,991	263,622,515	$
Total Direct Cost	214,846,727	2,578,160,727	$
Indirect Cost	142,462,635	1,709,551,614	$
Total Contingency	71,461,872	857,542,468	$
Total Capital Investment	509,256,225	5,408,877,325	$
Specific Capital Investment (Nuclear)	**5,093**	**4,507**	$/kW
Specific Capital Investment (CF)	**2,133**	**1,870**	$/kW
Production Costs			
Total Annual O&M	62,086,683	311,631,799	$
Fuel Cost (annual)	7,750,516	93,006,192	$
Decommissioning Cost (annual)	1,165,920	13,991,046	$
Overall Production Cost	71,003,119	418,629,037	$
Marginal Production Cost	**81.05**	**39.82**	$/MWh

A comparison of other methodologies of capital and O&M cost estimation, such as drop down or scaling to nuclear power plants currently under construction (e.g. AP1000's at Vogtle

and VC Summer), are subject to future study. Additionally, a cost comparison between competing generation technologies to the Mk1 is planned and to be performed.

6 Supplementary Cycle Configurations and NACC Alternatives

6.1 Introduction

Up to this point, only commercial scale NACC configurations were considered. There might however be some value in considering alternative applications or scales for the NACC or an altogether different power conversion system. This is the focus of this chapter.

One alternative configuration that might be applicable for the NACC is a mobile/small scale unit. NACC at such a scale might serve as a proof of concept initially and can be subsequently used for appropriate applications that demand power in the range of 10 MW_e, e.g. remote locations, small scale electricity/power generation.

It is also prudent to juxtapose the NACC to an alternative power conversion system that might be well suited for similar applications. To this end, a supercritical carbon dioxide (S-CO_2) Brayton cycle was explored for use with the Mk1 PB-FHR. A head to head technical comparison is then performed between it and the NACC.

6.2 Simple and Combined Cycle NACC for Mobile Applications

This section is an adapted version of the stimulated summary "Simple and Combined Cycle Power Conversion with Natural Gas Co-Firing, for Mobile PB-FHR" by Andreades et al. [61]*. Copyright granted 24 April, 2015 by the American Nuclear Society, La Grange Park, Illinois.*

Manufacturing a commercial scale system requires several iterations and a stepwise approach. Between studying performance on paper and a final product, an intermediate step to commercialization is the creation of a proof of concept or demonstration system. Such systems usually tend to be scaled down version of the final product.

In the NACC's case there is a multitude of smaller gas turbines (GT) that lend themselves readily to such a purpose. Aeroderivative GTs in the 10MW_e range are widely available from several manufacturers, as shown in Table 6-1, that can be used either for electricity production or mechanical drive applications.

Table 6-1. Commercially available 10MWe aeroderivative GTs.

Manufacturer	Model	Power output (MW)	Mass flow (kg/s)	PR	Efficiency (%)	RPM	Exhaust temp (°C)	Shaft
GE	10-1	11.25	47	15.6	31.1	11000	481	1
GE	10-2	11.7	47	15.6	32	11000	482	2
Hitachi	H15	13.9	49	14.3	31.1	7280	556	1
Rolls Royce	SpeySK15	11.6	57	18.5	39.6	5220	396	3
Siemens	SGT-400	12.9	39	16.3	34.8	9500	555	2
Solar	Titan 130	12.8	49	15.7	33.3	11218	474	1

Advancements and improvements in aeronautical GTs have trickled down to land based GTs; however, not all of the features of Aeroderivative machines are suitable for use with the

NACC. Therefore, it is important to select a machine that will make the proof of concept more manageable/easier to perform.

Proof of concept aside, due to its combined cycle configuration the NACC can perform several combined processes such as industrial steam production, hydrogen production, advanced multi-effect distillation, etc. Furthermore, its ability to co-fire with NG yields increased turbine inlet temperatures (TITs) and power output for peaking operation. The flexibility of NACC power conversion allows it to provide a wide range of grid support and process heat services. All these features are attractive for mobile applications. The small size of aeroderivative GTs allow for quick deployment, ease in servicing and maintenance (can be swapped out with loaner GTs), and suit themselves well to remote applications due to their ruggedness, ability to produce peak power on demand, and to couple to collocated processes.

This section examines the GT selection, namely the GE 10-1, several parameters that are important in coupling a commercial GT to a nuclear heat source, suggests a possible system configuration, necessary modification, and evaluates its performance. The cycle setup and optimization is similar to the commercial scale NACC outlined in an earlier chapter, therefore only performance results without in-depth methodology and a condensed modification list are presented.

6.2.1 Gas Turbine Selection and Modification

For the purposes of a mobile/small NACC the GE 10-1 (single shaft) GT was selected as a baseline. This particular GT has an external, silo-type combustor, which allows for easier modification and connection of air ducts that route back to a reactor to heat up the air. Its performance characteristics are shown in Table 6-2.

Table 6-2. GE 10-1 characteristics.

Description	Value	Unit
GT	GE 10-1	
PR	15.6	
TIT	1077	°C
TET	481	°C
Mass Flow	47	kg/s
Power	11.25	MW
Efficiency - LHV	31.1	%
Price	5.6	MM$

There are several configuration possibilities for setting up a nuclear heated GT, among which are a simple cycle, a simple cycle with reheat, and a combined cycle with reheat. For the purposes of this study, the procedure and results from the combined cycle with reheat are shown, since this is the most advanced and efficient configuration.

The basic layout is nearly identical to the Mk1 system and is as follows:

i) Air intake occurs through a filter bank, and the air is compressed and reaches a temperature between 380°C and 450°C, depending on compressor pressure ratio (PR) and ambient conditions.

ii) After the compressor outlet, the air passes through a high-pressure (HP) coiled tube air heater (CTAH) and is heated up to a TIT between 660 to 680°C.

iii) The air is then expanded down to approximately the same temperature as the compressor outlet temperature. This criterion determines the expansion ratio (ER) of the first expansion stage at design conditions.

iv) The air is then reheated back up to 660-680°C by passing through a second low-pressure (LP) CTAH.

v) After the LP CTAH, the air is above the auto-ignition temperature of natural gas. To provide power peaking, natural gas (or another fuel) can be injected and burned to increase the turbine inlet temperatures and the power output.

vi) The heated air is then expanded down to nearly atmospheric pressure and 300-650°C by passing through an additional set of turbine blades, before entering the HRSG.

A model of the proposed layout is shown in Figure 6-1 and Figure 6-2. The HRSG and steam cycle are not included.

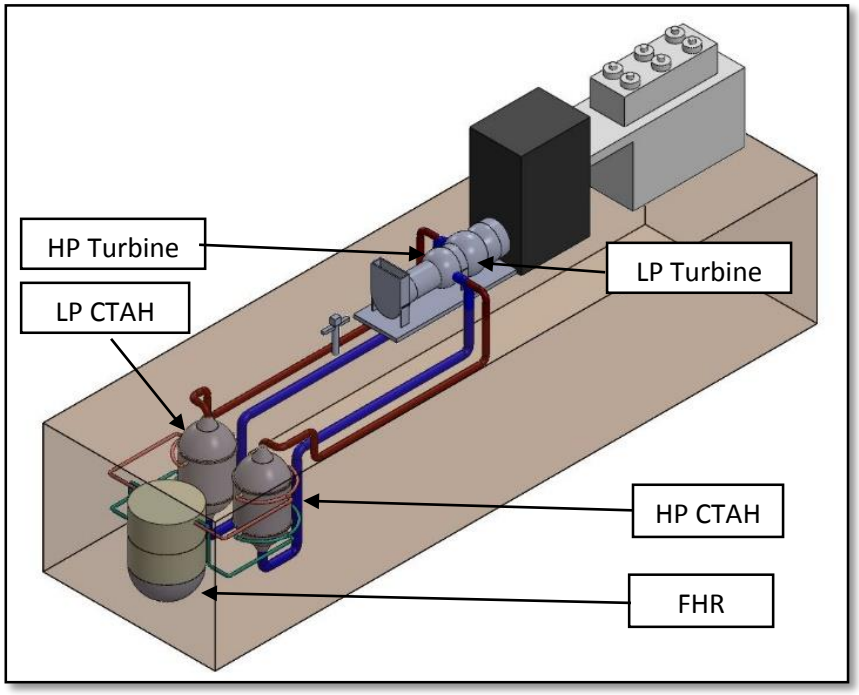

Figure 6-1. SC GE 10-1 layout w/ reactor - Isometric view.

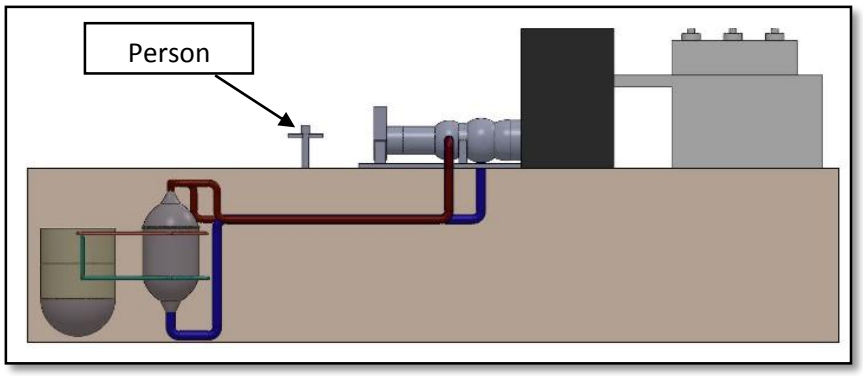

Figure 6-2. SC GE 10-1 layout w/ reactor - Elevation view.

To add the stage of reheat, the shaft between the first and second row of turbine blades needs to be expanded by adding a spool. Moreover, a second silo needs to be added to the casing in order to fit the ducting for the LP CTAH. Overall, the modifications are similar to the commercial Mk1 NACC and are not elaborated on further.

6.2.2 Modeling and Results

In order to model the NACC, THERMOFLEX® (v.23) was used. THERMOFLEX is a fully-flexible program for thermodynamic heat balance modeling and engineering with a graphical user interface. To configure and optimize the NACC it is necessary to first optimize the Brayton cycle separately and subsequently the Rankine cycle for maximum efficiency and power output. The optimization was performed at standard ISO conditions, i.e. 15°C, 60%RH, 0 m altitude.

The addition of reheat introduces a new parameter to be optimized to extract maximum power and efficiency from the system - the distribution of expansion ratios between the two turbines. Using THERMOFLEX®, a series of optimizing exercises was performed for both the baseload and co-firing operation modes. The results of each optimization are shown in Table 6-3 and Table 6-4.

Table 6-3. SC w/ reheat optimization – Baseload.

Description	Value	Unit
Turbine (1) Expansion Ratio	3.5	
Turbine (2) Expansion Ratio	3.84	
Turbine Exhaust Temperature	429.7	°C
Net Power	5797	kW
Net Efficiency	21.86	%
Heat Exchanger (1) UA	158.3	kW/°C
Heat Exchanger (1) Heat Transfer	13914	kW
Heat Exchanger (2) UA	156.6	kW/°C
Heat Exchanger (2) Heat Transfer	12337	kW

Table 6-4. SC w/ reheat optimization – Co-fired.

Description	Value	Unit
Turbine (1) Expansion Ratio	1.4	
Turbine (2) Expansion Ratio	9.6	
Turbine Exhaust Temperature	293.4	°C
Net Power	12229	kW
Net Efficiency	30.68	%
Heat Exchanger (1) UA	158.3	kW/°C
Heat Exchanger (1) Heat Transfer	13914	kW
Heat Exchanger (2) UA	320.3	kW/°C
Heat Exchanger (2) Heat Transfer	3665	kW

As the tables show, the baseload configuration is optimized when the pressure ratios for the two turbines are approximately equal, while the co-fired configuration is optimized when the expansion ratio for the second turbine is much larger than the first. This is evident since power extraction from the NG happens in the second expansion stage, therefore the larger the LP ER the larger the power extraction.

To best answer the question of how to best compromise the optimization of the baseload and cofiring configurations, better information on the specific energy markets which the reactor serves must be known. If the reactor is to spend most of its time in co-firing mode, then it should be optimized accordingly and vice versa. However, it is important to note an important difference between the results in the previous tables. In the case of the baseload optimization, both the heat exchanger sizes and turbine parameters are very similar, while in the co-firing optimization they are quite different. This addition of complexity and non-uniformity may contribute additional design difficulties as well as incur extra costs that may offset the benefits of increased power. A thorough cost-benefit analysis of these concerns provides an area of further research.

The next optimization step deals with the determination of the optimum conditions for the dual pressure Rankine cycle. This cycle allows the NACC to capture the maximum amount of useful power from the waste heat expelled by the air cycle.

As before, the addition of these components provides the loop with additional parameters for optimization, in this case the steam pressures. An optimization study was conducted in both baseload and co-firing. However, before these exercises were performed, a model was run for the co-firing operation to determine the proper size of the condenser such that it could be rated to reject the maximum amount of heat dealt to it.

To optimize the Rankine cycle, the inlet air temperature into the HRSG is fixed below 700°C - a material constraint - and the cycle's HP and LP values are varied iteratively until they converge at an optimum value. The results are summarized in Table 6-5 and Table 6-6.

Table 6-5. Rankine cycle optimization – Baseload.

Description	Value	Unit
HPT Design point inlet pressure	5.2	MPa
LPT Design point pressure	0.3	MPa
Net power	9882	kW
Net efficiency	35.17	%

Table 6-6. Rankine cycle optimization – Co-fired.

Description	Value	Unit
HPT Design point inlet pressure	12.6	MPa
LPT Design point pressure	1.9	MPa
Net power	22590	kW
Net efficiency	42.85	%

As before, the results for baseload optimization differ from the results for co-firing optimization. However, no cost-benefit analysis need be done on these results since the inlet pressures are sliding and can be adjusted online during operation. Alternatively, pressures can be fixed within a certain range with inlet valves.

One important parameter to look at is the cofiring efficiency, which is the efficiency with which natural gas burning is converted to electricity. Its definition is as follows:

When, calculating the cofiring efficiency for the simple cycle, cycle with reheat, and combined cycle, an important result is obtained as can be seen in Table 6-7. The nuclear heated GT system has a natural gas co-firing efficiency much greater than that of any conventional GT in its size range. Because of the fuel prices in carbon markets, this implies that an FHR coupled with natural gas co-firing will always have a distinct advantage over conventional natural gas plants; because of its higher efficiency in converting NG to electricity, its marginal cost will be lower and it will be dispatched before similar conventional NG plants.

Table 6-7. Co-firing efficiencies.

Description	Value	Unit
SC (GT – normal)	31.4	%
SC (nuclear heated)	43.1	%
CC w/ reheat	52.8	%

Finally, Figure 6-3 is a depiction of the thermodynamic T-s diagram of the proposed NACC. The lines connecting the operating states are arrows since the exact path between states is not known.

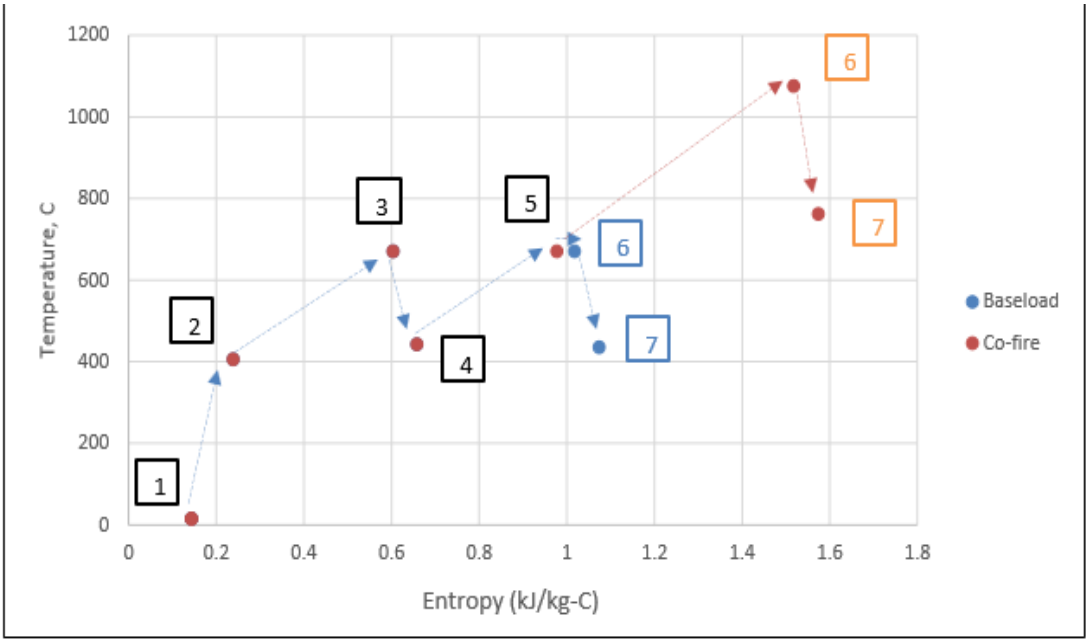

1. **Inlet of Compressor**
2. **Inlet of First Heat Exchanger**
3. **Inlet of Turbine (1)**
4. **Inlet of Second Heat Exchanger (Reheat)**
5. **Inlet of Combustor**
6. **Inlet of Turbine (2)**
7. **Exhaust to Atmosphere**

Figure 6-3. NACC T-s diagram - baseload and co-fired.

6.2.3 Discussion

It is concluded that the NACC system would be more efficient for electricity production with natural gas than conventional natural gas plants. This has important implications for the economic viability and competitiveness of small FHR reactors. This section features results of optimization exercises for both the simple cycle with reheat as well as the combined cycle. Further, as discussed earlier in this section, a more detailed study of economic environments in which the FHR will operate is necessary in order to better understand whether the models should be optimized to operate in baseload mode for the majority of their operation or with natural gas co-firing. This economic analysis will allow for practical optimization of each power conversion model.

Moreover, the fact that the NACC can push nuclear electricity production out of a baseload electric generator into a generator that can provide ancillary services can significantly benefit both the plant operator, by providing extra revenues, and the grid operator, by providing flexible capacity in times of need.

6.3 Supercritical Carbon Dioxide (S-CO_2) Power Conversion

S-CO_2 power cycles have been investigated for several decades, dating back to the 1940's, because of the performance benefits they could provide when operating near the critical point of CO_2. CO_2 shows properties of a real gas and its extremely high density near its critical point

allows the compression work in a Brayton cycle to be reduced significantly compared to an ideal gas. This in turn demands less turbine work to be used to drive the compressor so that more power is available for the generator. Several cycle options have been discussed and analyzed including condensing, intercooled, reheated, and recompressing among others [62, 63, 64]. Recently, S-CO_2 power conversion development has focused primarily on TITs in the range from 480°C to 550°C, appropriate for current-generation SFR technologies. Here we examine high temperature S-CO_2 cycle designs, which could be coupled to higher-temperature heat sources, allowing turbine inlet temperatures in the range from 600°C to 700°C, such as FHRs and CSP. In this temperature range current structural materials such as 316 stainless steel and Alloy N have significantly reduced allowable stresses than at lower temperatures, creating challenges in the design of the high temperature heat exchangers. Here one must trade off the pressure differential in the heat exchangers, where lower pressure differentials reduce stresses, against lower turbine inlet temperatures, which increase allowable stresses. The initial steps of studying high-temperature S-CO_2 cycles involved validating that the power cycle simulation software, THERMOFLEX® [24], is capable of handling S-CO_2 as a working fluid. To this end, the modeling and validation of results of other high-temperature S-CO_2 power conversion cycle studies were performed in a code-to-code comparison. Once completed, a proposed high-temperature cycle layout was developed, described and subsequently optimized. Additionally, design issues focused around material selection and performance at design conditions are discussed.

6.3.1 Code to Code Comparison

6.3.1.1 Methodology

In order to perform a code-to-code comparison and to validate that THERMOFLEX® can properly handle S-CO_2 cycles, two other independent S-CO_2 Brayton cycles were chosen as references, an Argonne National Laboratory (ANL) 104.8 MWe, 42.27% efficient recompression cycle [65] and a Sandia National Laboratory (SNL) 252 kW_e, 780 kW_{th} test cycle [66]. Both of these cycles were recreated in THERMOFLEX® with the parameters provided in the above-cited references. The main parameters for the two cycles are shown in Table 6-8.

Table 6-8. Main performance parameters for ANL and SNL S-CO2 Brayton cycles.

Parameter	ANL	SNL	Unit
Core Outlet Temperature	550	-	°C
Net Power	105.7	0.252	MW
Thermal Power	250	0.78	MW
η_{net}	42.27	32.3	%
Pressure Ratio	2.62	1.8	
Compressor Inlet Temperature	32.8	32	°C
Turbine Inlet Temperature	516.6	537	°C
$\eta_{compressor}$	89.1	67	%
$\eta_{re\text{-}compressor}$	90.1	70	%
$\eta_{turbine}$	92.8	86/87	%

6.3.1.2 *Modeling of ANL S-CO_2 Brayton cycle.*

The first power cycle modeled was the SFR-100 S-CO_2 power conversion cycle, a 104.8 MWe, 42.27% (gross) efficient cycle. The details of the cycle were studied by Sienicki et al. [65]. Figure 6-4 shows a schematic of the cycle.

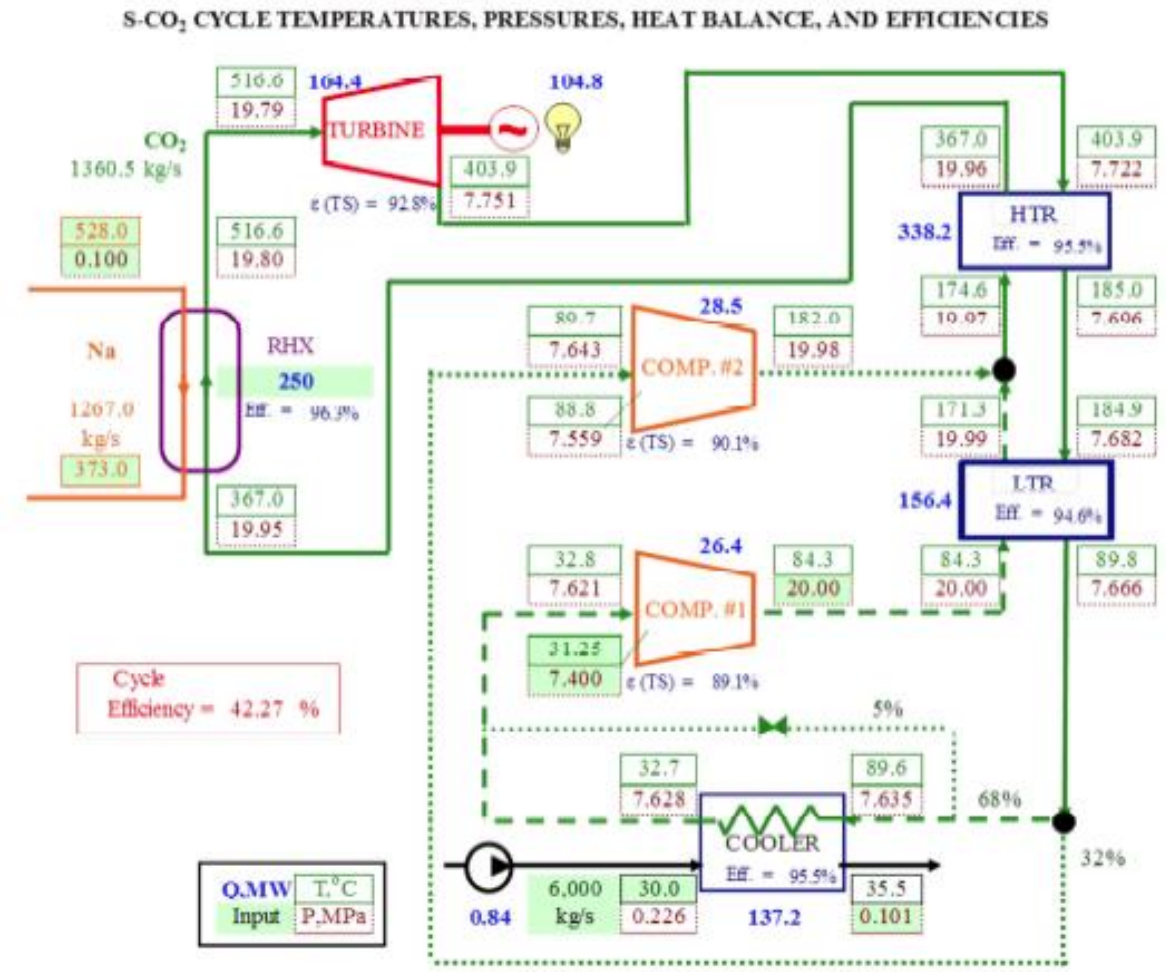

Figure 6-4. Optimized S-CO_2 Brayton cycle conditions for the SFR-100 [65].

The first step was to construct a model which involved building a simple S-CO_2 Brayton cycle with no recuperation and a single compressor rather than a split compressor model. This allowed the stepwise addition of detail and components to the model while also verifying that each component added did not cause the model to break down. The complete cycle with its performance results is depicted in Figure 6-5. The results obtained agree well with the ANL predictions, showing that THERMOFLEX® is able to model S-CO_2 cycles correctly with an approximate deviation of 1.9% to the report from Sienicki et al. [65]. This was deemed close enough since not all data needed for the model could be retrieved from the report (mainly parameters and the source of the thermodynamic properties for S-CO_2). THERMOFLEX® uses REFPROP thermodynamic values for CO_2, a database developed by the National Institute of

Standards and Technology (NIST) [43], with the original thermodynamic properties coming from Span and Wagner [67].

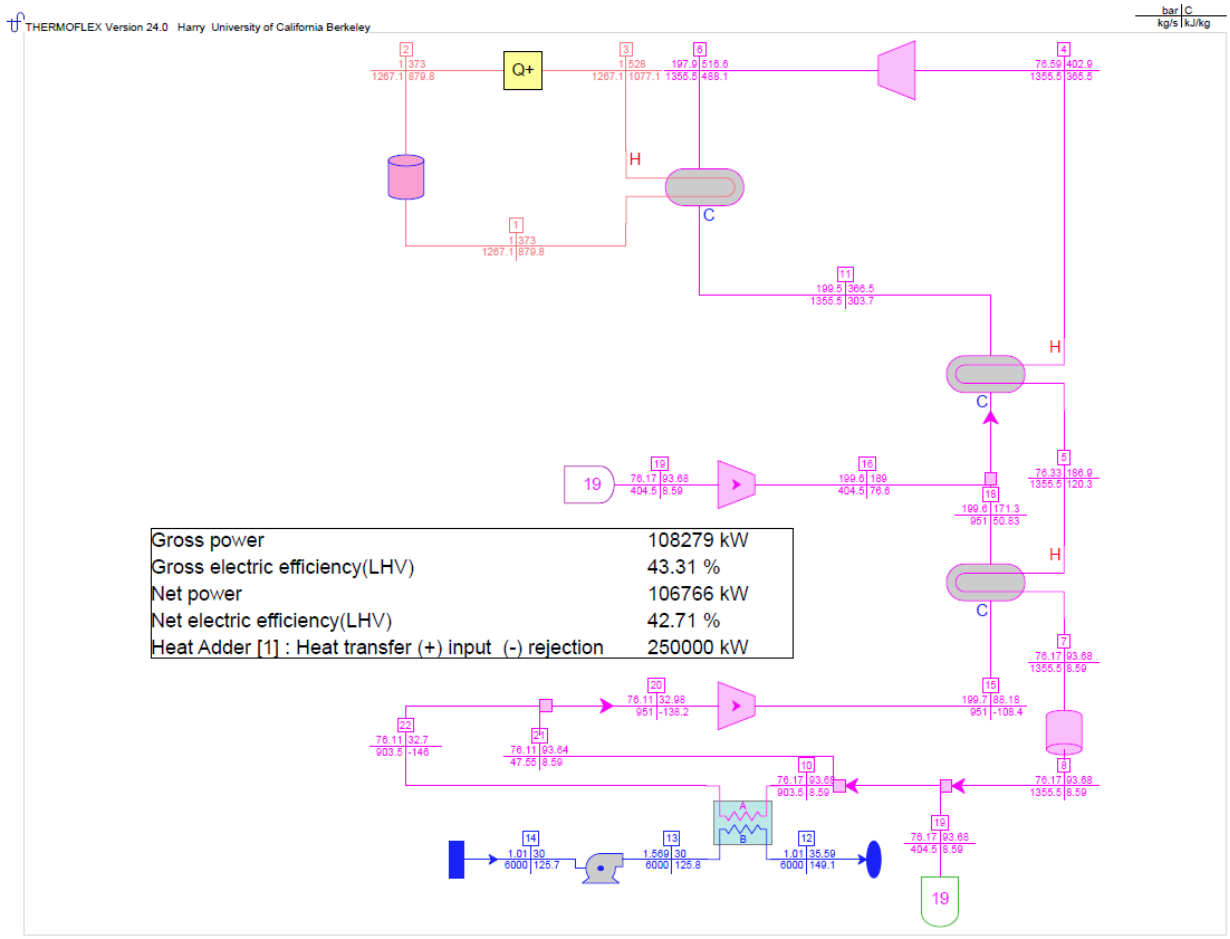

Figure 6-5. SFR-100 S-CO_2 ideal cycle results from THERMOFLEX®.

In Figure 6-5, the orange stream represents the primary reactor coolant (sodium), the pink stream represents S-CO_2, and the blue stream represents the water cooling stream. Sienicki et al. [65] reported outputs and results in terms of an idealized model that does not include some details required to implement the cycle in a power plant. Efficiency and power are reported as gross numbers as well, rather than net. A second iteration that considers these deficiencies was performed on the model by adding: (1) heat losses through the heat exchangers, (2) pressure drops through the primary liquid sodium loop and (3) wet cooling towers to the waste heat loop. A further step of detail would be to add more realistic pressure drops across the cycle branches. This has not been done here since the plumbing/piping distances of the cycle in question are unknown. With the above in mind and with the recalibrated model, it is evident that performance dropped significantly as seen in Figure 6-6. Net power and efficiency decreased from 106.8 MW_e and 42.71% to 101.9 MW_e and 40.76% with a constant 250 MW_{th} power input.

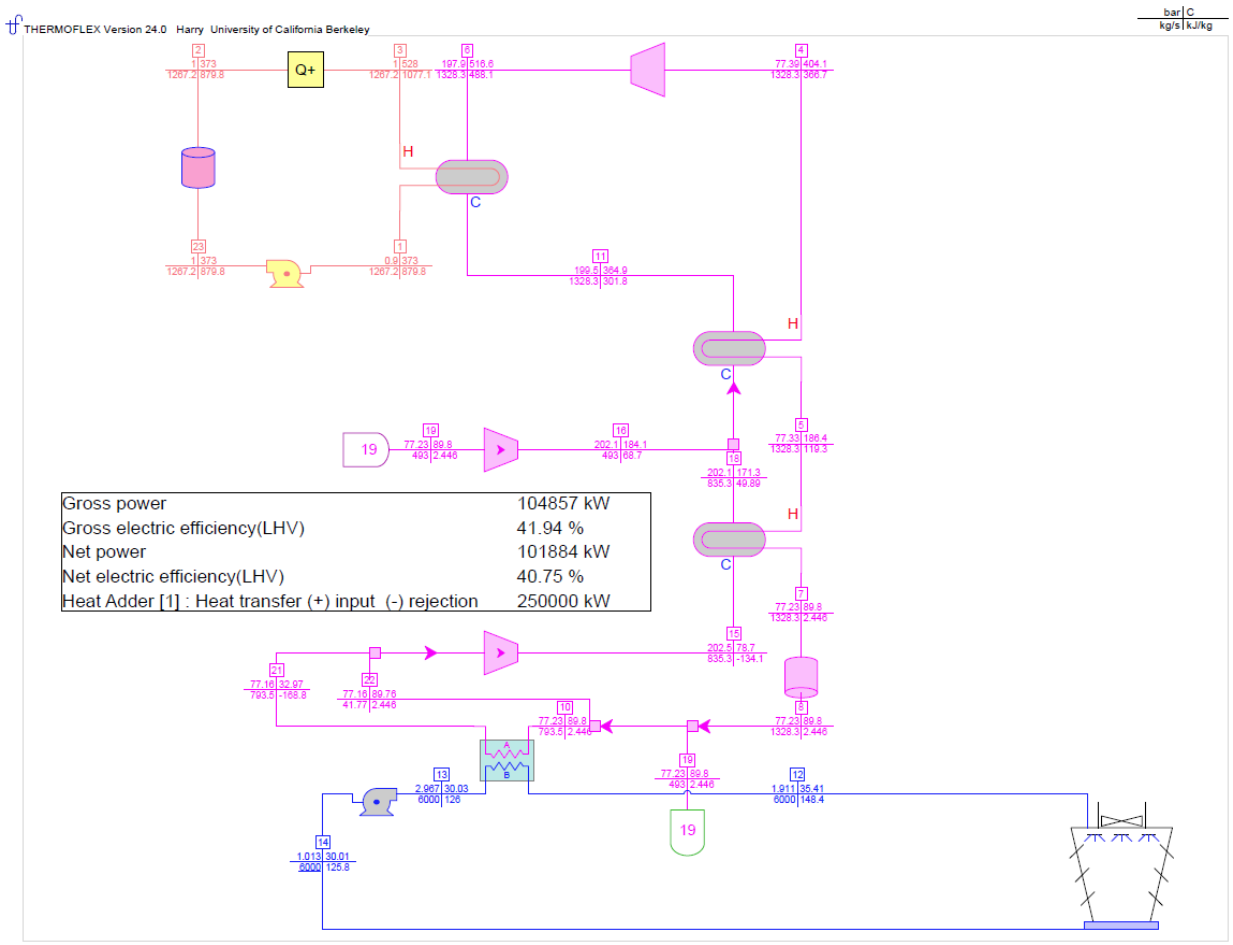

Figure 6-6. SFR-100 S-CO_2 detailed THERMOFLEX® results.

6.3.1.3 Modeling of SNL S-CO_2 Brayton Cycle

SNL is developing a S-CO_2 recompression Brayton cycle with an initial small test-stand already built and currently being tested to validate their modeling results [66]. A THERMOFLEX® model was built following the state points given in Figure 6-7, and is depicted in Figure 6-8.

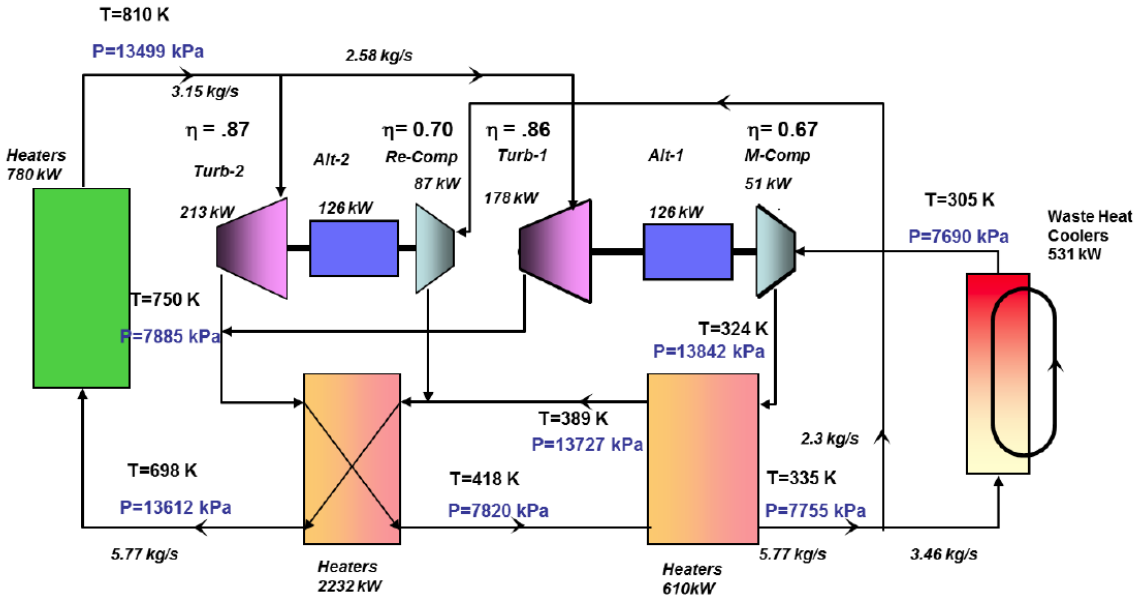

Figure 6-7. SNL S-CO_2 recompression Brayton cycle flow diagram [66].

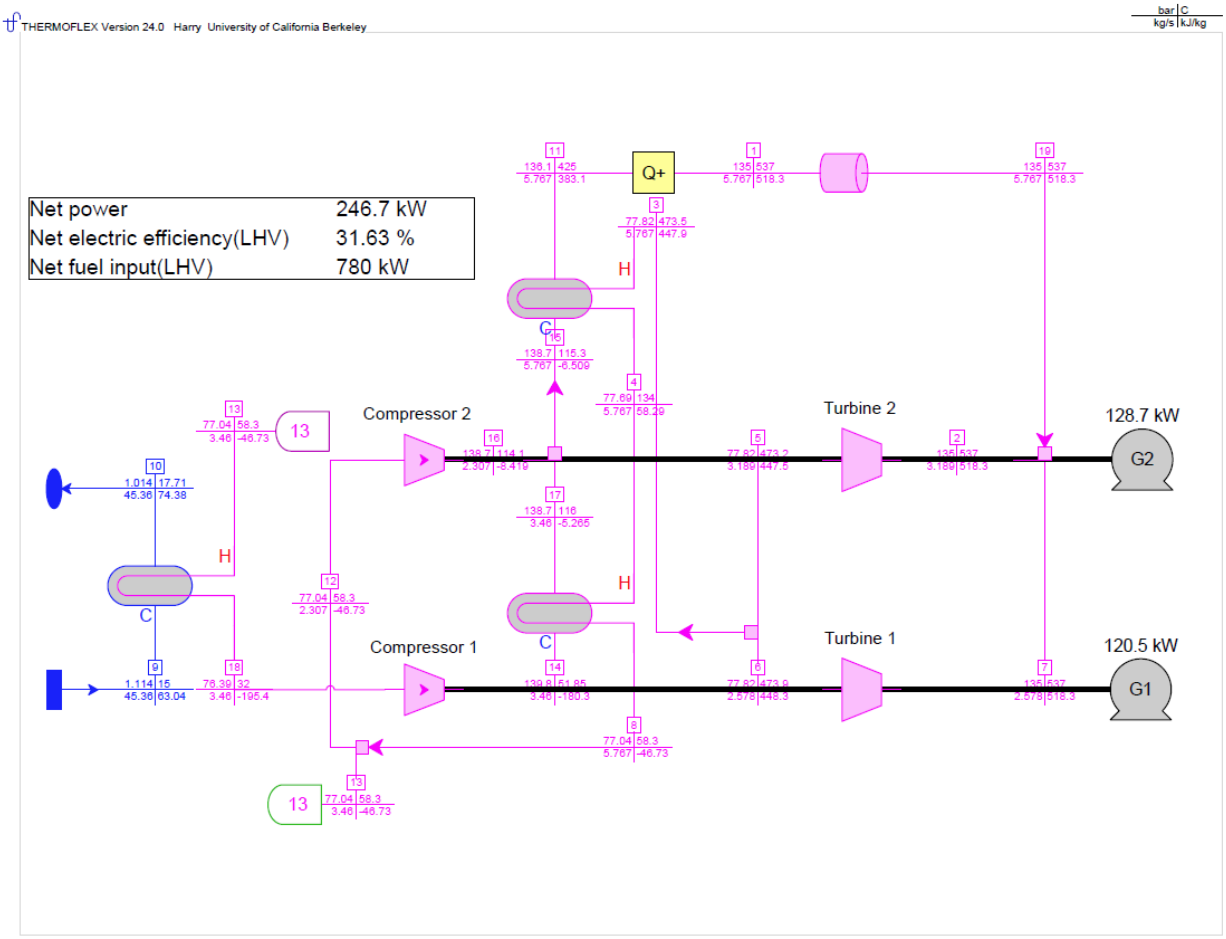

Figure 6-8. SNL S-CO_2 THERMOFLEX® cycle diagram.

The results of the THERMOFLEX® model and the model from SNL [66] are in good agreement: the source reference gives a power output of 252 kW_e and an efficiency of 32.3%, while the THERMOFLEX® results delivered an output of 246.7 kW_e and an efficiency of 31.6%, which is an overall deviation of roughly 2.1%. There was a slight imbalance in delivery of power from the two generators, which might have been due to slight configuration differences in the models, turbomachinery modeling techniques of the two software packages and/or assumed parasitic losses and mechanical losses for the generators, etc. Moreover, the output of the generators was not locked in THERMOFLEX® to match the source reference. These results however were deemed to be close enough for validation of THERMOFLEX®'s capabilities of modeling S-CO_2 cycles.

6.3.2 PB-FHR S-CO_2 Cycle Modeling and Considerations

6.3.2.1 Initial layout and configuration

A high-temperature S-CO_2 power conversion system is to be coupled to a 236 MW_{th} PB-FHR: the Mark-1 PB-FHR [68]. Using this thermal power and reactor coolant temperatures allows a direct performance comparison to a NACC power conversion cycle studied earlier [39] [40]. The cycles referenced in the previous sections have fundamental differences from an S-CO_2 cycle used for a PB-FHR, primarily due to the different size and power scale of the cycle. The SNL test stand is relatively small (0.78 MW_{th} of heat input), and thus uses radial-flow turbomachinery rotating at high frequency. At commercial scale power levels above 100 MW_{th}, axial-flow turbomachinery is more appropriate. This dictates that a comparison between an S-CO_2 cycle and a NACC might have to perform sensitivity studies on turbomachinery efficiencies for the S-CO_2 cycle, as it is yet an unproven turbomachinery technology at commercial scale. Additionally, S-CO_2 cycle operating characteristics will differ markedly from a NACC due to the recuperation and closed nature of the S-CO_2 cycle. These are topics for further research and study.

The initial layout of an appropriate cycle configuration for an S-CO_2 cycle coupled to a FHR took guidance from Dostal et al. [9]. It was suggested that a recompression cycle performs best and avoids low-temperature recuperator problems, namely a pinch point within the recuperator, when CO_2 is near its critical point with highly varying physical properties between the high and low pressure streams. Additionally, a sensitivity study demonstrated that reheat does yield better performance but at an added cost to the reactor design that might not warrant it. Keeping in mind these two findings, it was deemed appropriate to use a recompression cycle with reheat. Reheat was applied due to the improved performance; the added complication in the power conversion cycle does not add complication to the FHR design. A schematic diagram of the S-CO_2 FHR power conversion cycle is shown in Figure 6-9.

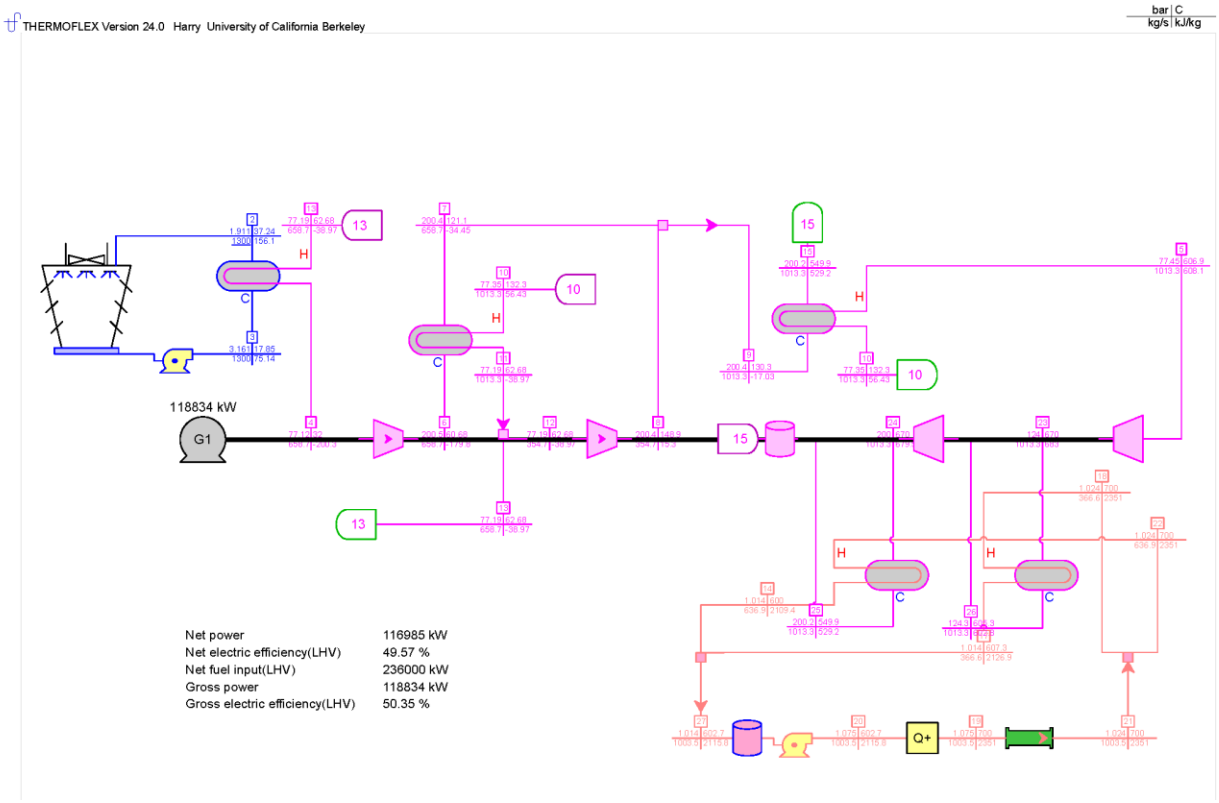

Figure 6-9. PB-FHR S-CO_2 power conversion schematic.

In Figure 6-9, the orange stream represents the reactor primary coolant (flibe), the pink stream represents S-CO_2, and the blue stream represents the water stream used as a heat sink. CO_2 enters the heaters at 550°C and is heated to 670°C, while the reactor coolant is cooled from 700°C to 600°C.

6.3.2.2 Cycle optimization

As with all Brayton cycles, there are various ways to optimize parameters and layouts in order to improve performance. Optimization of TIT, pressure ratio (PR), compressor inlet temperature, amount of regeneration, and reheat stages are a few examples [20].

Dostal et al. [9] performed an extensive survey of previous S-CO_2 studies and conducted sensitivity studies to determine general operating points and conditions that yield optimal performance for most S-CO_2 cycle layouts. For instance, operating slightly above the critical point at the main compressor inlet yields a higher PR and in general better performance. Deviating from the critical point reduced performance and also increased work needed by the compressor, in essence reducing the main benefit of using S-CO_2. Furthermore, a turbine inlet pressure of 20 MPa is a practical limitation for currently available materials. Though higher pressures are desirable as they yield higher efficiencies, material constraints related to the specific geometry of the heat exchangers used may limit the inlet pressure to this level. With the two above mentioned points, when using a recompression cycle an optimal PR of around 2.6 was produced.

Reheat can increase efficiency for a given maximum turbine inlet temperature. To study the effect of reheat on efficiency, the TIT was set at 670°C for both turbine stages to match the conditions used earlier in the Mk1 PB-FHR NACC system, outlined by Andreades et al. [39]. Core heat delivery was set at 236MW_{th}. Compressor efficiencies of 89% and turbine efficiencies of 90% were conservatively set. Compressor efficiencies and turbine efficiencies were set to 95.5% and 92.9% respectively under best estimate (B.E.) scenarios according to Dostal et al. [9]. A source of inefficiency not explicitly taken into account and modeled, is bypass flow due to leakage at location where seals are used (at points between high and low pressure flows). The overall fixed parameters are given in Table 6-9.

Table 6-9. PB-FHR S-CO_2 cycle conservative and best estimate fixed operating parameters.

Parameter	Cons.	B.E.	Unit
FHR Core Inlet Temperature	600	600	°C
FHR Core Outlet Temperature	700	700	°C
FHR Thermal Power	236	236	MW
Pressure Ratio	2.6	2.6	
Compressor Inlet Temperature	32	32	°C
Turbine Inlet Temperature	670	670	°C
$\eta_{compressor}$	89	95.5	%
$\eta_{turbine}$	90	92.9	%
$T_{ambient}$	15	15	°C

Having set the above mentioned parameters, the remaining parameters that needed to be optimized to yield optimal performance were the following: (1) expansion ratio (ER) split between reheat stages, (2) amount of heat regenerated from the high-temperature (HT) recuperator, (3) amount of heat regenerated from the low-temperature (LT) recuperator, (4) flow split between main and recompressing compressors, and (5) the mass flow rate of the cooling water (CW) stream. A sensitivity study was performed within a reasonable range for each of the five parameters separately, which was followed by subsequent iterations with the new parameters until results converged. Thermoflow MACRO 24.0, a multi-run application for Thermoflow software, was used to perform the sensitivity studies. All calculations were performed at ISO 3977 conditions (15°C, 60% relative humidity, 0 m altitude). THERMOFLEX® innately adds parasitic losses (house loads, generator losses, etc.) to its net efficiency numbers, which yield more accurate performance estimations.

Results of the optimization are presented in Table 6-10 along with a temperature-entropy diagram of the resulting conservative cycle in Figure 6-10.

Table 6-10. FHR S-CO_2 optimized parameters.

Parameter	Cons	B.E.	Unit
Net Electric Power	117.8	121.9	MW
Gross Power	119.9	124.1	MW
η_{net}	49.9	51.7	%
η_{gross}	50.8	52.6	%
FHR Thermal Power	236	236	MW
Expansion Ratio$_1$	1.6	1.6	
Expansion Ratio$_2$	1.61	1.61	
Recompressed Fraction	0.405	0.411	
$T_{cold,out,HT\ Recup}$	556.2	552.9	°C
$Q_{th,HT\ Recup}$	548	534.2	MW
$T_{cold,out,LT\ Recup}$	150.3	146.2	°C
$Q_{th,LT\ Recup}$	124.3	120.9	MW
m_{cw}	1800	1750	kg/s

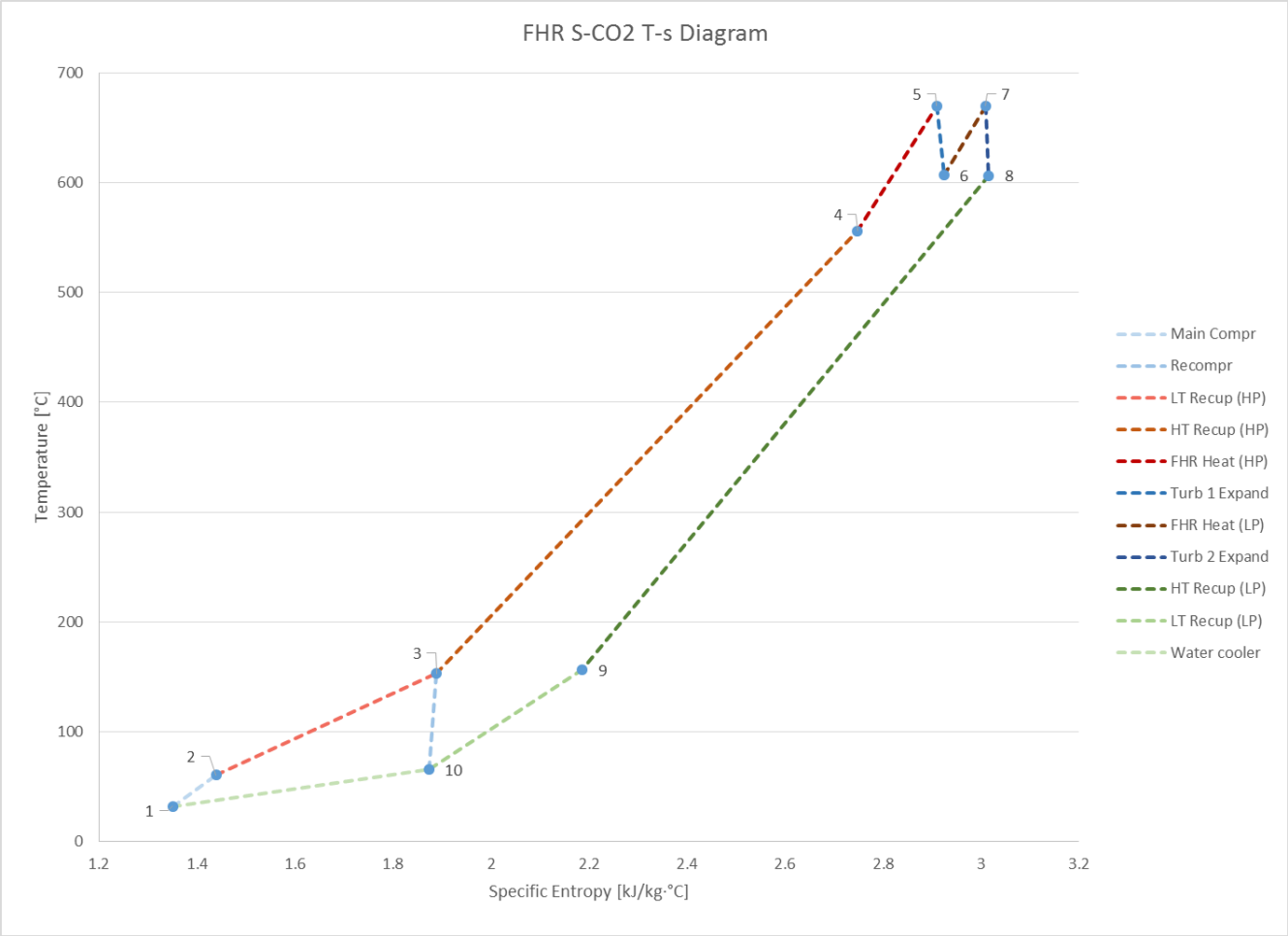

Figure 6-10. FHR S-CO_2 T-s diagram.

The results demonstrated quite good performance, in line with previous studies for the proposed design conditions. For the conservative (B.E.) turbomachinery assumptions the resulting power was 117.8 MW_e (121.9 MW_e) with a net efficiency of 49.9% (51.7%). As pointed out in Dostal et al. [9] the optimized recompression flow fraction is close to 0.40 which was confirmed here with a value of 0.405 (0.411). Moreover, in optimum configuration, the LT recuperator provided just enough heat to get the main compressor stream up to the temperature of the recompressing compressor outlet temperature. Any less or more regeneration by the LT recuperator would be suboptimal. The rest of the regeneration up to approximately 556°C was done by the HT recuperator.

Thermodynamically, work output maximization for reheat occurs when both turbines expand by the same pressure ratio. This was confirmed by the previous results and had an implication for the primary S-CO_2 heaters. The HP heater needed to deliver 150.9 MW_{th}, while the LP heater needed to deliver the remaining 82.7 MW_{th} from the reactor (assumed 1% heat loss for both heaters). This resulted in dissimilarly sized primary heaters. Unfortunately, this problem was hard to alleviate since the overall pressure ratio was not high enough to plausibly and efficiently split between the two expansion stages in any other manner.

An interesting note to make is that lower cooling water mass flow rates resulted in increased net efficiency at the expense of a higher air exhaust temperature by reducing pumping power. However, this might lead to a visible exhaust plume. It was deemed prudent to find the lowest water cooling mass flow rate in order to balance efficiency gain against exhaust plume visibility. At a cooling water mass flow rate of 1800 kg/s the exhaust plume is essentially invisible, while losing approximately 0.15% in efficiency compared to about half the cooling water requirement. At higher ambient temperatures this problem becomes less pronounced and lower cooling water mass flow rates can be selected.

6.3.2.3 Comparison to NACC

The primary motivation of the work here is the design of an appropriate power conversion system for the PB-FHR. An initial power conversion system is the NACC which is described in detail by Andreades et al. [39], and uses a modified GE 7FB gas turbine (open air Brayton cycle) in a combined cycle configuration. The system modeled in the previous sections, namely an indirect recompressing S-CO_2 closed Brayton cycle, is a second option. Both cycle configurations deliver enhanced performance compared to traditional LWR systems, in addition to providing additional operating and economic advantages. A comparison between the two cycle configurations using standard reference conditions might also provide some initial feedback as to which cycle provides the most optimal coupling to a PB-FHR. The operating parameters of the two cycles are presented in Table 6-11.

Table 6-11. Operating parameter comparison of NACC and S-CO2 cycles.

Parameter	NACC	S-CO_2	Unit
Power (Co-fired)	100 (240)	117.8 (-)	MW_e
TIT	670	670	°C
$T_{comp,in}$	15	32	°C
$p_{comp,in}$	0.1013	7.71	MPa
$p_{comp,out}$	1.874	20	MPa
Pressure Ratio	18.5	2.6	
η_{net} (Co-fired)	42.4 (66)	49.9 (-)	%
Thermal Power (Co-fired)	236 (447.6)	236 (-)	MW_{th}
Mass Flow Rate	418.5	1058.8	kg/s
W_{turb}	275.3	158.5	MW
W_{comp}	175.3	36.9	MW
W_{comp}/W_{turb}	0.637	0.233	
m_{CW}	5098	1800	kg/s

The S-CO_2 cycle delivers approximately 18 MW more power using the same core heat input and is therefore 17.6% more efficient than the NACC. Additionally, turbomachinery work is much smaller for the S-CO_2 cycle, with the compressors requiring only 23% of the turbine output at design point conditions. Another advantage of the S-CO_2 cycle compared to the NACC is its compactness and therefore smaller footprint. The power conversion system is to be vertically contained within an integral pressure vessel of an approximate diameter of 3.5 m. Although similarly ducted to the primary heaters as the NACC, this configuration removes the need for a large heat recovery steam generator, and possibly shorter ducts.

On the other hand, the NACC has the ability to provide quick peak power by injecting natural gas into the reheat turbine stage. This enables the NACC to deliver a large range of flexible capacity to the grid in times of need, as well as provide various ancillary services such as black-start services, regulation, and spinning reserves, among others. Moreover, the open nature of the NACC allows it to respond to transients effectively by venting air through after the last air heater, giving the reactor a longer coast-down time. Control of the S-CO_2 cycle during transients becomes more complicated due to the closed and recuperated nature of the system, necessitating some form of bypass around the turbine and back into the turbine. This might also result in a large thermal transient for the recuperators. Furthermore, the recompression layout of the S-CO_2 cycle gives a smaller operating envelope for the system as a whole, unless a multi-shaft arrangement or variable geometry compressors are used. Finally, the NACC has a greater degree of "off-the-shelf" advantage since large industrial frame gas turbines are well developed and commercially proven, although not with the specific external heating and reheat configuration needed for NACC. Conversely, CO_2 turbomachinery has yet to be demonstrated at commercial scale. Scaling considerations relating to commercial level S-CO_2 power conversion systems are discussed by Fleming et al. [69].

Operating pressure for the S-CO_2 cycle is more than an order of magnitude higher when compared to the NACC. Although both cycles consider the same type of design for the flibe-to-gas coiled tube heat exchangers, the former is more challenging to design and operate. The high

pressure differentials of nearly 20 MPa are comparable to the ASME Boiler and Pressure Vessel Code 100,000-hour allowable stress of a range of metals typically used for heat exchangers at design point conditions.

An additional issue to consider in the design of the cycle and more specifically the coiled tube gas heaters is the small available log-mean temperature difference (LMTD) across each salt to S-CO_2 heat exchanger that results from the thermodynamic optimization of the cycle. A basic heat exchanger calculation yielded the summarized results displayed in Table 6-12.

Table 6-12. Coiled tube gas heater summarized performance characteristics.

Parameter	NACC	S-CO_2 Brayton	Unit
Required HP Heat Transfer	116	151	MW
Required LP Heat Transfer	116	83	MW
HP Coiled Tube Heater LMTD	84.1	36.5	°C
LP Coiled Tube Heater LMTD	84.1	10.3	°C
Overall HP Heat Transfer Coefficient U	301.5	357.0	W/m²·°C
Overall LP Heat Transfer Coefficient U	301.5	373.5	W/m²·°C
Assumed Effectiveness ε	0.9	0.9	
HP S.A. Requirement	5083	12307	m²
LP S.A. Requirement	5083	23972	m²

Although the overall heat transfer coefficient had a higher value for the S-CO_2 cycle coiled tube gas heaters, the much lower LMTD yielded a substantial increase in surface area (SA) requirement compared to the NACC. The resulting height of the NACC tube bank was around 5.92m, and by proportion a height of 14.3-27.9 m for the S-CO_2 cycle while maintaining the same tube geometry is required. This lead to the conclusion of the impracticality from a manufacturing perspective of the application of reheat even at the higher core outlet temperature of 700°C, while using coiled tube gas heaters rather than printed circuit heat exchangers. The small PR available in the cycle gave each turbine stage a small ER and high turbine exhaust temperature, ultimately resulting in a small LMTD and high SA requirement. The removal of reheat would alleviate the larger SA requirement but reduces overall performance.

In terms of economics, the smaller footprint of the S-CO_2 cycle needs to be weighed against the less demanding and conventional material and fabrication requirements of the NACC. These benefits from the S-CO_2 cycle also need to be weighed against the additional revenues that the NACC can generate from its flexible capacity. Further studies need to be performed to quantify these aspects of each cycle to allow for a more accurate comparison.

6.3.3 Discussion

The interest in S-CO_2 Brayton cycles has revived over the past two decades. This is due to the increased need for highly efficient and economic power conversion systems in an ever-expanding "green" energy market. This study focuses on exploring an appropriate layout for an S-CO_2 Brayton cycle coupled to a molten salt primary heat loop in the temperature range of 650-700°C and evaluates its performance. A validation of THERMOFLEX® as a S-CO_2 cycle modeling tool is performed, by comparing results obtained with THERMOFLEX® to two other independent codes. A deviation between the codes of approximately 2% is observed, giving confidence in the ability of the software to model S-CO_2 cycles accurately.

An FHR is used as a reference heat source for the S-CO_2 Brayton cycle. In re-compression and reheat configuration, indirect heating by flibe with a TIT of 670°C yields close to 50% efficiency from a 236 MW_{th} heat source. The coupling to an FHR also allowed for a direct performance comparison to a NACC cycle. Although, the S-CO_2 Brayton cycle will have a smaller footprint and performs better in baseload operation, it loses the flexibility in operation of an NACC and also has more demanding conditions for the design of its primary heaters. An economic analysis needs to be performed to compare the two power conversion systems and quantify the overall impact of each one.

7 Conclusion

The push for economic development and an overall increased standard of living necessitate access to adequate energy, part of which is electricity. The triad of energy access and security, competitiveness, and environmental sustainability are the cause célèbre of the current era when it comes to energy policy. At times however, when put to practice these three goals seem to contradict each other paradoxically. Electricity market liberalization/deregulation (the competitiveness aspect) has produced inconclusive evidence of increased competition and ultimately lower consumer prices. There are also suggestions that it has caused cyclic investment in generation [70], which runs counter to a reliable long term supply of electricity. Compounding the problem of supply reliability in the short term is the large strain placed on transmission by the fervent introduction of intermittent renewable energy sources. In all, the current electricity infrastructure is not well suited in its current guise, with its current generating technology mix, to see through the necessary directives. To ease a transition to a clean and reliable electricity grid this dissertation proposes a novel power conversion system, lays out its basic physical form, estimates its performance, and studies its economic merit.

The combination of a nuclear heat source with an open air-Brayton power conversion system could enable the production of both base-load electrical power as well as ancillary services, such as peaking, load following, spinning reserve, and black start capability, previously not possible by commercial nuclear reactors. This is possible due to the high-temperature, low-pressure heat delivered by these sources. Such operating characteristics allow for grid stabilization services to system operators and added revenue for generators.

The earlier modular SmAHTR FHR design considered both steam and supercritical CO_2 as power conversion fluids, which are predicted to give thermal efficiencies of approximately 45% and 48%, respectively. This is greater than the 42.5% base-load efficiency predicted for the GE 7FB based power conversion system that operates at similar temperature, but the capability of the NACC system to also generate large amounts of peak power using cofiring generates additional revenues that would greatly exceed those from these larger base-load thermal efficiencies.

Initially, currently available commercial GTs are surveyed, several parameters that are important in coupling a commercial GT to non-fossil, external heat sources are examined, and a possible setup to achieve it is suggested. Table 7-1 summarizes key design parameters for the proposed NACC configurations.

Table 7-1. Key NACC design parameters.

	GE 7FB	Alstom GT24
Nominal ambient temperature	15 °C	15 °C
Elevation	Sea level	Sea level
Compression ratio	18.52	35.4
Compressor outlet pressure	1,858,000 Pa	3,587,000 Pa
Compressor outlet temperature	418.7 °C	560.4 °C
Compressor outlet mass flow(total flow is 440.4 kg/s; conventional 7FB design uses balance for turbine blade cooling)	418.5 kg/sec	469.3 kg/sec
CTAH outlet temperature	670 °C	870 °C
Base-load net electrical power output	100 MW_e	178 MW_e
Base-load thermal efficiency	42.5%	51.2%
Cofiring turbine inlet temperature	1065 °C	1230 °C
Cofiring net electrical power output	241.8 MW_e	324.6 MW_e
Cofiring efficiency (gas-to-peak-power)	66.4%	70%

Various off-nominal ambient and transient scenarios are considered for NACC operation. In order for the NACC cycle to provide economic and system benefits to both plant operators and the electricity grid, such as peaking power, spinning reserves, black start services, and frequency regulation, it must be able to accommodate these off-nominal and transient conditions successfully. Qualitative methods for the NACC to meet safety and reliability performance requirements while maximizing the use of standard gas turbine and combined cycle components wherever possible are proposed. A numerical study of the NACC performance under different ambient and off-nominal conditions is also performed. Through “off-the-shelf” modifications, currently in use with conventional NGCC, NACC performance is stabilized at its nominal design point performance and at all varying ambient conditions considered.

An additional key figure of merit that is estimated for the NACC is its power ramp rate. During the initial warm-up phase of startup a TIT ramp rate of approximately 460°C/min is calculated, whereas during the acceleration phase a lower TIT ramp rate between 150 and 240°C/min is calculated. As the full power TIT is approached the TIT ramp rate is reduced accordingly. Regarding the NACC, one can assume that a TIT ramp rate of anywhere between 150-460°C/min is reasonable which in turn yields a power ramp rate from the Brayton cycle of 21.7 MW/min to 66.5 MW/min. Typical ramp rates for conventional gas turbine are around 8 MW/min, but can be ramped to a maximum of 8 times faster during emergency startups. The maximum calculated ramp rate for the NACC thus appears to fall within maximum ramp rates of conventional gas turbines. The slower ramp rate of the steam turbine also had to be taken into account and is subsequently added to the above power ramp rates. Assuming a 30 minute ramp time for the steam cycle yields a 2.8 MW/min ramp rate. Adding this to the gas turbine ramp rate yields an overall ramp rate for the NACC of 24.5 MW/min to 69.3 MW/min. Such large power ramp rates can prove critically important during situations such solar eclipses, or during early evening hours when renewable generation stops being produced in large capacities within short time intervals. When selecting a ramp rate between the calculated values one has to balance potential material degradation, shortening of maintenance intervals, and added operating and maintenance costs to the added revenue generated from providing flexible capacity to the grid. Additionally, one

has to take into account that although the TIT at baseload is above autoignition temperature of NG, the full air mass flow is running through the nozzles, which in turn necessitates careful nozzle placement and design for the establishment of a steady flame.

Shifting from the technical aspects of the NACC to its economic merits, a combination of top down and bottom up approaches are used to estimate the cost structure of the Mk1, a vitally important part of assessing its overall profitability. Capital costs are estimated using an inventory of major classes of materials and scaling their cost to those of known conventional system. An overall capital cost of $4,500-$5,093/kW base load is estimated depending on the number of units, ranging from one to twelve, present at the power plant site. Having more units on site spreads out fixed costs and reduces the specific cost. When comparing the Mk1 to other plants it is important to take into account its ability to produce added electricity at essentially no additional capital cost, since all infrastructure required is already present and accounted for, which reduces the specific capital to $1,870-2,133/kW for base load plus peaking. These numbers should be compared to capacity weighted average capital costs of a NGCC and a conventional nuclear power plant, rather than each separately. O&M costs, along with fuel and decommissioning costs, which together constitute the marginal cost of electricity production for the baseload nuclear output are also estimated. The marginal cost of production for the peaking output is simply the cost of NG, which is not considered here due to its highly volatile price. Similar to capital construction costs, O&M costs drop from $89.32/MWh (¢8.93/kWh) to $48.09/MWh (¢4.81/kWh) as the number of units per site increase from one to twelve. The overall results are demonstrated in Table 7-2.

Table 7-2. Overview of Mk1 costs.

Description	Single Unit	12 Unit	
Capital Construction Costs			
Preconstruction Costs	80,484,991	263,622,515	$
Total Direct Cost	214,846,727	2,578,160,727	$
Indirect Cost	142,462,635	1,709,551,614	$
Total Contingency	71,461,872	857,542,468	$
Total Capital Investment	509,256,225	5,408,877,325	$
Specific Capital Investment (Nuclear)	**5,093**	**4,507**	$/kW
Specific Capital Investment (CF)	**2,133**	**1,870**	$/kW
Production Costs			
Total Annual O&M	62,086,683	311,631,799	$
Fuel Cost (annual)	14,992,846	179,914,152	$
Decommissioning Cost (annual)	1,165,920	13,991,046	$
Overall Production Cost	78,245,449	505,536,997	$
Marginal Production Cost	**89.32**	**48.09**	$/MWh

A comparison of other methodologies of capital and O&M cost estimation, such as drop down or scaling to nuclear power plants currently under construction (e.g. AP1000's at Vogtle and VC Summer), are subject to future study. Additionally, a cost comparison between competing generation technologies to the Mk1 is planned to be performed.

A revenue and profitability study is also necessary to fully evaluate the economic merits of the Mk1 system. Such a study will be performed initially under a levelized cost of electricity model for a regulated market and subsequently under a deregulated market mechanism.

In the name prudency, alternative power conversion systems to the NACC or alternative NACC configurations are studied. The interest in S-CO_2 Brayton cycles has revived over the past two decades. This is due to the increased need for highly efficient and economic power conversion systems in an ever-expanding "green" energy market. An appropriate layout for an S-CO_2 Brayton cycle coupled to a molten salt primary heat loop in the temperature range of 650-700°C is explored and its performance evaluated. A validation of THERMOFLEX® as S-CO_2 cycle modeling tool is performed, by comparing results obtained with THERMOFLEX® to two other independent codes. A deviation between the codes of approximately 2% is observed, giving confidence in the ability of the software to model S-CO_2 cycles accurately.

An FHR is used as a reference heat source for the S-CO_2 Brayton cycle. In re-compression and reheat configuration, indirect heating by flibe with a TIT of 670°C yields close to 50% efficiency from a 236 MW_{th} heat source. The coupling to an FHR also allows for a direct performance comparison to an NACC cycle. Although the S-CO_2 Brayton cycle will have a smaller footprint and performs better in baseload operation, it loses the flexibility in operation of an NACC and also has more demanding conditions for the design of its primary heaters. An economic analysis needs to be performed to compare the two power conversion systems and quantify the overall impact of each one.

A small scale 10MW_e NACC configuration is also suggested and studied. Its performance is not near that of its larger brother, mainly due to its lower pressure ratio, but several applications where such a configuration might be useful and appropriate are identified, such as a demonstration plant or remote applications.

References

[1] California Independent System Operator, "What the duck curve tells us about," October 2013. [Online]. Available: https://www.caiso.com/Documents/FlexibleResourcesHelpRenewables_FastFacts.pdf. [Accessed 4 April 2015].

[2] C. Andreades, A. T. Cisneros, J. Choi, A. Chong, D. L. Krumwiede, L. Huddar, K. Huff, M. R. Laufer, M. Munk, R. Scarlat, J. Seifried, N. Zweibaum, E. Greenspan and P. F. Peterson, "Technical Description of the “Mark 1” Pebble-Bed Fluoride-Salt-Cooled High-Temperature Reactor (PB-FHR) Power Plant," University of California, Berkeley, Berkeley, CA, September 30, 2014.

[3] C. Andreades, R. Scarlat, L. Dempsey and P. Peterson, "Reheat Air-Brayton Combined Cycle (RACC) Power Conversion Design and Performance Under Nominal Ambient Conditions," *Journal of Engineering for Gas Turbines and Power,* p. Pending, 2014.

[4] H. G. MacPherson, "The Molten Salt Reactor Adventure," *Nuclear Science and Engineering,* vol. 90, pp. 374-380, 1985.

[5] P. F. Peterson, "Multiple-Reheat Brayton Cycles for Nuclear Power Conversion with Molten Coolant," *Nuclear Technology,* vol. 144, no. 3, pp. 279-288, December 2003.

[6] P. F. Peterson and Z. Haihua, "A flexible baseline design for the advanced high temperature reactor using metallic internals (AHTR-MI)," *ICAPP,* 4-8 June 2006.

[7] S. R. Greene, "Pre-Conceptual Design of a Fluoride- Salt-Cooled Small Modular Advanced High-Temperature Reactor (SmAHTR)," ORNL/TM-2010/199, Fig. 8-1, p. 8-2, Oak Ridge, TN, December 2010.

[8] C. Forsberg, "Economics of meeting peak electricity demand using hydrogen and oxygen from base-load nuclear or off-peak electricity," *Nuclear Technology,* vol. 166, pp. 18-26, April 2009.

[9] V. Dostal, P. Hejzlar and M. J. Driscoll, "The Supercritical Carbon Dioxide Power Cycle: Comparison to Other Advanced Power Cycles," vol. 154, no. 3, 2006.

[10] R. Eldrid, L. Kaufman and P. Marks, "The 7FB: The next evolution of the F gas turbine," GE Power Systems, Schenectady, 2001.

[11] V. Ferraro, F. Imineo and V. Marinelli, "An improved model to evaluate thermodynamic solar plants with cylindrical parabolic collectors and air turbine engines in open Joule–Brayton cycle," *Energy,* vol. 53, pp. 323-331, 1 May 2013.

[12] H. Zhao and P. F. Peterson, "Advanced MED Using Waste Heat from Closed Gas Brayton Cycles," *Transactions of the ANS,* vol. 96, pp. 791-792, 2007.

[13] Y. Jeong, P. Saha and M. Kazimi, "Attributes of a nuclear-assisted gas turbine power cycle," Nuclear Energy and Sustainability Program, Cambridge, MA, 2005.

[14] Kemika, "Material Safety Data Sheet: Natural Gas Feed," Air Liquide, Houston, TX, 2005.

[15] C. Jones and J. A. Jacobs III, "Economic and technical considerations for combined-cycle performance-enhancement options," General Elecitric, Schenectady, NY, October 2000.

[16] D. Chase and P. Kehoe, "GE Combined-Combined Cycle Product Line and Performance," GE Power Systems, Schenectady, NY, 2000.

[17] A. Franco and C. Casarosa, "On some perspectives for increasing the efficiency of combined cycle power plants," *Applied Thermal Engineering,* pp. 1501-1518, 2002.

[18] Y. C. Wenguo Xiang, "Performance improvement of combined cycle power plant based on the optimization of the bottom cycle and heat recuperation," *Journal of Thermal Science,* pp. 84-89, 2007.

[19] P. Gilli, K. Fritz, J. Lippitsch and G. Lurf, "Radial flow heat exchanger". USA Patent 3,712,370, 1973.

[20] M. P. Boyce, Gas Turbine Engineering Handbook, Burlington, MA: Gulf Professional Publishing, 2006.

[21] R. Matta, G. Mercer and R. Tuthill, "Power Systems for the 21st Century - "H" Gas Turbine Combined Cycles," GE Power Systems, Schenectady, NY, 2000.

[22] Alstom, Artist, *Alstom GT11N2 Gas Turbine.* [Art]. Brown Boveri Strasse 7,CH-5401 Baden, Switzerland, 2013.

[23] C. B. Meher-Homji and G. A. Gabriles, "Gas Turbine Blade Failures - Causes, Avoidance, and Troubleshooting.," in *Proceedings of the Twenty-Seventh Turbomachinery Symposium*, Houston, TX, 1998.

[24] Thermoflow, "Thermoflow.com," Thermoflow Inc., 2 Willow Street, Suite 100, Southborough, MA 01745-1020, USA, [Online]. Available: http://www.thermoflow.com.

[25] F. J. Brooks, "GE Gas Turbine Perfrormance Characteristics," GE Power Systems, Schenectady, NY, 2000.

[26] S. Lecheler and J. Hoffman, "The Power of Water in Gas Turbines: ALSTOM's Experience with Air Inlet Cooling," Sao Paulo, Brazil, November 11-13, 2003.

[27] C. Andreades, L. Dempsey and P. Peterson, "Reheat Air-Brayton Combined Cycle (RACC) Power Conversion Design and Performance Under Off-Nominal Conditions," *Journal of Engineering for Gas Turbines and Power,* vol. 136, no. 6, 2014.

[28] P. Walsh and P. Fletcher, Gas Turbine Performance, 2nd ed., Wiley-Blackwell, 2004.

[29] M. P. Boyce, Gas Turbine Engineering Handbook, 4th ed., Elsevier, 2011.

[30] S. Jolly and S. Cloyd, "Performance Enhancement of GT 24 with Wet Compression," in *Power-Gen International*, Las Vegas, NV, 2003.

[31] C. Meher-Homji and R. Bhargarva, "Response, Condition Monitoring and Diagnostic Aspects of Gas Turbine Transient," *International Journal of Turbo and Jet Engines,* vol. 11, no. 1, pp. 99-111, March 1994.

[32] J. Gravdahl and O. Egeland, Compressor Surge and Rotating Stall: Modeling and Control, London, UK: Springe, 2011.

[33] G. K. McMillan, Centrifugal and Axial Compressor Control, Research Triangle Park, NC, USA: Momentum Pres, 2010.

[34] R. Kurz and K. Brun, "Gas Turbine Performance-What Makes the Map.," in *29th Texas A&M Turbomachinery Symposium*, Houston, TX, September 18-21, 2000.

[35] GE Power Systems, "Variable Inlet Guide Vane System, GEK 106910A," General Electric, Schenectady, NY, April 1998.

[36] GE Power Systems, "Unit Operation/Turbine (Gas), GEK 107357A," General Electric, Schenectady, NY, July 2003.

[37] D. Balevic, S. Hartman and R. Youmans, "Heavy-Duty Gas TUrbine Operating and Maintenance Considerations," GE Energy, Atlanta, GA, October, 2010.

[38] C. Andreades and P. F. Peterson, "Nuclear Air Brayton Combined Cycle (NACC) Power Ramp Rate," in *American Nuclear Society Student Conference*, College Station, TX, 9-11 April, 2015.

[39] C. Andreades, R. Scarlat, L. Dempsey and P. Peterson, "Reheat Air-Brayton Combined Cycle (RACC) Power Conversion Design and Performance Under Nominal Ambient Conditions," *Journal of Engineering for Gas Turbines and Power,* vol. 136, no. 7, June 2014.

[40] C. Andreades, D. Lindsay and P. Peterson, "Reheat Air-Brayton Combined Cycle (RACC) Power Conversion Design and Performance Under Off-Nominal Conditions," *Journal of Engineering for Gas Turbines and Power,* vol. 136, no. 6, 2014.

[41] GE Power Systems, "Fundamentals of Speedtronic MKVI Control System," General Electric, Greenville, SC.

[42] Thermoflow, "Thermoflow.com," Thermoflow Inc., 2 Willow Street, Suite 100, Southborough, MA 01745-1020, USA, [Online]. Available: http://www.thermoflow.com.

[43] National Institute of Standards and Technology, "NIST Standard Reference Database 23," 6 May 2014. [Online]. Available: http://www.nist.gov/srd/nist23.cfm. [Accessed 20 November 2014].

[44] G. Rothwell and F. Ganda, "Electricity Generating Portfolios with Small Modular Reactors," Argonne National Laboratory, Argonne, IL, May 2014.

[45] International Atomic Energy Agency, "PRIS - Country Details - United States of America," IAEA, 15 April 2015. [Online]. Available: http://www.iaea.org/PRIS/CountryStatistics/CountryDetails.aspx?current=US. [Accessed 15 April 2015].

[46] A. Gandrik, B. Wallace, L. Demick, S. Melancon and M. Patterson, "Assessment of High Temperature Gas-Cooled Reactor (HTGR) Capital and Operating Costs," Idaho National Laboratory, TEV-1196, Idaho Falls, ID, 2011.

[47] INL, "NGNP Program Planning Bases for the Schedule and Cost Estimates," Idaho National Laboratory, PLN-2970, Idaho Falls, ID, December 2010.

[48] C. Andreades and e. al., "Technical Description of the “Mark I” Pebble-Bed Fluoride-Salt-Cooled High-Temperature Reactor (PB-FHR) Power Plant, UCBTH-14-002," Department of Nuclear Engineering, University of California at Berkeley, Berkeley, CA, 2014.

[49] N. Zweibaum, C. Andreades, S. Hong and P. Peterson, "Life Cycle Assessment of the Mark 1 Pebble-Bed, Fluoride-Salt-Cooled, High-Temperature Reactor," in *Proc. Int. Congress on Advances in Nuclear Power Plants (ICAPP '15)*, Nice, France, May 3-6, 2015.

[50] P. F. Peterson, H. Zhao and R. Petroski, "Metal And Concrete Inputs For Several Nuclear Power Plants," UCBTH-05-001, Berkeley, CA, February 2005.

[51] R. H. Bryan and I. T. Dudley, "Estimated Quantities of Materials Contained in a 1000-MW(e) PWR Power Plant," Oak Ridge National Laboratory, ORNL-TM-4515, Oak Ridge, TN, June 1974.

[52] U.S. Energy Information Administration, "Updated Capital Cost Estimates for Utility Scale Electricity Generating Plants," U.S. Department of Energy, Washington, D.C., April 2013.

[53] Bureau of Labor Statistics, "Electric Power Generation , Transmission and Distribution," NAICS 221100, 25 March 2015. [Online]. Available: http://www.bls.gov/oes/current/naics4_221100.htm. [Accessed 21 April 2015].

[54] Dominion Engineering, Inc., "Study of Construction Technologies and Schedules, O&M Staffing and Cost, Decommissioning Costs and Funding for Advanced Reactor Designs," Contract No. DE-AT01-020NE23479, Reston, VA, 2004.

[55] N. Kumar, P. Besuner, S. Lefton and D. Agan, "Power Plant Cycling Costs," National Renewable Energy Laboratory, Sunnyvale, CA, April 2012.

[56] J. R. Lamarsh and A. J. Barata, "Isotope Separation," in *Introduction to Nuclear Engineering*, Upper Saddle River, NJ, Prentice Hall, 2001, pp. 201-205.

[57] UxC, LLC, "Historical Ux Price Charts," Ux Consulting Company, LLC, 1 May 2015. [Online]. Available: http://www.uxc.com/review/UxCPriceChart.aspx?chart=spot-u3o8-full. [Accessed 1 May 2015].

[58] Nuclear Energy Agency, "The Economics of the Nuclear Fuel Cycle," NEA-OECD, Paris, France, 1994.

[59] D. E. Shropshire, K. A. Williams, W. B. Boore, J. D. Smith, B. W. Dixon, M. Dunzik-Gougar, R. D. Adams and D. Gombert, "Advanced Fuel Cycle Basis Cost," Idaho National Laboratory, INL/EXT-07-12107, Idaho Falls, Idaho, April 2007.

[60] U.S. Nuclear Regulatory Commission, "Report on Waste Burial Charges: Changes in Decommissioning Waste Disposal Costs at Low-Level Waste Burial Facilities (NUREG-1307, Revision 15)," Nuclear Regulatory Commission, Washington, DC, January 2013.

[61] C. Andreades and P. Peterson, "Simple and Combined Cycle Power Conversion with Natural Gas Co-Firing, for Mobile PB-FHR," *American Nuclear Society Transactions,* vol. 109, no. 1, pp. 1683-1686, November 2013.

[62] G. Angelino, "Carbon Dioxide Condensation Cycles For Power Production," *Journal of Engineering for Gas Turbines and Power,* vol. 90, no. 3, 1968.

[63] D. Gokhstein, E. Taubman and G. Konyaeva, "Thermodynamic cycles of carbon dioxide plant with an additional turbine after the regenerator," *Thermal Engineering,* vol. 20, no. 3, 1973.

[64] E. G. Feher, "The supercritical thermodynamic power cycle," *Energy Conversion,* vol. 8, pp. 85-90, 1968.

[65] J. Sienicki, A. Moisseytsev and L. Krajtl, "Utilization of the supercritical CO2 Brayton cycle with sodium-cooled fast reactors," in *The 4th Internation Symposium - Supercritical CO2 Power Cycles*, Pittsburgh, Pennsylvania, September 9-10, 2014.

[66] J. C. T. Pasch, D. Fleming and G. Rochau, "Supercritical CO2 recompression Brayton cycle: Completed assembly description," Sandia National Laboratories, Albuquerque, NM, October 2012.

[67] R. Span and W. Wagner, "A new equation of state for carbon dioxide covering the fluid region from the tiple-point temperature to 1100 K at pressures up to 800 MPa," *Journal of Physical and Chemical Reference Data,* vol. 25, no. 6, 1996.

[68] C. Andreades, A. T. Cisneros, J. K. Choi, A. Y. K. Chong, D. L. Krumwiede, L. R. Huddar, K. Huff, M. R. Laufer, M. O. Munk, R. O. Scarlat, J. Seifried, N. Zweibaum, E. Greenspan and P. F. Peterson, "Technical Description of the 'Mark 1' Pebble-Bed Fluoride-Salt-Cooled High-Temperature Reactor (PB-FHR) Power Plant," Department of Nuclear Engineering, U.C. Berkeley, Report UCBTH-14-002, 2014.

[69] D. D. Fleming, T. V. Holschih, T. M. Conboy, J. J. Pasch, S. A. Wright and G. A. Rochau, "Scaling Considerations for a Multi-Megawatt Class Supercritical CO2 Brayton Cycle and Commercialzation," Sandia National Laboratories, Albuquerque, NM, November 2013.

[70] S. Arango and E. Larsen, "Cycles in deregulated electricity markets: Empirical evidence from two decades," *Energy Policy,* vol. 39, no. 5, pp. 2457-2466, 2011.

[71] ECCO International, Inc., "ProMaxLT™," 2014. [Online]. Available: http://www.eccointl.com/downloads/ProMaxLT_Overview.pdf. [Accessed 20 November 2014].

[72] U.S. Energy Information Administration, "Annual Energy Outlook 2014 with projections to 2040," Department of Energy, Washington DC, 2014.

[73] D. F. Williams, L. M. Toth and K. T. Clarno, "Assessment of Candidate Molten Salt Coolants for the Advanced High-Temperature Reactor (AHTR)," Oak Ridge National Laboratory, Oak Ridge, TN, 2006.